The Kinetic Characterization of the Marginally Processive Motor, Dimeric Eg5/KSP

by

Troy Christopher Krzysiak

B.S. Biology and Chemistry Interdisciplinary Major, Loyola College of Maryland, 2002

Submitted to the Graduate Faculty of

The Department of Biological Sciences in partial fulfillment

of the requirements for the degree of

Doctor of Philosophy

University of Pittsburgh

2007

UNIVERSITY OF PITTSBURGH

Biological Sciences

This dissertation was presented

by

Troy Christopher Krzysiak

It was defended on

August 30th,2007

and approved by

_____

Jeffrey Brodsky, PhD, Biological Sciences, University of Pittsburgh

_____

Roger Hendrix, PhD, Biological Sciences, University of Pittsburgh

_____

William Saunders, PhD, Biological Sciences, University of Pittsburgh

_____

E. Michael Ostap, PhD, Physiology, University of Pennsylvania School of Medicine

_____

Dissertation Advisor: Susan P. Gilbert, PhD, Biological Sciences, University of Pittsburgh

The Kinetic Characterization of the Weakly Processive Motor, Dimeric Eg5/KSP

Troy Christopher Krzysiak

University of Pittsburgh, 2007

The Kinesin-5 subfamily of the kinesin superfamily of molecular motors has been shown to play an integral role in the transfer of genetic material from mother-cell to daughter-cell. These homotetrameric kinesins function by crosslinking two microtubules in the mitotic spindle and imparting a force necessary to both assemble and maintain the spindle. The purpose of this dissertation has been to gain a better understanding of how Eg5/KSP, a member of the Kinesin-5 subfamily, coordinates the biochemical activities of its motor domains, to fulfill its cellular role.

This dissertation focuses on a truncation of the human Eg5 gene that produces a dimeric motor. Analysis of this motor has indicated that the two motor domains, which interact with the same microtubule, function cooperatively. In some respects, dimeric Eg5 resembles conventional kinesin. Both motors are capable of translocating along the microtubule by taking successive steps before dissociating. To achieve this phenomenon, both motors couple the turnover of a single molecule of ATP to each advancement while maintaining the two motor domains out of phase through alternating catalytic cycles. Also, both motors have their stepping gated by ATP binding.

The mechanistic commonalities between dimeric Eg5 and conventional kinesin, however, do not reach beyond a similar mechanism of stepping. This work has uncovered a novel biphasic, microtubule associated mechanochemical cycle. Dimeric Eg5 is the first kinesin known to begin the microtubule associated phase of its ATPase cycle with both motor domains associated with the microtubule. Furthermore, the transition to this two-motor-domain-bound

state is the slow step governing steady-state ATP turnover. This slow transition only occurs once in the cycle and prior to processive movement. During processive movement, the catalytic step governs the rate of motor stepping. Dimeric Eg5 is also the first kinesin motor to have a rate-limiting catalytic step.

TABLE OF CONTENTS

LIST OF TABLES

LIST OF FIGURES

PREFACE

I guess the best way to sum up graduate school is that nothing was the way I had expected it to be. I don't mean this in necessarily a bad way, but the process of science is much different than it appears as an undergrad. As an undergrad you learn science predominantly from text books and assume/believe what you are reading about is fairly well understood and/or widely accepted. It never ceased to amaze me how little people agree in the various fields of scientific research and how many processes have a huge "magical" component to them. I suppose it is just the nature of the practice that when you work with extremely complicated microscopic and submicroscopic systems, it is impossible to directly examine an object in a truly direct way as is possible in the macroscopic everyday world. A mechanic can figure out how a new engine works by taking it apart with their hands and seeing what happens with their own eyes if a particular part would be removed. In science, everything is a shadow-game. By this I mean that nothing is ever truly directly examined without one complication or another. It is these complications that lead to multiple possible interpretations resulting from every experiment. If anything this is the double-edged-sword of science. It is great in that a researcher can have a seemingly endless supply of avenues to take when experiments give unexpected results, but bad in that everyone has a tendency to get so wraped up in their particular models and doggedly defend them well beyond reason.

On a slightly related note, I thoroughly love the scientific breakthrough press releases detailed on the evening news. The general public just gets told so much junk based off of preliminary or predominantly circumstantial evidence. It is no wonder that the general public has such little understanding of the way things really are.

Well, enough of my perspective on things. If anything, my perspective usually gets me in trouble. As my Mom always would tell me before we would go somewhere with people out of the immediate family: "Now don't give anyone your opinion because they really don't want to hear it." This then leads me in to the people that I need to thank for various things during the course of this dissertation.

First and foremost I need to thank my family; Mom, Dad, Sean (Bonz), Pap, and Gram. If I would go on and list all the things that they do for me or have done for me it would make whomever is reading this jaw drop. I would probably need to double the size of this dissertation to list all of them. Not many graduate students get to begin grad school with their own townhouse. You can't beat going home to your own nice house instead of some cruddy, old, overpriced, apartment that most gradstudents are stuck with. I even had tons of help keeping it nice. My Mom and Gram spent countless hours helping me clean and take care of it. Really, my Mom has always just done so much for me. She has always gone out of her way to do everything and anything for me so that my life could always be as convienient as possible. My Mom is the best.

Next in line would be the Boss, Susan. On the core course third module exam I got an invitation to rotate in the lab and it turned into this document. We have certainly argued over our fair share of scientific data over the last four years but it was obviously all for the best. I have been thinking for a while about what is the most important thing I have learned over the last four

years and what I came up with basically led to some of the more important point in this dissertation. At times when experimental data has given results so much different than what I would have predicted it was imensly beneficial to try experiments that had worked in the past from a different angle.

Along these same lines, I need to thank my thesis committee: Jeff Brodsky, Roger Hendrix, Mike Ostap, and Bill Saunders. For the duration of this project they have taken the time to critically evaluate my project and make sure I am accomplishing as much as possible.

The next group of people I need to thank are all the people I have worked with in the Gilbert lab. I couldn't have been luckier in getting Jared and Lisa as fellow grad students and friends. Jared and I basically conqurered Eg5 together. Every morning we would have Eg5 project meeting time as we cycle microtubules. It is amazing, some of the ideas we came up with, and how those ideas turned out to be true; well as true as anything can be in science. Lisa, what can I say, you were my best friend, my twin, and someone I will always be very close too. Being nonbiological twins we don't look alike but we always had the ESP connection and would finish each others sentences all the time. As I promised, when I have kids one day I will have them call you Aunt Lisa.

Of course, as lab personel continually changes, there are plenty of people that impact your life. Dave, it was great having someone in the lab with the same interests as me. Nothing beats the way Lisa would describe us when we would talk about video games and such: "Oh you boys." You're a good friend. Vince, I'm glad you came to the lab. It has been definitely fun having a lab of you, me and Dave. Good luck up in Troy, NY. Karen, Yuan Yuan, Amy Ewing, Brian, and Karli, everyone I have trained to do kinetics at some point or the other, trying to teach

you guys things taught me a lot about both kinetics, conveying a message, and (not to name any names) to make sure the person you are training isn't blowing something up. Ha!

The last person I need to thank is Amy Mucka. As everyone that knows me is aware, I think I know everything. For one of the many reasons that you have become as special to me as you are, you also think that you know everything. I love the fact that you are able to challenge me and on occasion point out that I am not entirely correct. Coupling that with the fact that we enjoy just about all the same things results in the role you have played in my thesis. For the last year you have been the person that makes me excited. For what? Well, just about anything.

To sum up grad school: I am so glad this is all finally over!

1.0 INTRODUCTION

While the definition of what makes a particular entity alive is not a settled matter, all definitions of a "living" organism involve it possessing the ability to reproduce. At the core of reproduction is the accurate passage of genetic material to the offspring. For this to happen, two things must occur: the accurate replication of DNA and the exact segregation of the duplicated genome into the offspring. Both processes occur because there are proteins capable of producing a force that will mechanically drive the process. By studying these molecular motors it should be possible to learn what events are crucial to the fidelity of these processes and how science can manipulate them to correct imbalances caused by disease.

1.1 MITOSIS

Looking at the cell cycle as a whole, it seems that the amount of time devoted to performing cell division, 5% of the total cell cycle, would indicate that it is a rapid and rather simple process. On the contrary, successful cell division putatively requires the coordination of 200-800 proteins in a massive apparatus called the mitotic spindle [1, 2]. There are also several checkpoint mechanisms to ensure that the process results in two daughter cells with a complete copy of the genome [3-10].

Mechanically speaking, the mitotic spindle has two main components, microtubules and motor proteins, that allow for the physical alignment of the genetic material and its subsequent separation into the cell poles [11-19]. Physically, the spindle is an interdigitating mesh of a noncovalent protein polymer called microtubules. This mesh is maintained through interaction with motor proteins from the kinesin and dynein superfamilies. These motors provide a way for the microtubules to connect to other objects in the spindle, such as the DNA, as well as remain focused in a structure competent for separating the genetic material. These motor proteins are not just static glue holding the spindle together, but are, more importantly, a way for the cell to both maintain and modulate the force balance within in the spindle, allowing for spatiotemporal control over necessary rearrangements.

1.2 MICROTUBULES

Microtubules are a very dynamic structural element in eukaryotic cells (Figure 1.1). As their name suggests, microtubules are long hollow cylinders approximately 25 nm in width and can be many microns in length [20]. These tubes form from the polymerization of αβ-tubulin heterodimers in a head-to-tail fashion [20, 21]. Initially, heterodimers come together to form linear protofilaments which will laterally interact with other protofilaments to form the final cylinder [22]. Microtubules have been seen to posses 8-19 protofilaments, however, most contain 13 protofilaments *in vivo* [20, 23-25]. Because the individual protofilaments are formed in a head to tail fashion, there is an intrinsic polarity to the microtubule with one end being capped by the β-tubulin subunit, termed the plus-end, and one end capped with the α-tubulin subunit, termed the minus-end [20, 22, 26-29]. This structural polarity directly contributes to the

dynamics of the microtubule with the net rate of subunit addition being faster at the plus-end [30]. Furthermore, while both tubulin subunits bind GTP, only the β-tubulin subunit is capable of hydrolyzing bound nucleotide [31-34]. *In vivo*, the minus-end of the microtubule is generally anchored in another protein structure leaving the plus-end as the dominant source of dynamics [35]. While heterodimers with GTP bound at the β-subunit are being added on, the microtubule is stable, however, when the GTP cap is lost due to hydrolysis, the individual protofilaments will begin to curve outward and a rapid phase of depolymerization, called catastrophe, will ensue [34, 36-42].

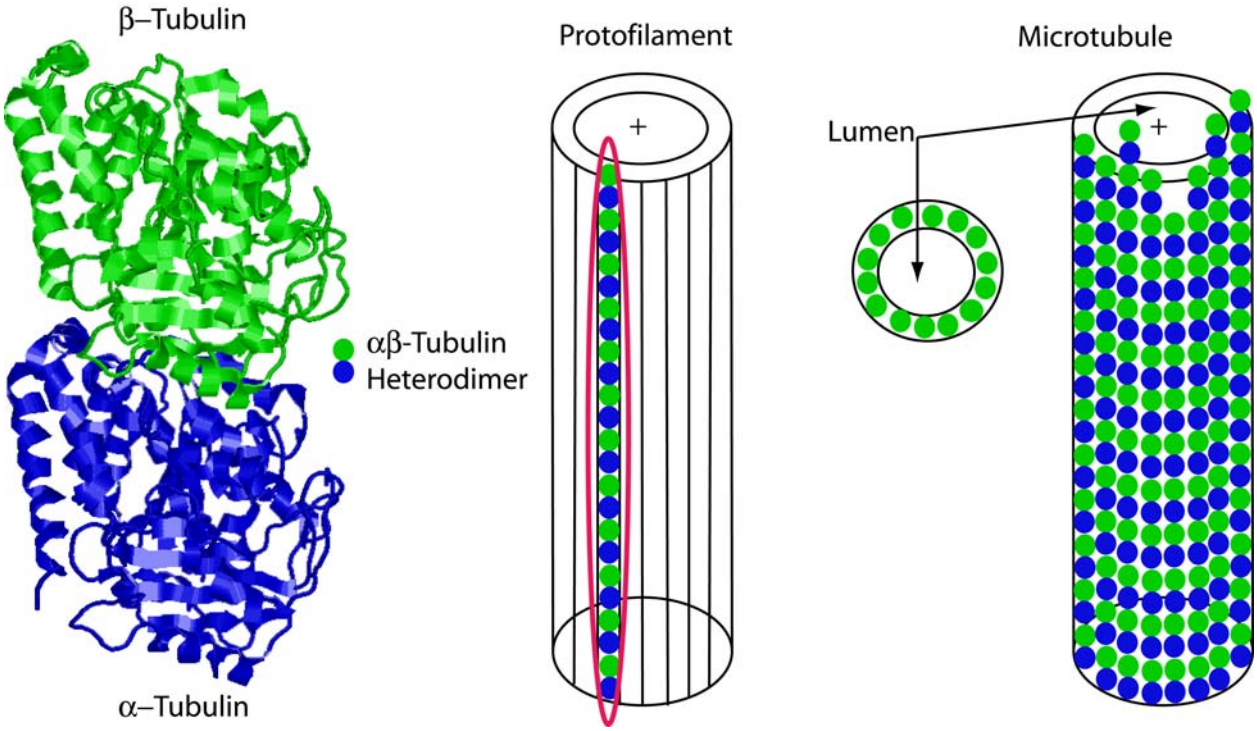

Figure 1.1 The Microtubule Polymer

Figure 1.1 is an adaptation from [43] using the αβ-Tubulin heterodimer crystal structure from [44]. Microtubules are polar polymers formed by the initial interaction of the α-subunit of one tubulin heterodimer with the β-subunit of another tubulin heterodimer to form a linear protofilament. Lateral contacts made between several protofilaments induce the formation of hollow, cylindrical microtubules.

Functionally, microtubules serve several purposes in the cell. At all points in the cell cycle, microtubules serve as the roads for motor proteins in the kinesin and dynein superfamilies as they transport various cargos [45-47]. During mitosis, microtubules become akin to the actin filaments of muscle; they become the intermediary through which various motor proteins are able to separate the two spindle poles. Microtubule dynamics are greater during mitosis [33, 48-50] and play an important role in the search and capture of the paired chromosomes and their proper alignment [20, 51-53]. After proper alignment of the chromosomes occurs, it is the depolymerization of those microtubules attached to the kinetochores of the chromosomes that drives the separation of the homologous pairs and their localization to the two cell poles [54-57].

1.3 FAMILIES OF MOLECULAR MOTORS

Molecular motors are a class of enzymes that transforms the chemical energy stored in a small molecule or concentration gradient into mechanical energy. In some cases the result is the translocation of the protein along a filament, i.e., cytoskeletal motors, polymerases, and helicases, and in others, it is a stationary conformational change to force a small molecule against a concentration gradient, e.g., V-ATPases.

There are three families of cytoskeletal motors (Figure 1.2): the actin based myosins, the kinesins and the dyneins, both of which are microtubule based. Within each family, members share a 30-50% amino acid sequence identity in their enzymatic globular domains, termed motor domains [58]. All three families of motors are ATPases, and function by imparting a force on their protofilament partner. Each superfamily has developed a unique mechanochemical cycle with respect to how ATP modulates motor behavior; however, each mechanism is able to

produce both processive and nonprocessive motors. The ability to be processive, literally to take multiple steps along the appropriate filament, or nonprocessive is crucial to the various functions each motor performs.

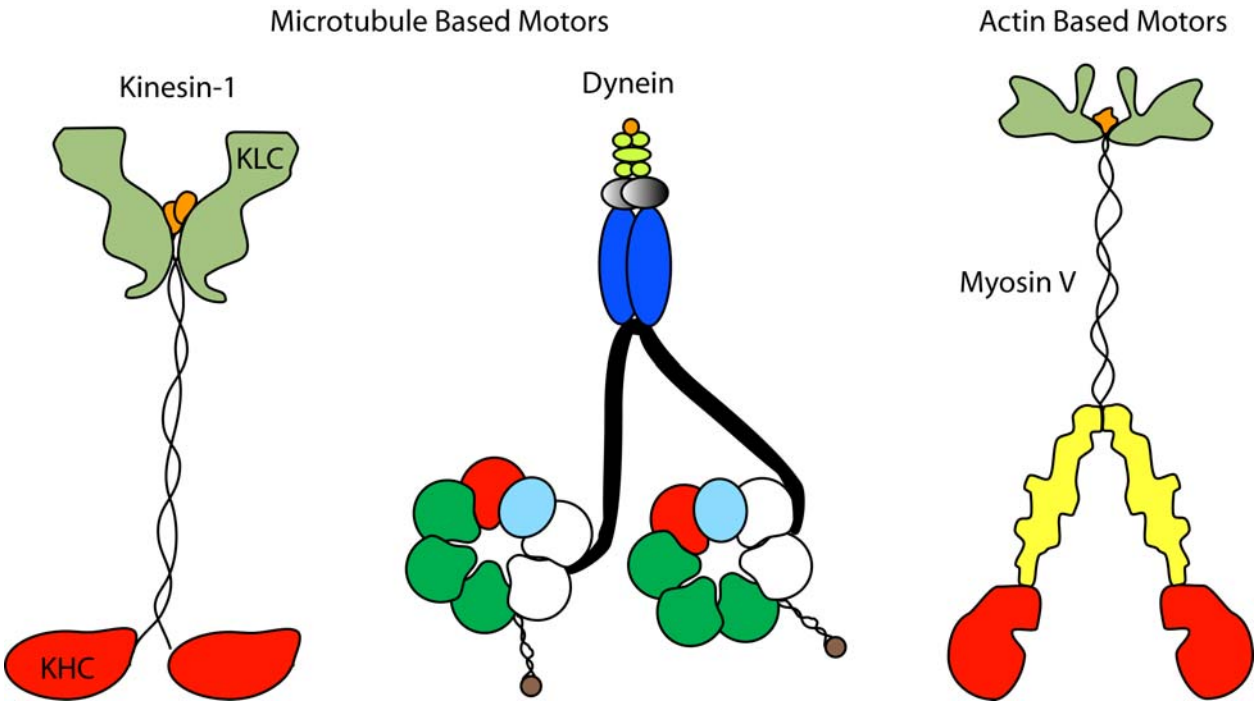

Figure 1.2 The Three Families of Cytoskeletal Motors

Figure 1.2 is a cartoon adapted from [59], depicting representative members of the three families of cytoskeletal motors, kinesins, dyneins and myosins. The motors are not drawn to scale. With regard to Kinesin-1, KHC and KLC stand for **k**inesin **h**eavy **c**hain and **k**inesin **l**ight **c**hain respectively. With regard to Dynein, the 4 AAA containing domains with P-loops are in green and red with red representing the domain acting as the primary site of the ATP hydrolysis. The light blue oval represents the non-AAA density in the dynein motor domain ring. With regard to Myosin V, the jagged yellow region represents the lever arm.

1.3.1 Dyneins

Dyneins are one of the two families of microtubule-based motor proteins. In comparison to the other families of cytoskeletal motors, they are extremely large proteins with the dynein heavy

chain mass ~520 kDa and a molecular mass of up to 2 MDa [60]. There are two broad classifications of dynein motors based on their subcellular localization, axonemal or cytoplasmic, and 7 subclassifications [61]. Axonemal dynein motors, Dynein-3 through Dynein-7, are either monomeric, heterodimeric, or heterotrimeric motors that are responsible for generating the oscillatory motion of cilia and flagella [60, 61]. Cytoplasmic dynein motors, Dynein-1 and Dynein-2, are homodimeric motors responsible for the retrograde transport of cargo during interphase [60, 61]. During mitosis their role shifts to a more structural one as they are responsible for focusing microtubules at the spindle poles as well as functioning in the attachment of astral microtubules to the cell membrane [61].

While being one of the earliest known motors, there is much less known about dynein mechanistically, than any other cytoskeletal motor. The size of the motor has contributed to the difficulty of studying dynein, however, the motor is also highly complex. Dynein is a member of the AAA+ (**A**TPases **a**ssociated with various cellular **a**ctivities) superfamily which is comprised of multisubunit ATPases that form ring like structures [60, 62, 63]. The motor domain of dynein, is a ~380 kDa ring composed of 7 distinct domains with 6 AAA domains; 4 of which have been shown to bind ATP and only one acts as the primary site of ATP hydrolysis [60, 62-66]. Functionally the four AAA domains that bind ATP are highly cooperative and modulate the motors interactions with the microtubule and response to an applied load [60, 62, 67, 68].

1.3.2 Myosins

Myosins are the actin-based family of molecular motors. There are 18 classes of myosin motors that function as monomers, homodimers, or much higher order oligomers [69]. This family of motors was originally identified for their role in muscle contraction but also play important roles

in cell locomotion, membrane trafficking, signal transduction, transcription, and vesicular transport [70-72]. Unlike the dyneins, the myosins are evolutionarily related to G-proteins instead of AAA+ ATPases [58, 73, 74].

Generally speaking, there is a good deal of knowledge on the ATPase cycle of these motors. There are both processive and nonprocessive myosins, which are mechanistically defined by the event that slows their ATPase cycle [75]. Most myosin motors, the only known exclusion being Myosin IXb [76], will dissociate from the actomyosin complex upon the binding of ATP. These motors will hydrolyze the ATP when detached actin, and rebind to the filament with the products ADP and P_i at the active-site [77-81]. The transition to tight binding is caused by the release of P_i resulting in a motor in the ADP bound state [77-81]. For myosins such as Myosin II that spend the majority of their cycle detached from the actin filament, the ATPase cycle is dominated by having the slowest step in the cycle occur upon association with the actin filament, i.e. P_i release [77-81]. For the processive myosins like Myosin V and VI, the release of P_i is rapid but the release of ADP is slowed, elongating the duration of the time the motor is bound to its filament partner [82-91].

1.3.3 Kinesins

Kinesins are probably best known for their role in intracellular transport since the founding member, conventional kinesin or Kinesin-1, was demonstrated to carry vesicles long distances down the axon in neurons [92-94]. The kinesin superfamily has grown substantially in the last two decades (Figure 1.3) and now comprises 14 subfamilies and a group of unclassified kinesins called Orphans [95]. Amongst these motors are monomers, homodimers, heterodimers with two catalytic motor domains, heterodimers with only one catalytic motor domain, heterotrimers,

heterotetramers and homotetramers [96]. Kinesins are also grouped into three broad classes based on the location of their motor domain in the peptide sequence [97]. The Kin-N motors, Kinesin-1 through Kinesin-12 subfamilies, have their motor domain located at the N-terminus and either walk or direct their force vectors to the plus-ends of microtubules. Kin-C motors, the Kinesin-14 subfamily, have their motor domain located at the C-terminus and walk or direct their force vectors to the minus-ends of microtubules. There are also Kin-I motors, the Kinesin-13 subfamily, that have their motor domains located in the middle of the protein sequence. These motors do not demonstrate any motor driven movement and instead use a diffusive mechanism to translocate along the microtubule until they reach their intended binding site at the microtubule ends [98, 99]. All this diversity in the kinesin superfamily has not evolved to have a different motor carry a different cargo; that role is often carried out by adapter proteins called light chains [100-103]. Besides playing a role in transport, kinesins have been demonstrated to play important roles in modulating microtubule dynamics, chromosome segregation, and ensuring the fidelity of the mitotic spindle [104-115].

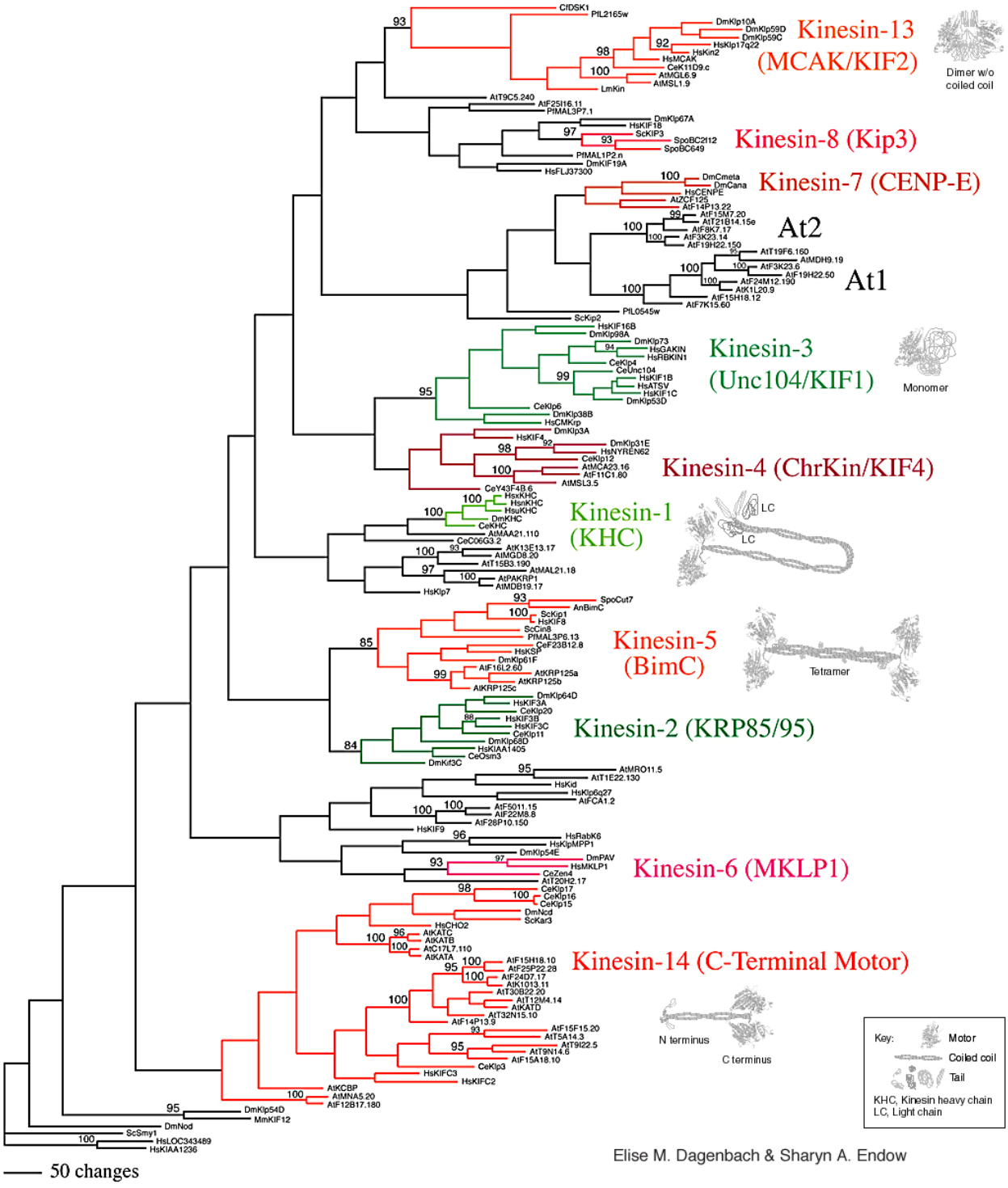

Figure 1.3 Kinesin Family Tree

Figure 1.3 is the latest depiction of the Kinesin superfamily containing 14 subfamilies and a group of unclassified Kinesins called the Orphans. The tree is originally presented in [95] and can be obtained at the Kinesin Home Page, www.proweb.org/kinesin.

Members of the both the Kinesin-13 and Kinesin-14 subfamilies have been demonstrated to posses the ability to modulate microtubule dynamics by promoting depolymerization [98, 113, 116-122]. The Kinesin-13s are mitotically active Kin-I motors that use their ATPase mechanism to peel apart a microtubule's protofilaments and induce the rapid depolymerization, catastrophe, of microtubules that are improperly attached to kinetochores [98, 116-122]. The Kinesin-14s, Kin-C motors, also have the ability to depolymerize microtubules, however, they appear to function by a different mechanism than that of the Kinesin-13s [113, 123]. Furthermore, while the ability to depolymerize microtubules has been seen in all Kinesin-14s examined, only one family member, Kar3, has a biological role, karyogamy in budding yeast, associated with its depolymerization ability [113].

The importance of Kinesins to the mitotic spindle does not end with their ability to depolymerize microtubules. There is increasing evidence that kinesin motors are the linkages between the chromosomes and the microtubules [105, 124-132]. One of these linking motors, an Orphan *Drosophila melanogaster* motor called Nod has been seen to actively facilitate the polymerization of microtubules [112]. The most important role for kinesins in the mitotic spindle, however, comes from their ability to slide microtubules towards either the plus-end or the minus-end. The plus-end-directed Kinesin-5s and the minus-end-directed Kinesin-14s generate opposing forces that maintain a balance in the spindle, allowing it to both assemble and maintain its structure [11, 14, 109, 133-137]. The Kinesin-5s are absolutely crucial to the fidelity of chromosome segregation, because a loss of their function results in a loss of spindle bipolarity and will induce the cell to apoptose [7, 8, 138].

Though the kinesins are microtubule-based motors, they are more closely related to the myosins and G-proteins than dyneins [58, 73, 74, 139, 140]. Structurally, a kinesin motor is

predominantly 8 β-sheets sandwiched between 6 α-helices [58, 141]. While not showing any sequence homology to myosins or resembling myosins in overall morphology, kinesins can be aligned with myosins based on the P-loop. All α-helices and 7 of the 8 β-sheets of the kinesin motor domain align in the region of the myosin motor domain containing the active-site [58]. There are also two highly conserved regions in this β-sheet sandwich termed Switch-I and Switch-II that alter their position depending out the presence of nucleotide at the active-site in an effort to coordinate the attack of a water molecule on the γ-phosphate of ATP [58, 73, 74, 139-142]. The gross morphological differences between the two motor families can be related to insertions that each family utilizes as their filament binding domains [58]. Mechanistically ATP has the opposite effect on kinesins as compared to myosins; instead of promoting dissociation of the motor from the filament, the ATP bound state is a strong microtubule binding state for the kinesin [143-147].

1.4 THE ATPASE CYCLES OF CONVENTIONAL KINESIN AND NCD

Prior to this dissertation there were only two homodimeric kinesin motors, conventional kinesin and Ncd, with highly characterized mechanochemical cycles. While conventional kinesin is a highly processive motor [148-151], Ncd is not processive [152-158]. Furthermore, the direction of motion by these two motors is reversed; conventional kinesin walks towards the plus-end of microtubules [92, 159] while Ncd is a minus-end directed motor [160, 161]. Nevertheless, the mechanisms of the two motors share several similarities. Following the initial collision with the microtubule, both motors initially interact through only one of the two motor domains [147, 162-171]. The motor domains of both motors display cooperativity: events need to occur on one of

the motor domains before they can occur on the other motor domain [156, 162, 168, 172-174]. Also, the ATP bound state, while a tight microtubule binding state [165], is transitory for both motors as rapid ATP binding is followed by rapid ATP hydrolysis [143, 150, 156, 158, 172, 174-182]. It is the positioning of the slow step in the reaction that has apparently determined why one motor can take multiple steps along the microtubule and why one cannot.

1.4.1 Conventional Kinesin

Key to processive motion by conventional kinesin is its ability to keep both motor domains from being in the same biochemical state [183-191]. Both motor domains have ADP tightly bound to the active-site off of the microtubule and appear biochemically indistinguishable from each other [174, 176, 192]. However, a recent study by Alonso *et al*. has suggested that the conformation of the motor might bias the abilities of the motor domains to interact with microtubules [193]. Upon association with the microtubule a structural and biochemical asymmetry between the two motor domains is present: only one motor domain will interact sufficiently with its binding site to cause the release of bound ADP (Figure 1.4 state 1) [162, 168, 170, 172]. ATP binding to the motor domain associated with the microtubule occurs (Figure 1.4 state 2). This necessary to trigger a conformational change, docking of the neck-linker (see Chapter 1.6 and Figure 1.8), which causes the second motor domain to interact with its binding site [168, 172, 193, 194] on the next β-tubulin subunit, 8 nm in front of the bound motor domain (Figure 1.4 state 3) [195-197]. The bound ADP can now be release from this "Head-2." Hydrolysis of the ATP bound to "Head-1," the rearward motor domain, rapidly occurs leaving Head-1 with ADP•P_i on its active-site and Head-2 nucleotide-free (Figure 1.4 state 4). The release of P_i occurs from Head-1 while it is still associated with the microtubule leaving that motor domain weakly bound to the

microtubule in the ADP state [190]. Dissociation of Head-1 occurs leaving the motor in an identical position to how it began the microtubule associated part of its mechanochemical cycle (Figure 1.4 state 6). It is important to point out that the alternation between which motor domain is tightly bound to the microtubule is made possible, in part, by the position of the slow step in the mechanism. The slowest step in the ATPase cycle, the release of P_i, occurs after the motor domain that was previously detached from the microtubule, associates with its new binding site [190]. If a slow step did not guard the dissociation of the rearward head from the microtubule, there would be a race between two rapid steps in the cycle, dissociation and ADP release, to determine whether the motor stays attached to the microtubule and completes a step or enters a state where both motor domains are weakly bound to the microtubule favoring dissociation of the entire motor from the microtubule.

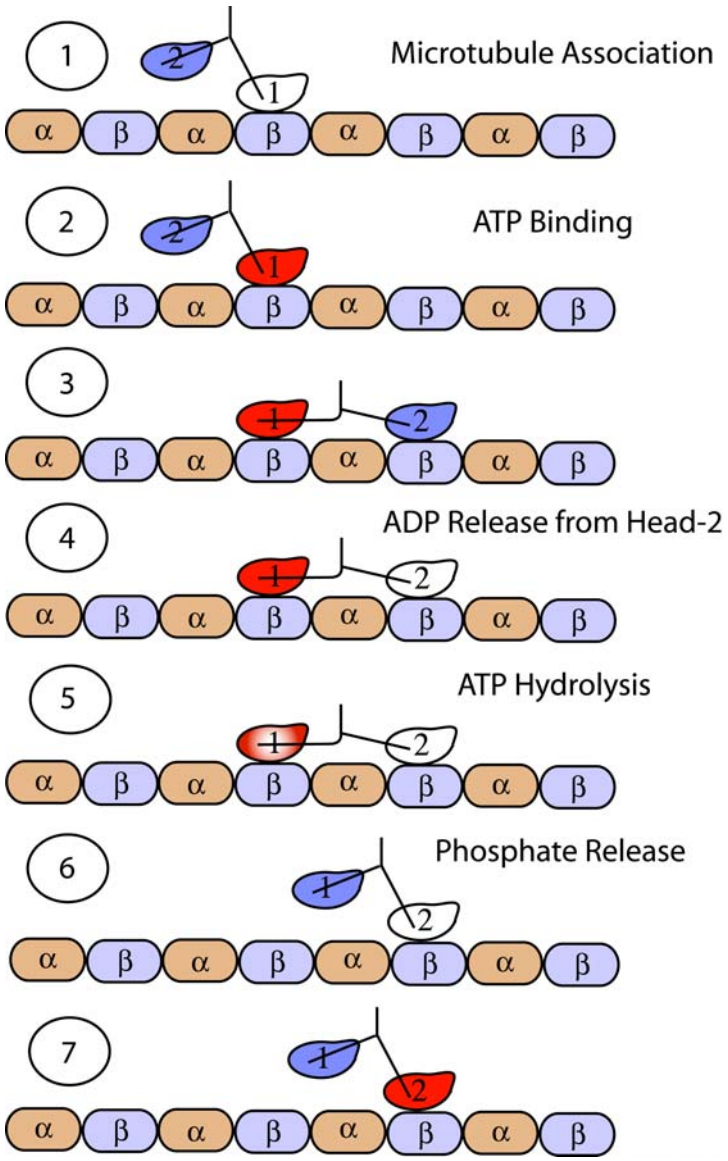

Figure 1.4 Conventional Kinesin ATPase Cycle

Figure 1.4 depicts the established ATPase cycle of conventional kinesin adapted from [190]. Conventional kinesin initially interacts with the microtubule through only one motor domain (1), labeled 1 in the figure. ATP binding to that motor domain (2) triggers neck-linker docking (3) (discussed elsewhere) and the release of ADP from the second motor domain (4), labeled 2 in the figure. Hydrolysis of the bound ATP to Head-1 occurs and the interactions of Head-2 with the microtubule strengthen (5). Following P_i release, ADP is present on Head-1 and the motor domain will dissociate from the microtubule; however, Head-2 is tightly associated with the microtubule (6). ATP can now bind to Head-2 and the cycle will repeat (7). Motor domains that are nucleotide-free are in white, ATP bound are in red, ADP bound are in blue, and ADP•P_i bound are a gradient of red.

1.4.2 Ncd

The ATPase cycle of Ncd is more controversial than that of conventional kinesin (Figure 1.5). There is general agreement that the motor will initially rapidly associate with the microtubule and release bound ADP from only one of the two motor domains [156, 174]. The microtubule bound motor domain binds ATP rapidly [156, 158, 174, 180, 182] and undergoes a conformational change directing the unbound head towards the minus-end of the microtubule [166, 193]. ATP hydrolysis is rapid [156, 158, 174, 180, 182], and there is a general consensus that the motor domains dissociate from the microtubule in the ADP•P_i state [173]. Functionally, the motor's force production is believed to occur in a lever arm mechanism like many myosins [171, 198]. The ADP states are the more controversial points.

In the Pechnatikova and Taylor model [156], the rate of ADP release upon the initial collision with the microtubule is considered to be the rate-limiting step in the mechanism. After releasing ADP, the motor domain attached to the microtubule will proceed through its ATPase cycle and rapidly dissociate from the microtubule in the ADP•P_i state (Figure 1.5 states 1-4). Unlike conventional kinesin, the second motor domain does not bind to the microtubule and the entire motor is dissociated from the microtubule (Figure 1.5 state 5P). The motor will then rebind to the microtubule using the partner motor domain (Figure 1.5 state 6P). The authors concluded that the entire cycle of one motor domain is roughly twice as fast as steady-state ATP turnover, and the observed steady-state rate could be achieved through the alternation of enzymatic cycles by the two motor domains.

In the Foster, Mackey, and Gilbert model [174, 182], the release of ADP from the first motor domain to associate with the microtubule is rapid with respect to the cycle. Unlike in the model of Pechatnikova and Taylor, the teathered motor domain, "Head-2," is able to interact

with the next tubulin binding site prior to the complete dissociation of the motor from the microtubule (Figure 1.5 state 5F). Release of ADP bound at the second motor domain is rate-limiting in the cycle (Figure 1.5 state 5F), and the entire motor will dissociate from the microtubule upon formation of ADP•P_i at its active-site (Figure 1.5 state 9F). In this model dimeric Ncd is proposed to hydrolyze two molecules of ATP per 8 nm advance of the motor and then dissociate. An unresolved aspect of this model, though, is the means by which Ncd would be able to essentially take one step before motor dissociation. Cryo-EM (**e**lectron **m**icroscopy) studies have been able to capture conventional kinesin bound to the microtubule using both motor domains in the presence of AMPPNP, consistent with models of processive motion [199, 200]. Unlike conventional kinesin, the simultaneous interaction of both Ncd motor domains with the microtubule has not been observed in either the ADP, nucleotide-free, or AMPPNP (ATP-like) states [169, 198, 200, 201].

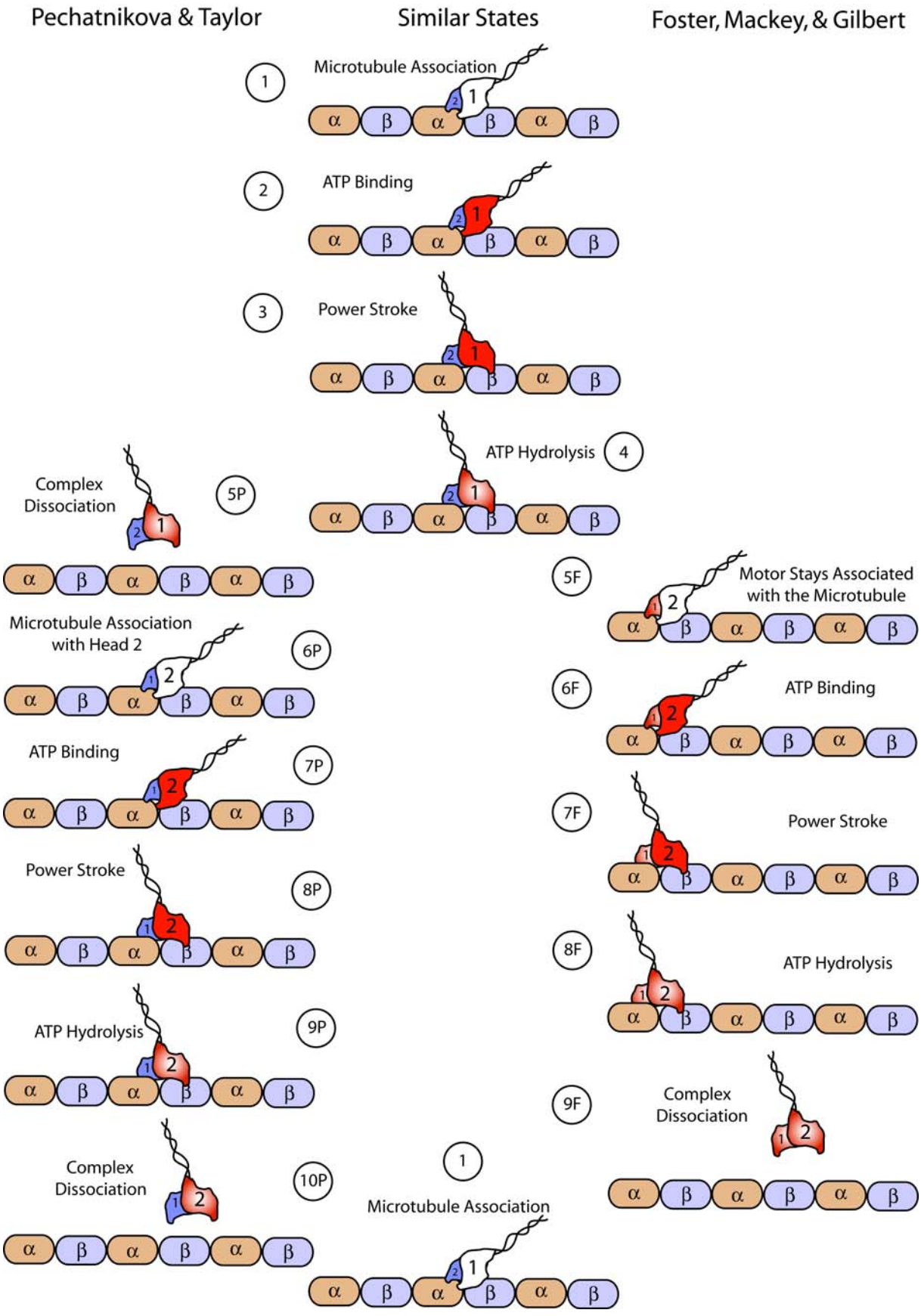
Pechatnikova & Taylor
Similar States
Foster, Mackey, & Gilbert
1
Microtubule Association
2
ATP Binding
3
Power Stroke
ATP Hydrolysis
4
Complex Dissociation
5P
Microtubule Association with Head 2
6P
ATP Binding
7P
Power Stroke
8P
ATP Hydrolysis
9P
Complex Dissociation
10P
5F
Motor Stays Associated with the Microtubule
6F
ATP Binding
7F
Power Stroke
8F
ATP Hydrolysis
9F
Complex Dissociation
1
Microtubule Association

Figure 1.5 ATPase Cycle of Ncd

Figure 1.5 depicts the two models for the ATPase cycle of Ncd. Species particular to the model of Pechatnikova and Taylor [156] are on the left and species particular to the model of Foster *et al*. [174] are on the right. The species in the middle column are shared between the two models. The artistic representation of the Ncd dimer is an adaptation from [198]. PLEASE NOTE, THE MOTOR DOMAIN DRAWN SMALLER IS **NOT** TO BE CONSIDERED ASSOCIATED WITH THE MICROTUBULE. Ncd initially interacts with only one motor domain (1), labeled 1 in the figure. ATP binding to Head-1 (2) causes a power-stroke towards the minus-end of the microtubule (3). ATP will be hydrolyzed on Head-1 (4). In the model of Pechatnikova and Taylor, the entire motor will dissociate from the microtubule when the ADP•P_i state is reached on Head-1 (5P). Ncd will then reassociate with the microtubule using its other motor domain, labeled 2, and have ADP bound to Head-1 (6P). Head-2 then proceeds through ATP binding (7P), the power-stroke (8P), ATP hydrolysis (9P) and dissociates in the ADP•P_i state as did Head-1 (10P). In the model of Foster *et al*., the presence of ADP•P_i on Head-1 (4) only causes Head-1 to dissociate from the microtubule but Head-2 will be bound to the microtubule at the next binding site. The ADP•P_i state is proposed to be maintained on Head-1 while Head-2 proceeds through its catalytic cycle (5F-8F). The entire motor will only dissociate from the microtubule after the ADP•P_i state is reached on both motor domains (9F). Motor domains that are nucleotide-free are in white, ATP bound are in red, ADP bound are in blue, and ADP•P_i bound are a gradient of red.

1.5 EG5/KSP

Eg5, also known as KSP (**k**inesin **s**pindle **p**rotein), is a homotetrameric motor in the Kinesin-5 subfamily [202, 203]. These homotetramers have long been hypothesized to be formed through the antiparallel coiled-coil interactions of two dimers oligomerized through parallel coiled-coil interactions. While this has not been explicitly verified, evidence from the fusion yeast Kinesin-5 motor Cin8p [204] and work in this dissertation involving human Eg5 [205] would suggest this assumption is accurate. Kinesin-5 motors function predominantly in mitosis and meiosis. During interphase their expression is repressed, however, in late G2 the expression is up regulated and the protein localizes to the cytoplasm [206, 207]. At the C-terminus, there is a globular regulatory domain containing a conserved phoshorylation site among all Kinsen-5

members termed the BimC box after the founding member, BimC (**b**locked **i**n **m**itosis) from *Aspergillus nidulans* [208]. Once the threonine in the BimC box gets phosphorolated by $p34^{cdc2}$ kinase, the motors become targeted to the spindle microtubules [209-211]. Though this regulatory mechanism is present in higher organisms, mutation of the conserved threonine in *S. pombe* homologue Cut7, does not prevent motor localization to the spindle microtubules or cause abnormal cell growth [212]. In the spindle, Eg5 will crosslink two microtubules (Figure 1.6) and slide them against each other [109, 203]. This function is initially necessary for separation of the two centrosomes to occur and continued activity is necessary to maintain spindle bipolarity prior till anaphase B [111, 135, 206, 210, 213-220]. When Eg5 function is blocked, the bipolar spindle will either not assemble or if blocking occurs after assembly, the spindle will collapse into a monoaster. This phenotype can be rescued if cytoplasmic dynein function is also inhibited [213, 216, 221]. Inhibition of Eg5 after anaphase B does not have an effect on spindle bipolarity, however, the overlapping microtubules, that link the two daughter cells during cytokinesis, appear shorter, though they do not compromise cytokinesis [206, 222].

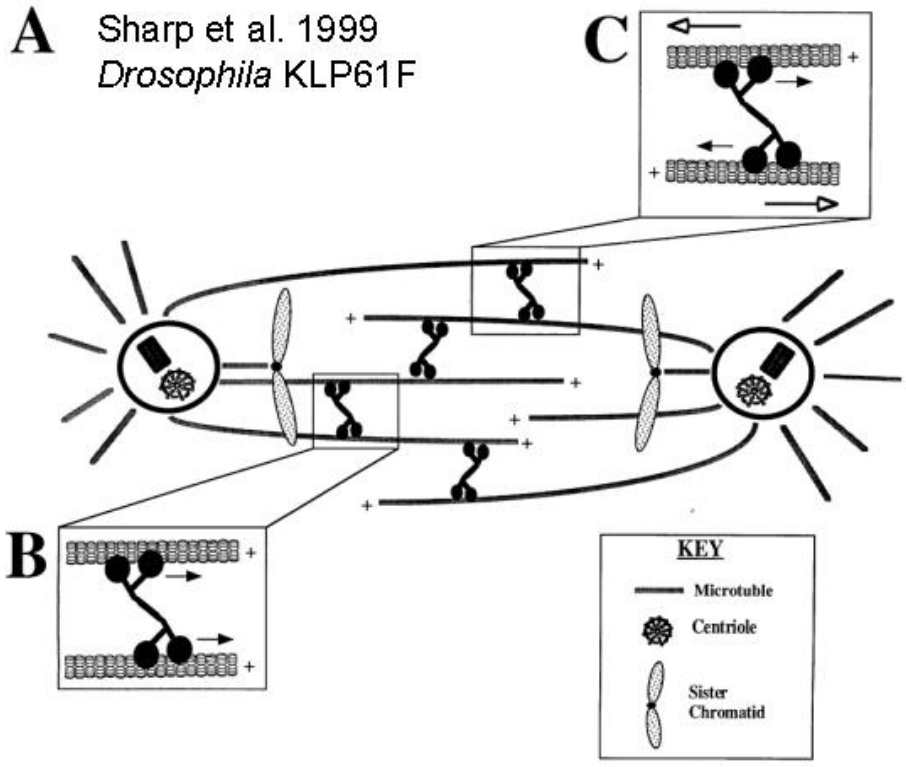

Figure 1.6 Eg5 in the Mitotic Spindle

Figure 1.6 is the model of Sharp *et al.* [109] depicting the Eg5 homologue from *Drosophila melanogaster*, KLP61F, cross-linking and sliding two microtubules in the mitotic spindle. *B*, *C* An enhancement of Eg5 cross-linking two parallel microtubules, microtubules with their plus-ends pointing in the same direction, and two antiparallel microtubules, microtubules with their plus-ends pointing in opposite directions, respectively.

Being the lynchpin of mitosis, Eg5 has become an intriguing target for chemotherapeutic agents in cancer treatment. At present there are several specific Eg5 inhibitors that bind to an allosteric site on the motor domain [217, 223-239]. These inhibitors target a particular loop [240-242], loop L5, in the Eg5 motor domain that is longer than in other kinesin superfamily members [243]. Crystallographic, FRET (**f**luorescence **r**esonance **e**nergy **t**ransfer), and kinetic evidence would suggest that these inhibitors, in the presence of nucleotide, cause a decrease in the mobility of loop L5 and leave the motor in a state not competent for generating force [244-247]. However, the motor has not lost its ability to bind microtubules. Immunostaining

indicates that homotetrameric Eg5 can still localize to the microtubules (Figure 1.7) in the presence of the inhibitor [218]. Microtubule pelleting experiments using monomeric Eg5 motor domains has indicated that while the inhibitor weakens the affinity of the motor domain for the microtubule, formation of a microtuble•motor complex does occur [248]. Prior to work in this dissertation, there wasn't a structural model of how microtubule association could occur without force generation.

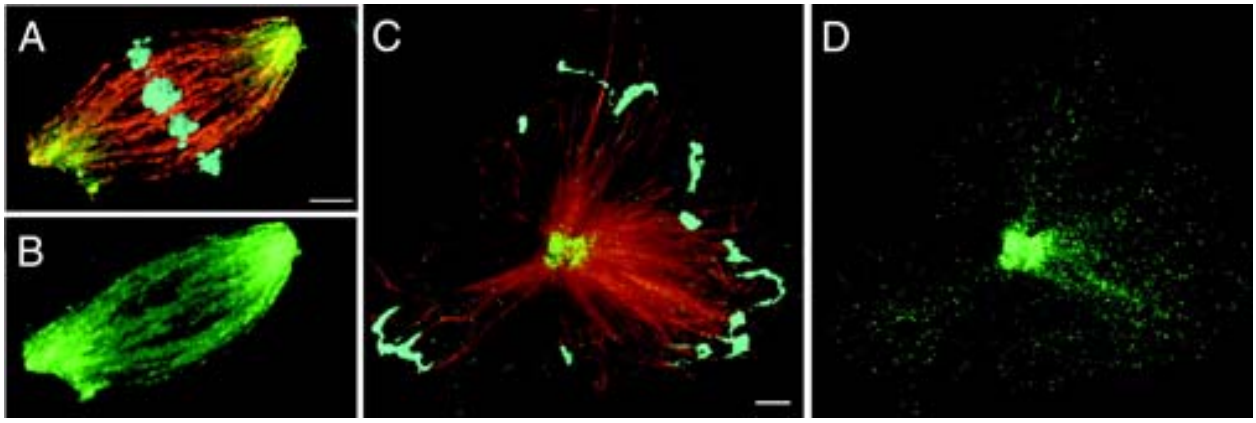

Figure 1.7 Inhibition of Eg5 Function

Figure 1.7 is a reconfiguration of a figure from Kapoor and Mitchison [218]. *A, B* display a normal bipolar spindle with the chromosomes lined up along the metaphase plate while *C, D* display the monaster that results from the addition of the Eg5 inhibitor, monastrol, to spindles formed from *Xenopus* egg extracts. *B, D* display antibody staining for Eg5 while *A, D* display the merge DNA, rhodamine labeled microtubules, and the α-Eg5 antibody.

1.5.1 Monomeric Eg5 Motor Domains

The vast majority of the mechanistic information on Eg5 has come from work using momomeric motor domains. Kinetically speaking, monomeric Eg5 appears very similar to monomeric conventional kinesin motor domains. Both associate with the microtubule rapidly, release ADP rapidly upon association, bind ATP rapidly, hydrolyze ATP rapidly, and hit the rate-limiting step

with the kinetically coupled release of P_i to the dissociation of the motor domain from the microtubule [146, 177, 179, 181, 249-251]. While mutational analysis has suggested that P_i release is the rate limiting step for conventional kinesin [190], comparable work to decouple P_i release and microtubule•motor complex dissociation has not been performed for Eg5. It is interesting that monomeric Eg5 motor domains, more closely resemble conventional kinesin with regards to having tight microtubule interactions and a rate-limiting step coupled to dissociation from the microtubule instead of a fellow spindle motor, Ncd, that displays very weak microtubule interactions and a rate-limiting step occurring upon microtubule association [180, 182].

Off of the microtubule, monomeric Eg5 provided an important tool to study how microtubules modulate kinesin motors. All kinesins release ADP much more slowly off of the microtubule and this in conjunction with the copurification of ADP with kinesin motors has made it difficult to study kinesins without their filament partner [176, 192, 252, 253]. Furthermore, both conventional kinesin and Ncd are unstable in the absence of nucleotide, which has thwarted attempts to begin analyses in a nucleotide-free state [175, 176, 180, 252]. Eg5 is the only kinesin known at present that is stable in the nucleotide-free state and can be purified in mg quantities [246]. Two very interesting results came of this work: (1) the microtubule not only accelerates the ATPase cycle by increasing the rate of ADP release but also enhances the rate of ATP binding, and (2) the microtubule limits the potential conformations of the motor domain such that a productive ATPase cycle is favored. To expound on (2), it was seen that within a population of monomeric Eg5 motor domains, the entire population was capable of binding ATP with the same relative affinity for the nucleotide; however, a fraction of the population was either in or entered into a state that did not support the hydrolysis to ADP•P_i.

1.5.2 Tetrameric Eg5

Mechanistically, very little is known on how the homotetramer physically coordinates its four motor domains to slide two microtubules. Work with *Xenopus laevus* egg extracts indicates that the motor will localize along the length of the spindle placing the motor in contact with both parallel (microtubules with the plus-ends facing in the same direction) and anti-parallel (microtubules with the plus-ends facing opposite directions) microtubules [109, 209, 218, 254]. This would place the motor in situations where it would either have all four motor domains walking in the same direction, the parallel case, or two motor domains walking in one direction and the other two walking in the other direction, the anti-parallel case (Figure 1.6). *In vitro* microtubule sliding experiments suggest that Eg5 can slide microtubules in both cases [255]. This would imply that the motor has a sensing mechanism for the orientation of one microtubule in relationship to the other. The exact basis of this is unknown at this point as well as how the motor might change its behavior depending on the orientation of the microtubules.

With regards to motility, Eg5 exhibits two different phases of motility. There is motor powered movement that is processive, akin to the way conventional kinesin takes multiple steps along the microtubule [149], and a one dimensional diffusional component initially observed to be utilized by the Kin-Is [98, 99] as they rapidly move along the microtubule in search of the microtubule end [256]. The nature of the diffusive movement appears to be tied to having ADP bound to the motor domains as the Eg5 inhibitor monastrol, which has been shown to stabilize the ADP bound state of monomeric Eg5 motors [248, 257], appears to promote this type of movement [245, 256]. From present published work on the homotetramer, it is unclear as to what causes the change from motor powered to diffusive movement and vice-a-versa, let alone the mechanism for accomplishing the switch. The work presented in this dissertation on a

dimeric Eg5 motor; however, proposes a suitable mechanism for the switch from motor driven to diffusional movement.

1.6 KINESIN MOTOR DOMAIN STRUCTURE

At present, there are 47 structures of kinesin family members in the protein data bank (http://www.pdb.org/pdb/home/home.do). As more structures of kinesins belonging to the various subfamilies are being determined, the subtle features corresponding to the cellular function of the motor are becoming clearer; however, more often than not, the relevance of a flexibility change caused by a particular insertion or deletion (the mobility comparison is made to conventional kinesin) is unknown. One feature of kinesin motors with a breadth of literature is the nucleotide binding pocket, which is similar among all known kinesins as well as myosins and G-proteins [58, 73, 74, 139, 140, 142, 258, 259]. There are four conserved motifs, N-1 through N-4, that contribute to the binding of nucleotide and its proper alignment for the nucleophylic attack of a water molecule on the γ-phosphate. One of these regions termed the P-loop (N-1), is a Walker A motif with a concensus sequence of GXXXXGKS/T with X representing any amino acid. This region is important for binding the oxygens of the β and γ-phosphates of ATP. Region N-4 coordinates with residues at the end of the P-loop to bind the adenosine base. Regions N-2 and N-3 are more commonly called Switch-I (NXXSSR) and Switch-II (DXXGXE) respectively. A conserved serine of Switch-I and the conserved glycine of Switch-II hydrogen bond to the γ-phosphate of the bound nucleotide causing larger scale conformational changes in these regions and their associated clusters. In the presence of a γ-

phosphate, the arginine of Switch-I and the glutamate of Switch-II form a salt bridge and coordinate the nucleotide-bound magnesium atom.

Besides helping to coordinate the nucleotide at the active-site, Switch-II is also crucial in relaying the nucleotide bound state of the motor to the microtubule binding interface [142, 194, 260-266]. The Switch-II cluster (α4, L11, L12, α5, L13) is located on the positively charged microtubule binding interface [140]. In particular helix-α4 and loop L11 are hypothesized to make the majority of the motor contacts in the interface between the α-tubulin and β-tubulin subunits of the two neighboring heterodimers making up the microtubule binding site [260, 267, 268]. The position of this cluster in relation to the rest of the motor domain and the size of helix-α4 are proposed to change in response to the nucleotide bound at the active-site [142, 258, 262, 264, 269-274]. The other regions of the motor domain contributing to microtubule interactions have also been mapped by means of protease digestion/protection experiments, scanning alanine mutagenesis, and docking of crystal structures of the αβ-tubulin heterodimer and various kinesin motor domains into cryo-EM maps of the microtubule•kinesin complex. The microtubule binding interface is made up of β5-L8, and the Switch-II cluster [167, 199, 260, 267, 273, 275-277] with minor contribution from L2-α6 in the case of Ncd only [167, 267]. It should be noted however, that in the absence of the microtubule•kinesin motor domain co-structure, the exact interactions of binding interface are not known.

The last highly studied region of the kinesin motor domain is a 14-20 amino acid stretch termed the neck-linker. Structurally, this region of the protein is responsible for tethering the motor domain to the coiled-coil oligomerization interface [278, 279]. Functionally, this region is responsible for the directional bias of a particular motor [153, 279-283] and could potentially be the force transducing element in the motor [153, 194, 284, 285]. In most crystal structures of

kinesin motor domains, the neck-linker is disordered in the ADP state [139, 142, 243, 272], and would be oriented perpendicular to the motor domain if the motor were bound to the microtubule. In crystal structures representing the ATP-like state, the neck-linker is visible and seen stabilized along the β-sheet core of the motor domain [142, 229, 244, 272, 286]. If the motor were bound to the microtubule, the neck-linker would appear parallel to the microtubule [167, 244, 272, 287]. In the cases of conventional kinesin, and Kif1A, several studies indicate that the neck-linker alters its position from the perpendicular or "undocked" state to the parallel or "docked" state in response to ATP binding to the active-site [142, 194, 272, 288-291]. The only kinesin seen to display a different neck-linker behavior is Eg5. In both the ADP and the ATP-like states, the neck-linker has been visible in the crystal structures suggesting that it undergoes an order-to-order transition [229, 238, 239, 243, 244]. Also, FRET evidence would suggest that the transition from the undocked to docked states for Eg5 might be a result of motor binding to the microtubule instead of ATP binding at the active-site [251]. Work presented in this dissertation further supports the concept of the Eg5 neck-linker altering its position in response to microtubule binding instead of ATP binding.

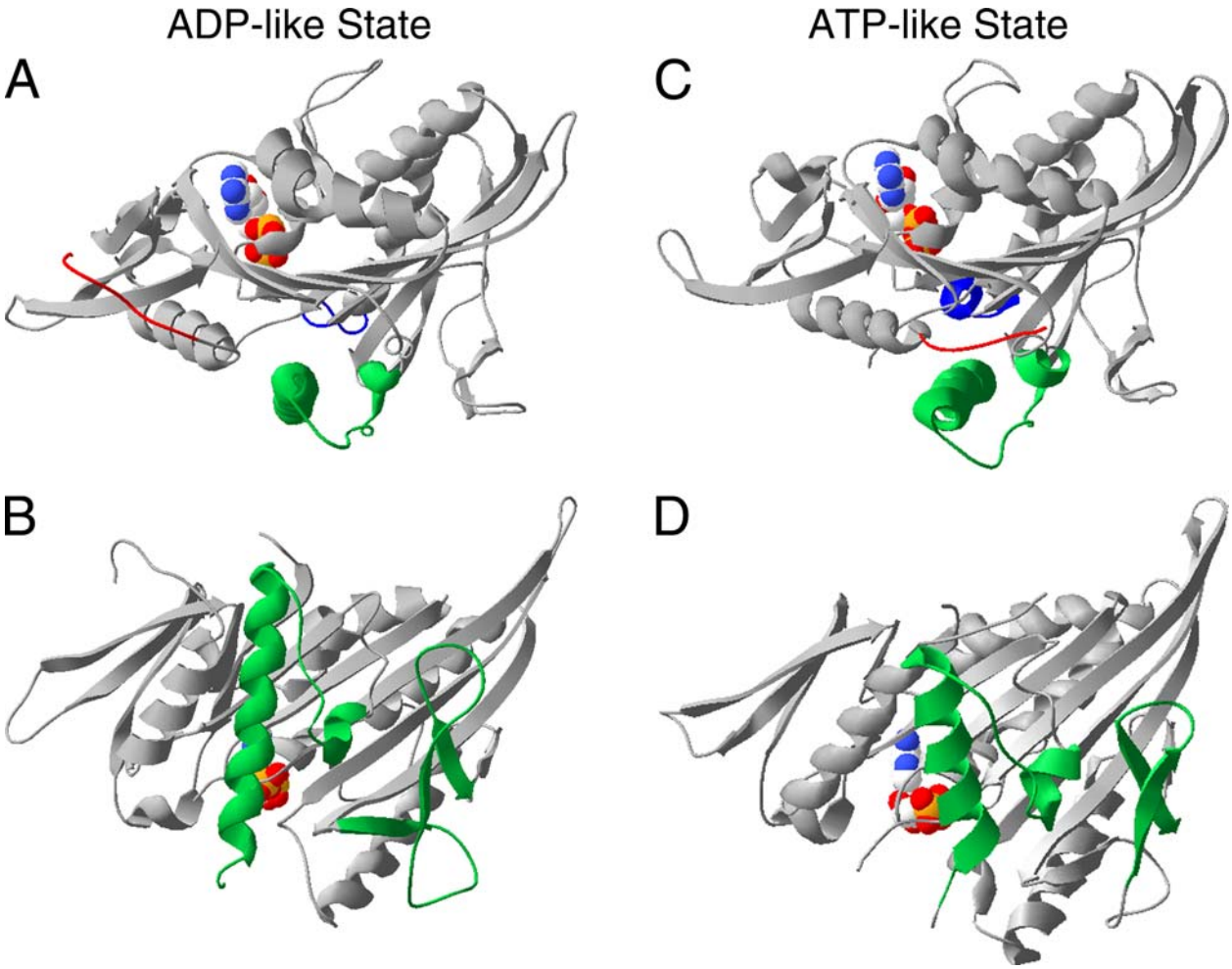

Figure 1.8 Eg5 Crystal Structure

Figure 1.8 depicts the crystal structure of human Eg5 complexed with (*A, B*) ADP [243] or (*C, D*) ADP and the specific Eg5 inhibitor monastrol [244]. The ADP is represented by the space fill model to indicate the motor active-site; however monastrol is not shown. *A*, *C* highlight three specific regions of the Eg5 motor domain: the beginning of the neck-linker (red), Switch-I (blue), and the Switch-II cluster (green). The motor is displayed such that a side view is given if the motor would be bound to a microtubule. The plus-end of the microtubule is to the right and the microtubule itself would be located below the Switch-II cluster. *B*, *D* highlight (green) the regions thought to directly interact with the microtubule. Note, the microtubule binding regions of Eg5 have not been experimentally mapped out; the highlighted regions represent regions of conventional kinesin demonstrated to interact with the microtubule. This view is a 90° clockwise rotation about the x-axis such that the viewer would be looking through the microtubule.

1.7 DISSERTATION OVERVIEW

The purpose of this work has been to further the understanding of how homotetrameric Eg5 is modulated by nucleotide to facilitate the establishment and maintenance of the mitotic spindle. Also, this work sought to increase the understanding of how the communication between two kinesin motor domains can be modulated to perform a particular function. In order to do this, a truncation of the human Eg5 gene was constructed that yielded a homodimeric motor. A kinetic analysis of this motor was performed to understand how the two motor domains that interact along the same microtubule are able to communicate with each other. A minimal kinetic mechanism was developed indicating that dimeric Eg5 has a more complicated ATPase cycle than other previously characterized kinesins. The major findings from this work include: (*1*) unlike conventional kinesin and Ncd, dimeric Eg5 initially binds the microtubule with both motor domains, (*2*) the catalysis of ATP to ADP•P_i is the rate-limiting step for Eg5 driven motility, and (*3*) a mildly processive motor can be engineered by weakening the coupling between the nucleotide states of the two motor domains. These findings will be related to potential mechanistic properties of homotetrameric Eg5 as well as other dimeric kinesin motors.

2.0 BUFFERS, CLONING, AND GENERAL METHODS

This section contains a detailed description of procedures used to generate common reagents. This section also contains a table of all buffers requiring more than two components. Also, the cloning strategy for the generation all motor constructs as well as a table containing all primers is present in this section. Details of specific experimental designs can be found in the chapter where the data from that experiment is discussed.

2.1 STANDARD BUFFERS

The following table lists all complex buffers used throughout this work. In subsequent sections, buffers will only be referred to by the name listed in this subsection.

Table 1 The Big Buffer List

BUFFER NAME	CONCENTRATION	COMPONENT
ATPase Buffer	20 mM	HEPES pH 7.2 w/KOH
	5 mM	Magnesium Acetate
	50 mM	Potassium Acetate
	100 μM	EDTA
	100 μM	EGTA
	1 mM	DTT

PM Buffer	100 mM	PIPES pH 6.7 w/KOH
	5 mM	Magnesium Acetate
	1 mM	EDGTA
Blue Goodies	0.05 %	$CuSO_4$
	0.1 %	Potassium Sodium Tartrate
	10 %	Na_2CO_3
	0.05 N	NaOH
Lysis Buffer	10 mM	$NaPO_4$ pH 7.2
	20 mM	NaCl
	2 mM	$MgCl_2$
	1 mM	EGTA
	1 mM	DTT
	2 mM	PMSF
S-Sepharose Column Buffer	10 mM	$NaPO_4$ pH 7.2
	20 mM	NaCl
	2 mM	$MgCl_2$
	1 mM	EGTA
	1 mM	DTT
S-Sepharose Elution Buffer	10 mM	$NaPO_4$ pH 7.2
	600 mM	NaCl
	2 mM	$MgCl_2$
	1 mM	EGTA
	1 mM	DTT
MCAC Column Buffer pH 7.6	10 mM	$NaPO_4$ pH 7.2
	150 mM	NaCl
	2 mM	$MgCl_2$
	20 μM	ATP
MCAC Elution Buffer pH 7.6	10 mM	$NaPO_4$ pH 7.2
	200 mM	Imidazole
	150 mM	NaCl
	2 mM	$MgCl_2$
	20 μM	ATP
Tubulin Column Buffer	100 mM	PIPES pH 6.7 w/KOH

	5 mM	$MgCl_2$
	1 mM	EGTA
	200 mM	KCl
	50 μM	GTP
Tubulin Elution Buffer	100 mM	PIPES pH 6.7 w/ KOH
	5 mM	$MgCl_2$
	1 mM	EGTA
	500 mM	KCl
	50 μM	GTP
Lauria Broth (LB)	10 g/L	Tryptone
	5 g/L	Yeast Extract
	5 g/L	NaCl
PBP Minimal Media pH 7.5	100 mM	HEPES
	20 mM	KCl
	15 mM	$(NH_4)SO_4$
	1 mM	$MgCl_2$
	10 μM	$FeSO_4$
	1 μg/ml	Thiamine
	0.25%	Glycerol
	2 mM	KH_2PO_4

2.2 TUBULIN PREPARATION

2.2.1 Tubulin Extraction From Bovine Brains

Tubulin was initially extracted from bovine brains using a series of polymerization and depolymerization cycles [292, 293]. Bovine brain matter was homogenized on ice in PM buffer supplemented with 1 mM PMSF at a ratio of 1g brain matter per ml of buffer to extract the

tubulin. The extraneous brain matter was subsequently pelleted out of solution (24,000 X g / 20 min / 4°C). The resulting supernatant was adjusted to 500 μM PuTP (purine triphosphate, both ATP and GTP) and clarified by centrifuging at 180,000 X g for 30 min at 4°C. The clarified supernatant was adjusted to 25% glycerol, and the extracted microtubules were polymerized by incubating at 34°C for 30 min. Microtubules were then pelleted by centrifuging at 100,000 X g for 45 min at 34°C. The microtubule pellets were resuspended in PM supplemented with 250 μM PuTP and incubated on ice for 30 min to depolymerize the microtubules. Another cold, high-speed spin was performed (180,000 X g / 30 min / 4°C), and the resulting supernatant was again adjusted to 25% glycerol. Microtubules were polymerized one final time by incubating at 34° for 30 min. At the end of the incubation, the solution was adjusted to 1 mM MgATP and 200 mM KCl and centrifuged (180,000 X g / 30 min / 34°C). The addition of MgATP and salt prior to pelleting helps to dissociate and therefore remove any microtubule based motors that have accompanied the microtubules during purification. The microtubule pellets were resuspended one last time in PM buffer supplemented with 250 μM PuTP, incubated at 34° for 10 min to encourage polymerization, and flash-frozen with liquid N_2.

2.2.2 Tubulin Purification by Ion Exchange Chromatography

The series of polymerization and depolymerization cycles resulted in a solution of both MAPs (**m**icrotubule **a**ssociated **p**roteins) and tubulin. In order to remove the MAPs, the solution was subjected to anion exchange chromatography [294, 295]. DEAE sepharose resin (GE Healthcare) was first charged with 1 M KCl and then equilibrated in 10 column volumes (30-50 ml columns) of tubulin column buffer. The solution of tubulin and MAPs was adjusted to 500 μM GTP and incubated on ice for 30 min. The solution was then centrifuged (40,000 X g / 30

min / 4°C) and the supernatant was adjusted to 200 mM KCl before loading on to the column. In this design, the tubulin will stick to the DEAE column and the MAPs should pass through the column in the flowthrough. Tubulin was eluted using the tubulin elution buffer and the pooled fractions were dialyzed against PM buffer supplemented with 250 μM PuTP. The dialysate was adjusted to 7% DMSO, and microtubules were polymerized at 34°C for 45 min. After polymerization, the solution was adjusted to 500 μM MgATP and 200 mM KCl and centrifuged (40,000 X g / 30 min / 34°C). The final microtubule pellet is resuspended in PM supplemented with 500 μM GTP and aliquots were flash frozen with liquid N_2.

2.2.3 Cycling of Microtubules

For each day's experiment, microtubules were cycled from a polymerized state, to a depolymerized state, and back to a polymerized state in order to remove any tubulin not competent for microtubule assembly [296]. An aliquot of microtubules was diluted 1:1 with PM buffer, supplemented with 500 μM GTP, and depolymerized on ice for 30 min. In order to separate any tubulin aggregates from the soluble tubulin, the solution is centrifuged at 18,000 X g for 15 at 4°C. Microtubules are then polymerized from the soluble tubulin by incubating at 34° for 10 min. To stabilize the microtubules, 20 μM taxol, Paclitaxel from *Taxus brevifolia* (Sigma-Aldrich Co.), was added, and the solution was incubated for another 10 min at 34°. The polymerized microtubules were pelleted (18,000 X g / 30 min / 25°C) and resuspended in ATPase buffer with 20 μM taxol. To determine the concentration of polymerized tubulin, the Lowry protein assay was performed using BSA as a standard [297, 298].

2.3 PHOSPHATE BINDING PROTEIN PURIFICATION AND CHARACTERIZATION

In order to monitor the release of P_i following hydrolysis of ATP by dimeric Eg5, the enzyme coupled system utilizing the A197C *E. coli* phosphate binding protein (PBP) mutant, originally developed in the laboratory of M. R. Webb, was used [299]. In this system, an attached 7-diethylamino-3-((((2-maleimidyl)ethyl)amino)carbonyl)coumarin fluorophore (MDCC) to C197 enhances it fluorescence upon the conformational change caused by the protein binding P_i.

2.3.1 Purification of MDCC Labeled Phosphate Binding Protein

The following protocol for the expression, purification, and labeling of PBP with MDCC is that of Brune *et al*. [299] with modifications enhancing prep efficiency by H. White (unpublished). E. coli strain BW 24777 was inoculated into two 100 ml flasks containing 10 ml LB supplemented with 12.5 μg/ml tetracycline. The cultures were grown for 6 hrs at 37°C with shaking. The two cultures were then used to inoculate two 500 ml flasks containing 90 ml LB supplemented with 12.5 μg/ml tetracycline. These larger cultures were then allowed to grow for 16 hrs. Ten ml of the most rapidly growing culture was inoculated into 8 X 2L flasks containing 500 ml of minimal media. When the cultures reached an OD_{600} of ~0.2, expression of the PBP was induced by adjusting the culture to 2 mM *L*-rhamnose pH 7.5. The rhamnose inducible expression of PBP was developed by E. W. Taylor and W. Epstein [300].

Cells expressing PBP were harvested by centrifugation (16,000 X g / 10 min / 25°C) and resuspended in 10 mM Tris-HCl pH 7.6 / 30 mM NaCl. The cells were then washed to remove

all traces of minimal media by pelleting followed by resuspension. The cells were pelleted one more time and resuspended in 33 mM Tris-HCl pH 7.6 to prepare the cells for osmotic lysis. The lysis was performed by diluting the cell suspension further with 40% sucrose / 0.1 mM EDTA / 33 mM Tris-HCl pH 7.6 and incubating at room temperature for 10 min. The cells were then pelleted (16,000 X g / 10 min / 4°C) and rapidly resusupended in ice cold 0.5 mM $MgCl_2$. Because PBP is a periplasmic protein, osmotic lysis will rupture the periplasmic space releaseing the protein while leaving the majority of the cell structure intact, allowing PBP to be separated from the majority of the other *E. coli* proteins by centrifugation. The lysis solution was clarified of cellular debris (16,000 X g / 10 min / 4°C) and dialyzed into 5 mM Tris-HCl pH 8.0.

To separate the PBP from the remaining periplasmic proteins, ion exchange chromatography was performed using Q-sepharose resin (GE Healthcare). The dialysate was clarified with a high speed spin (180,000 X g / 45 min / 4°C) and applied to a 25 ml Q-sepharose column (binding capacity is ~10 mg PBP/ml resin). PBP was eluted using a 200 ml linear 5 mM Tris-HCl pH 8.0 / 1-100 mM KCl gradient. The fractions containing PBP separate from other contaminants were determined using SDS-PAGE with a 12% gel (Figure 2.1). The concentration of PBP (ε = 60,880 $M^{-1}cm^{-1}$, M_r = 34,440 Da) in the pooled fractions was determined by subtracting the absorbance at 320 nm from the absorbance at 280 nm. Subsequently the pooled PBP was concentrated to ~100 μM using Centriprep 10 concentrators (Millipore Corp.) and dialyzed against 20 mM Tris-HCl at 4°C overnight. The S-sepharose column was also regenerated (washed with 100 ml 5 mM Tris pH 8.0 / 2 M NaCl followed by 3 L of 5 mM Tris pH 8.0).

Before labeling of PBP with MDCC (Invitrogen Corp.), any P_i present in solution was removed by incubating at 25°C for 30 min with a "P_i mop" comprised of 0.2 units/ml PNPase

(Sigma-Aldrich Co.) and 200 μM 7-methyguanosine. Any P_i present in solution needed to be removed prior to labeling because the covalent linkage of the MDCC to C197 at the active site is extremely inefficient when P_i is bound to the active site. The "mopped" PBP was then incubated with 150 μM MDCC dissolved in *N,N*-dimethylformamide at 25°C with end-over-end rotation for 30 min. To separate the MDCC-PBP from free PBP, the solution was diluted to 5 mM Tris-HCl and loaded back onto the Q-sepharose column. The column was washed with 5 mM Tris-HCl pH 8.0 to remove any free MDCC, and the MDCC-PBP was eluted using 5 mM Tris-HCl pH 8.0 / 200 mM NaCl. Stoichiometric labeling of PBP with MDCC is represented by an A_{280}/A_{430} ratio of 1.6. Fractions displaying a ratio of 1.5-1.7 were pooled, and dialyzed into 10 mM Hepes pH 7.2. Following dialysis the protein solution was diluted to 100 μM MDCC-PBP, clarified (180,000 X g / 45 min / 4°C), and aliquots were flash frozen with liquid N_2. The prep resulted in a yield of 90 mg of MDCC-PBP.

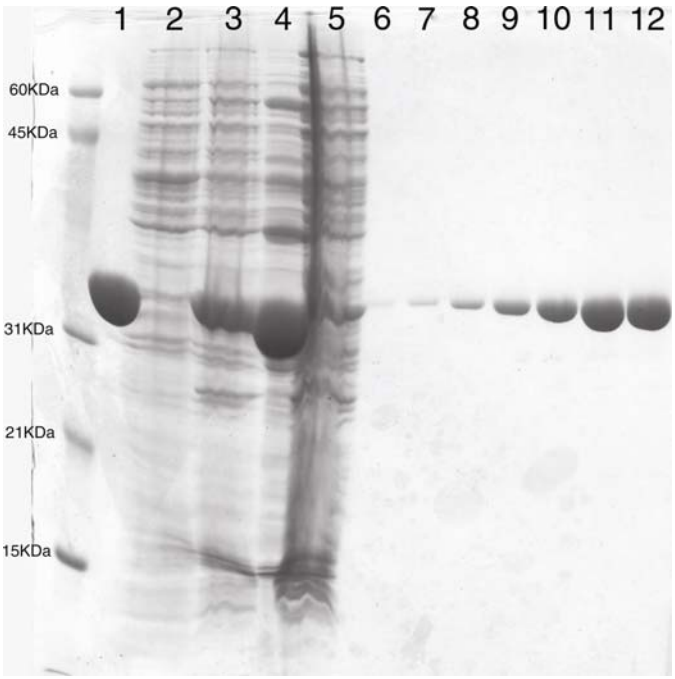

Figure 2.1 PBP Prep Gel

Figure 2.1 is a 12% acrylamide / 2 M urea SDS-polyacrylamide gel representing the elution of PBP from the Q-sepharose column. (1) is a PBP standard; (2) BW 24777 in the absence of *L*-rhamnose; (3) BW 24777 in the presence of *L*-rhamnose; (4) osmotic lysis supernatant; (5) osmotic lysis pellet; (6-12) fractions of the elution of PBP from Q-sepharose.

2.3.2 Characterization of MDCC-PBP

To verify that the MDCC-PBP prep was able to rapidly bind phosphate and display the expected fluorescence response, both fluorimetry and stopped-flow experiments were performed. MDCC labeled PBP has been demonstrated to both enhance its fluorescence as well as undergo a blue-shift in its emission spectrum when P_i is bound [299]. The fluorescence yield as well as the emission spectrum was monitored in the presence and absence of P_i using an Aminco-Bowman Series 2 luminescence spectrometer (Thermo Spectronic). The MDCC-PBP prep displays a 4-fold increase in fluorescence as well as the expected blue-shift in peak emission intensity from 474 nm to 466 nm (Figure 2.2A).

The MDCC-PBP prep was further characterized by examining the kinetics of P_i binding and the shape of the fluorescence response. To examine the kinetcs of P_i binding, the MDCC-PBP was mixed in the Kin-Tek stopped-flow instrument (Kin-Tek Corp.) with KH_2PO_4. The MDCC-PBP prep displays an apparent second-order rate constant of P_i binding at ~100 $\mu M^{-1}s^{-1}$ with an off-rate of 98 s^{-1} (Figure 2.2B). When 1 μM MDCC-PBP (final concentration) was mixed with increasing KH_2PO_4 in the stopped-flow, the fluorescence enhancement predominantly displayed a linear dependence on the KH_2PO_4 concentration, with curvature as the KH_2PO_4 concentration approached 1 μM, leading to a maximal fluorescence inhancement at ~ 1 μM KH_2PO_4 (Figure 2.2C). A deviation from linearity as the MDCC-PBP approaches saturation with P_i has been observed previously [299].

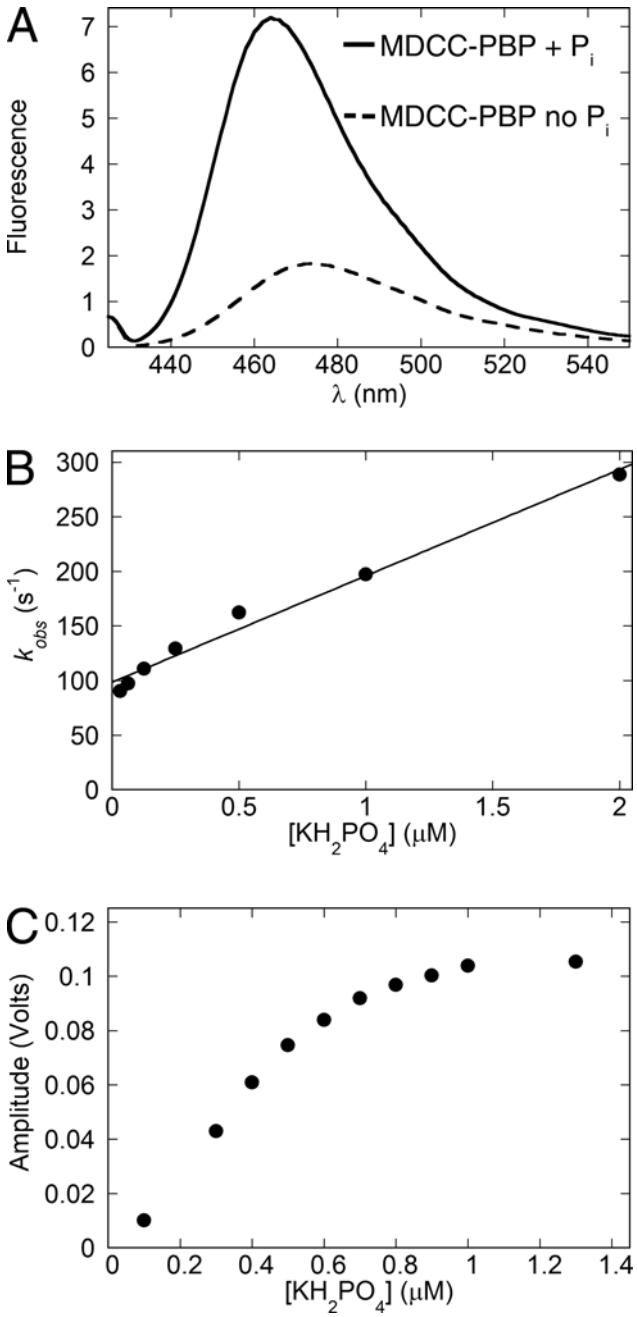

Figure 2.2 Characterization of MDCC-PBP

Figure 2.2 depicts the characterization of the MDCC labeled PBP. *A*, An emission scan (λ = 425 nm) of MDCC-PBP in the presence or absence of KH_2PO_4. In the presence of P_i the maximum fluorescence emission increases 4-fold and undergoes a blue-shift from 474 to 466 nm. *B*, The observed rate of fluorescence enhancement when MDCC-PBP was mixed with KH_2PO_4 in the stopped-flow instrument is plotted as a function of KH_2PO_4 concentration (Final: 5 μM MDCC-PBP, 0.025 U/ml PNPase, 75 μM MEG). The apparent second-order rate constant of substrate binding is 97 ± 5 $\mu M^{-1}s^{-1}$ with an off-rate defined by the y-intercept of 98 ± 5 s^{-1}. C, The fluorescence amplitude obtained from mixing MDCC-PBP with increasing KH_2PO_4 in the

stopped-flow instrument is plotted (Final: 1 μM MDCC-PBP, 0.025 U/ml PNPase, 250 μM MEG).

2.4 CLONING

This section details the cloning procedure used to generate 12 different Eg5 motor constructs: Eg5-464, Eg5-474, Eg5-481, Eg5-488, Eg5-495, Eg5-513, Eg5-513-5His, R234K, CysLight V1, CysLight N358C V1, CysLight V2, and CysLight N358C V2. All motors have been expressed and purified except for Eg5-481. All primers used have been listed in Table 2 along with the primer name. All primers will be referred to in the text by their primer name and not by the sequence.

Table 2 List of Primers

Primer Name	5′-Sequence-3′	T_m (°C)
TKF1HsEg5-513	GCG TAT GGC CAA ACT GGC AC	60.5
TKR1HsEg5-513	ATC CAG CTC GAG TTA GAG ACC AGA TAC ATC	62.4
pRSET A reverse	CTA GTT ATT GCT CAG CGG TGG	56.6
TKF SeqM HsEg5-513	GAT GTT TCT GAG AGA CTA C	47.4
TKR3HsEg5-464	TTG CAC CTC GAG TTA AGT GGT TTC AAG TTC	62.9
TKR4HsEg5-474	CAC TTT CTC GAG TTA TTG TAA TTT AGT TTC	53.1
TKR5HsEg5-481	CAC CAA CTC GAG TTA GAT ATA TTC TTC TTT CAA	56.5
TKR6HsEg5-488	GCG TTT CTC GAG TTA ACT TTC CAA AGC TGA TGT GA	62.8
TKR7HsEg5-495	CAG CTT CTC GAG TTA ATC ATG AAG TTT CTC CTC	59.8

HsEg5-513 rev 5His	ATC CAG CTC GAG TTA GTG GTG GTG GTG GTG CAT GGC CTT GTG GAG ACC AGA TAC ATC	71.9
Asn 358 F	CTC ATA GAG CAA AGT GCA TAT TGA ATA AGC	56.3
Asn 358 R	GCT TAT TCA ATA TGC ACT TTG CTC TAT GAG	56.3
Cys 25 F New	GTG GTG GTG AGA GTC AGA CCA TTT AAT	58.4
Cys 25 R New	ATT AAA TGG TCT GAC TCT CAC CAC CAC	58.4
Cys 43 F	CGT AGA GGA TCA GAT TCT ACT ATT G	52.5
Cys 43 R	CAA TAG TAG AAT CTG ATC CTG TAC G	52.5
Cys 87 F	CCG AAG TGT TGT TGC TCC ATT CTG GAT G	61.4
Cys 87 R	CAT CCA GAA TGG AGC AAC AAC ACT TCG G	61.4
Cys 99 F	ATG GGC TAT AAT GCC ACT ATC TTT GCG T	60.1
Cys 99 R	ACG CAA AGA TAG TGG CAT TAT AGC CCA T	60.1
Cys 450 F	GAA CTT GAC CAG TCT AAA TCT GAC CTG	57
Cys 450 R	CAG GTC AGA TTT AGA CTG GTC AAG TTC	57
TK C25S F	GTG GTG GTG AGA TCC AGA CCA TTT AAT	58.6
TK C25S R	ATT AAA TGG TCT GGA TCT CAC CAC CAC	58.6
TK C87S F	CCG AAG TGT TGT TTC TCC AAT TCT GGA TG	59.6
TK C87S R	CAT CCA GAA TTG GAG AAA CAA CAC TTC GG	59.6
TK C99S F	ATG GGC TAT AAT TCC ACT ATC TTT GCG T	58.1
TK C99S R	ACG CAA AGA TAG TGG AAT TAT AGC CCA T	58.1
TK R234K Forward 2	GCA TAC TCT AGT AAG TCC CAC TCA GTT TTC	58.1
TK R234K Reverse 2	GAA AAC TGA GTG GGA CTT ACT AGA GTA TGC	58.1

2.4.1 Cloning of Eg5-464, 474, 481, 488, 495, 513, and 513-5His

The template for all Eg5 constructs was a plasmid containing human Eg5 cDNA (generously provided by Anne Blangy, Centre de Recherches de Biochimie Macromoléculaire). The Eg5 cDNA was excised from the plasmid by means of an EcoRI restriction digest and used as the template for polymerase chain reaction (PCR) designed to amplify bases 307 to the desired truncation point (base pairs 1392, 1422, 1443, 1464, 1485, or 1539 respectively) as well as to insert a TAA stop codon followed by a XhoI restriction site after the truncation point. For all constructs, the TKF1HsEg5-513 primer was used to amplify bases beginning with 307. Each construct had a different truncation primer, TKR3HsEg5-464, TKR4HsEg5-474, TKR5HsEg5-481, TKR6HsEg5-488, TKR7HsEg5-495, TKR1HsEg5-513, and HsEg5-513 rev 5His respectively. The PCR product was purified by agarose gel electrophoresis followed by extraction from the gel matrix using a QIAquick Gel Extraction Kit (Qiagen). Both the purified PCR product and a pRSET A plasmid containing HsEg5-405 [224] were digested with BstEII and XhoI. The various PCR amplifications were then ligated to the piece of the plasmid containing the first 306 base pairs of the Eg5 gene. The ligation reaction was then transformed into the Nova Blue cell line (EMD Chemicals Inc.) for amplification and storage. Plasmids were harvested from the clones using QIAprep Spin Miniprep Kits (Qiagen), verified by restriction digest with BglI and sequenced. Sequencing of the gene was accomplished using three primers: one at promoter, T7 Promoter Primer (EMD Chemicals Inc.), one in the middle, TKF SeqM HsEg5-513, and a primer in the reverse orientation beginning just outside the stop codon, pRSET A reverse. Plasmids bearing the expected sequence were transformed into the BL21-CodonPlus(DE3)-RIL cell line (Stratagene) for protein expression.

2.4.2 Cloning of R234K

The cloning, purification, and initial kinetic characterization of R234K were performed with the assistance of Yuan Yuan Duan, a rotation student from the Biophysics and Structural Biology Graduate Program. Mutation of arginine 234 to lysine was accomplished through PCR site-directed mutagenesis with the primers, TK R234K Forward 2 and TK R234K Reverse 2, using the pRSET A plasmid containing Eg5-513-5His as the template. The amplified plasmids containing the mutation were separated from the template DNA by DpnI digestion (New England Biolabs Inc.) and transformed into the Nova Blue Cell line. Plasmids were extracted from the clones and sequenced as described in section 2.4.1.

2.4.3 Cloning of the CysLight Constructs

In an unpublished collaboration with the Selvin lab at the University of Illinois examining the mechanism of dimeric Eg5 stepping along the microtubule, four dimeric Eg5 constructs were generated that only encode for a single cysteine. These mutants were engineered in order to allow for site specific labeling of the motor such that the motion of individual motor domains could be followed as dimeric Eg5 steps along the microtubule. Two different mutational approaches were used to generate the mutant constructs. One mutational design, constructs termed V1, converted each cysteine to the most commonly used amino acid at the position of the particular cysteine by other Kinesin-5 family members [251]. The other, constructs termed V2, was to conserve the biochemical properties by converting all the cysteines to serines.

The cloning of CysLight V1 and CysLight N358C V1 were accomplished through a series of 4 or 6 rounds, respectively, of PCR site directed mutagenesis using the pRSET A

plasmid containing Eg5-513-5His as the template as described in section 2.4.2. For CysLight V1 the following mutations were made: C25V using the primer pairs Cys 25 F New and Cys 25 R New, C43S using the primer pairs Cys 43 F and Cys 43 R, C99A using the primer pairs Cys 99 F and Cys 99 R, and C450S using the primer pairs Cys 450 F and Cys 450 R. In this mutant, only one naturally occurring cysteine is still present at position 87. According to the Eg5 crystal structure [243], this residue is completely solvent exposed and is located on sheet-β3 on the top of the motor domain, diametrically opposite the microtubule binding domain. For the CysLight N358C V1 mutant, the two additional rounds of mutagenesis made the following mutations: C87A using the primers Cys 87 F and Cys 87 R, and N358C using the primers Asn 358 F and Asn 358 R. This mutant also only contains one cysteine residue; however, it was introduced at the juncture of helix-α6 and the neck-linker.

The cloning of CysLight V2 and CysLight N358C V2 required 2 and 3 rounds of site-directed mutagenesis as CysLight V1 and CysLight N358C V1 were used as the respective templates. For CysLight V2 the following mutations were made: V25S using the primer pair TK C25S F and TK C25S R, and A99S using the primer pair TK C99S F and TK C99S R. The CysLight N358C V2 construct required the same two mutations and the additional A87S mutation using the primer pair TK C87S F and TK C87S R.

2.5 PROTEIN PURIFICATION

2.5.1 Purification by Microtubule Affinity

Purification of the Eg5-464, Eg5-474, Eg5-488, Eg5-495, Eg5-513, Eg5-513-5His, and all 4 CysLight mutants proteins was accomplished by microtubule affinity as previously described [301] with modification (Figure 2.3). Cells were grown in LB medium supplemented with 100 μg/ml ampicillin and 50 μg/ml chloroamphenicol at 37 °C until cultures reached an $A_{600} \leq 0.4$ (yield ~ 2.5 g cells/L). Protein expression was then induced with 400 μM IPTG, and the cultures were allowed to grow overnight at 20 °C. The cells were collected by centrifugation (16,000 X g / 10 min / 4°C) and diluted at 10 g/100 ml lysis buffer. After lysis by freeze-thaw, the lysate was clarified (180,000 X g / 30 min / 4°C) and the supernatant was adjusted to 8 μM microtubules, 0.1 mM MgGTP, 20 μM Taxol, and 0.5 mM MgAMPPNP. The supernatant was incubated at 34°C for 5 min to warm the solution back to room temperature and then incubated for another 15 min to promote MT•Eg5 complex formation. The MT•Eg5 complexes were pelleted (40,000 rpm / 35 min / 25°C), and the resultant pellet was resuspended in 15 ml of ATPase buffer supplemented with 60 μM Taxol plus 0.5 mM MgAMP-PNP. MT•Eg5 complexes were again centrifuged (33,000 rpm / 35 min / 25°C) to remove any proteins that were nonspecifically bound to the microtubules. The resulting microtubule pellet was resuspended in 15 ml ATPase buffer supplemented with 1 mM MgATP, 0.1 mM MgGTP, 100 mM KCl, plus 100 μM Taxol and allowed to incubate at room temperature for 10 min prior to centrifugation (33,000 rpm / 35 min / 25°C). The supernatant contained the Eg5 protein. The ATP-dependent release of Eg5 from the microtubules was repeated. The supernatants were pooled, adjusted to 20 μM Taxol plus 0.1 mM MgGTP, allowed to incubate at room temperature for 10 min, and centrifuged (160,000 rpm / 35 min / 25°C). This step was used to drive the polymerization of any soluble tubulin in the supernatant to microtubules and to separate the microtubules from the soluble Eg5 protein. The Eg5 supernatant was then concentrated (Amicon

Ultra 50K molecular weight cutoff, Millipore Corp.) to ~ 1 ml and subjected to gel filtration (Superose-6 HR 10/30 gel filtration column, Amersham Biosciences). The fractions enriched with Eg5 were pooled, adjusted to 5% sucrose, clarified (160,000 rpm / 25 min / 4°C), and concentrated to ~1.5 ml. Motor domain concentration was subsequently determined by the Bio-Rad Protein Assay (Bio-Rad Laboratories Inc.) using IgG as the protein standard. The approximate yield of an Eg5-513 preparation is ~ 7-8 mg.

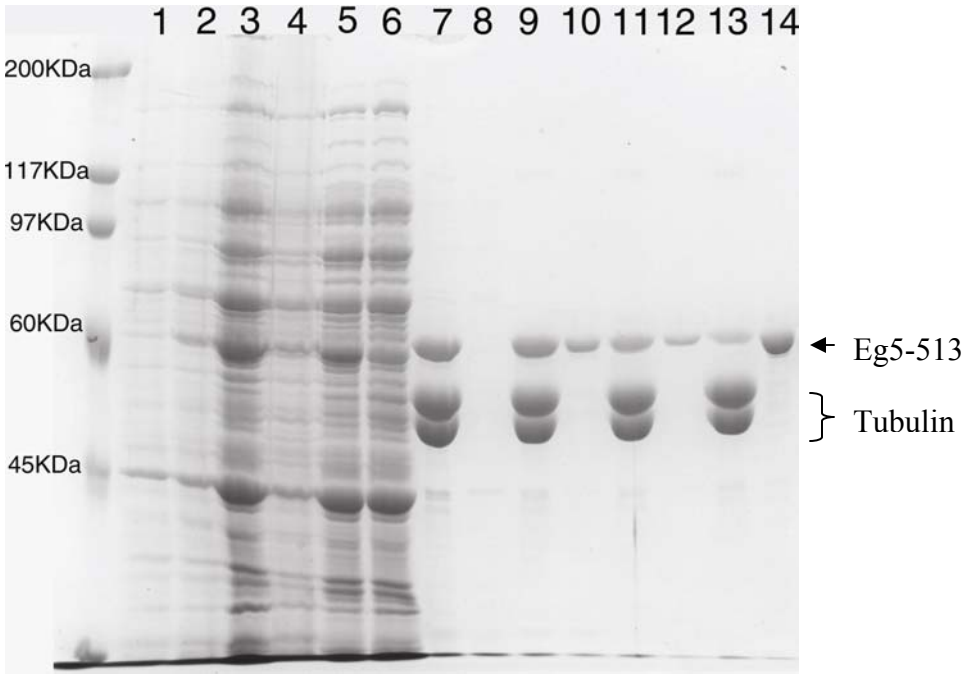

Figure 2.3 Eg5-513 Microtubule Affinity Prep

Figure 2.3 is an 8% acrylamide / 2 M urea SDS-polyacrlyamide gel representing the purification of Eg5-513 using the motor's affinity for the microtubule. (1) cell sample before induction; (2) IPTG induced cell sample; (3) 18K spin supernatant; (4) 18K spin pellet; (5) 40K spin supernatant; (6) supernatant after pelleting the MT•Eg5 complexes; (7) formation of a MT•Eg5 pellet;(8) wash supernatant; (9) wash pellet; (10) ATP Eg5 release 1 supernatant; (11) ATP Eg5 release 1 pellet; (12) ATP Eg5 release 2 supernatant; (13) ATP Eg5 release 2 pellet; (14) final sample.

2.5.2 Purification of R234K by Column Chromatography

The R234K mutant was purified by means of ion exchange chromatography followed by affinity chromatography as described for monomeric Eg5-367 (Figure 2.4, [250]). *E. coli* cells were grown in LB supplemented with 100 μg/ml ampicillin and 50 μg/ml chloroamphenicol and expression was induced as described in section 2.5.1. The cells were harvested by centrifugation (16,000 X g / 10 min / 4°C), resuspended 1 g/ 10 ml in lysis buffer, and lysed by freeze thaw. The solution was clarified by two successive rounds of centrifugation; a low speed spin (24,000 X g / 30 min / 4°C) followed by high speed spin (180,000 X g / 45 min / 4°C). The clarified supernatant was then applied to a 50 ml S-sepharose column (Sigma-Aldrich Co.) equilibrated in S-sepharose column buffer. Bound protein was eluted using a linear gradient from 20-600 mM KCl. Fractions containing R234K were determined by SDS-PAGE, pooled and dialyzed overnight against MCAC column buffer. The next day, the dialysate was clarified (180,000 X g / 45 min / 4°C) and applied to a 6 ml Ni-NTA agarose column (Qiagen). Bound protein was eluted using a linear 0-200 mM imidazole gradient. As with the S-sepharose column, fractions enriched for R234K were resolved using SDS-PAGE, pooled, and dialyzed overnight against ATPase buffer supplemented with 20 μM ATP and 150 mM NaCl. On the last day of the prep, the pooled protein underwent three successive rounds of dialysis into ATPase buffer supplemented with 5% sucrose. The protein was then clarified (180,000 X g / 45 min / 4°C) and concentrated to ~ 100 μM active-sites. Protein concentration was determined in the same manner as with microtubule affinity purification.

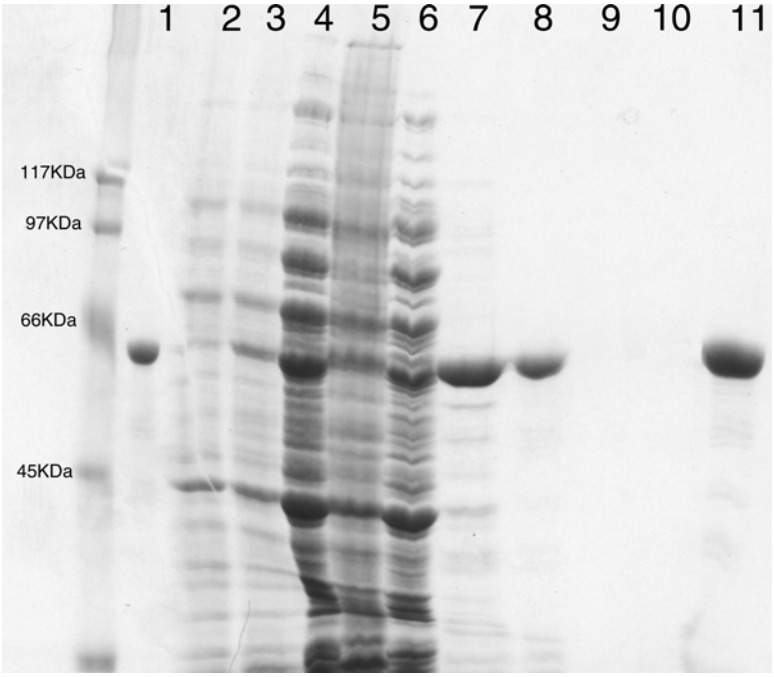

Figure 2.4 Purification of R234K

Figure 2.4 is an 8% acrylamide / 2 M urea SDS-polyacrlyamide gel representing the purification of R234K by a series of ion exchange and affinity chromatography. (1) Eg5-513 standard; (2) cell sample before induction; (3) IPTG induced cell sample; (4); low speed spin supernatant; (5) low speed spin pellet; (6) high speed spin supernatant; (7) Ni-NTA load; (8) post dialysis; (9) pellet from final clarification spin; (10) concentrator flowthrough; (11) final sample.

3.0 EQUILIBRIUM CHARACTERIZATION OF EG5-513

Eg5 or KSP is a homotetrameric Kinesin-5 involved in centrosome separation and assembly of the bipolar mitotic spindle. In an effort to understand how two Eg5 motor domains that interact with a single microtubule communicate, the human Eg5 gene was truncated in order to generate a construct capable of producing a dimeric motor. Analytical gel filtration of purified protein and cryo-electron microscopy (cryo-EM) of unidirectional shadowed microtubule-Eg5 complexes have been used to identify the stable dimer, Eg5-513. Eg5-513 exhibits slow ATP turnover (k_{cat} = 0.48 s^{-1}), high affinity for ATP ($K_{m,ATP}$ = 7.9 μM), and a weakened affinity for microtubules when compared to monomeric Eg5 ($K_{½,Mt}$ = 1.8 μM versus 0.7 μM for Eg5-367). Microtubule cosedimentation assays indicate that dimeric Eg5 has the highest affinity for the microtubule prior to ATP hydrolysis and the weakest in the presence of ADP. The effect of the Eg5 specific inhibitor, *S*-monastrol, was also examined. *S*-monastrol caused a 10-fold reduction in the steady-state ATPase rate, and in large part, negated the enhanced affinity that dimeric Eg5 has for the microtubule in the presence of AMPPNP. The binding of monomeric Eg5 to microtubules in the presence of AMPPNP and *S*-monastrol, under equilibrium conditions, was predominantly unaffected, suggesting that the inhibition of homotetrameric Eg5 by *S*-monastrol is probably a result of impaired cooperativity between motor domains.[1]

---

[1] The data presented in this chapter is reprinted with permission from the Nature Publishing Group. The original form of this data is by Krzysiak *et al*. and can be found it EMBO Journal, *25***:** 2263-2273.

3.1 INTRODUCTION

Molecular motors are prominent participants in mitosis and not only provide the force necessary to assemble the spindle, but they also strike a delicate balance of forces to generate the synchronized set of movements necessary for chromosome segregation [reviewed in [11, 12, 14-19]]. One of the mitotic motors, Eg5 or KSP, is a member of the homotetrameric BimC Kinesin-5 subfamily. These N-terminal kinesins are responsible for providing a plus-end-directed force associated with sliding microtubules during centrosome separation to assemble the bipolar spindle and for prevention of bipolar spindle collapse prior to anaphase [104, 109, 111, 133, 202, 203, 210, 213, 217-219, 302].

Of the Kinesin-5 members, human Eg5 is of particular interest because of its potential as a therapeutic target for cancer treatment. A number of small molecule inhibitors have been identified that can specifically and reversibly inhibit Eg5 function leading to monoaster formation, arrested cell division, and apoptosis [7, 8, 138, 217, 223-239, 303, 304]. The best known of these inhibitors, monastrol, has been shown to slow ADP release, significantly alter Eg5 interactions with the microtubule, and alter the conformation of both the Switch-II region and neck-linker of the catalytic core [224, 243-245, 247, 248, 250, 256]. However, for these initial experiments, a monomeric Eg5 was used. To understand the mechanochemical properties of Eg5 for its mitotic function and the mechanism of inhibition by the monastrol class of small molecule inhibitors, it is critical to define the cooperative interactions that occur between the two

motor domains that interact on a single microtubule and to define the pathway of communication between the catalytic active site and the motor-microtubule interface.

The section presents an anlysis of monomeric and dimeric Eg5 motors comprising the N-terminal 367 (Eg5-367) and 513 (Eg5-513) amino acids of the human gene sequence expressed in *E. coli*. Analytical gel filtration and cryo-electron microscopy (cryo-EM) in combination with high-resolution surface shadowing [e.g. see [305]] indicate that Eg5-513 forms a stable dimer. Steady-state kinetics, equilibrium binding, and cryo-EM 3-D analyses have been used to compare the monomeric and dimeric motors in the presence and absence of monastrol. The results indicate that in dimeric Eg5-513, the cooperative head-head interactions slow ATP turnover, tighten ATP binding, and weaken binding to microtubules. While monomeric Eg5 can bind to microtubules in the presence of monastrol in the ATP and nucleotide-free state, monastrol disrupts dimeric Eg5-513 interactions with the microtubule at every nucleotide condition. Based on the reorientation of the neck-linker and Switch-II cluster in the Eg5•ADP [243] and Eg5•ADP•monastrol [244] crystal structures, monastrol is proposed to weaken the interactions of Eg5 with the microtubule by stabilizing a conformation with the neck-linker of each motor domain docked onto its catalytic core.

3.2 MATERIALS AND METHODS

The biochemical analysis of Eg5-513 was performed in ATPase buffer at room temperature (25°C). Paclitaxel in DMSO was used throughout to stabilize the microtubule polymer. The

concentrations reported are final concentrations after mixing. For the cloning and purification of all motors see chapter 2.

3.2.1 Analytical gel filtration

Gel filtration was performed using a Superose-6 HR 10/30 gel filtration column with the System Gold high-pressure liquid chromatography system (Beckman Coulter Inc.). Elution was monitored using intrinsic protein fluorescence (λ_{ex} = 280, λ_{em} = 340) with a Jasco RP-2020 detector (Jasco Inc.). All proteins were eluted in ATPase buffer at a flow rate of 0.5 ml/min at room temperature. The void volume was determined using bacteriaphage HK97 proheads (generously provided by Roger Hendrix, University of Pittsburgh), and the included volume was determined using *L*-tryptophan. The protein standards used were aldolase (158 KDa), catalase (232 KDa), ferritin (440 KDa), and thyroglobin (669 KDa). The apparent molecular weight (M_r) of Eg5-513 was determined using a semilog plot of K_{av} versus the log of M_r.

3.2.2 Steady-state ATPase kinetics

Steady-state kinetics were determined by monitoring the hydrolysis of [α-^{32}P]ATP [306]. In Figure 3.4, the observed rate of ATP turnover as a function of MgATP concentration was fit to the Michaelis-Menten equation, and the ATPase rate as a function of microtubules (tubulin concentration) was fit to quadratic Equation 1.

$$\text{Rate} = 0.5*k_{cat}*\{(E_0 + K_{1/2,Mt} + MT_0) - [(E_0 + K_{1/2,Mt} + MT_0)^2 - (4E_0MT_0)]^{1/2}\} \quad \text{Eq. 1}$$

Rate is the concentration of product formed per second per active site, and k_{cat} is the maximum rate constant for product formation at saturating microtubules and MgATP conditions. The $K_{m,ATP}$ and $K_{1/2,MT}$ are the constants at which the concentration of substrate yields half the maximal velocity. E_0 is the concentration of motor active sites in the reaction, and MT_0 is the tubulin concentration as microtubule polymer.

For the inhibition of Eg5 steady-state ATPase as a function of *S*-monastrol concentration (Figure 3.4C), the data were fit to the following quadratic equation,

$$\text{Rate} = -0.5*\{(A_{inh} + K_{d\text{-}Mon} + S_0) - [(A_{inh} + K_{d\text{-}Mon} + S_0)^2 - (4A_{inh}S_0)]^{1/2}\} + k_{max} \quad \text{Eq. 2}$$

A_{inh} is the amplitude of *S*-monastrol inhibition defined by k_{max} (k_{cat} in the absence of *S*-monastrol) minus k_{min} (k_{cat} at saturating *S*-monastrol), $K_{d\text{-}Mon}$ is the apparent dissociation constant for *S*-monastrol, and S_0 is the *S*-monastrol concentration.

3.2.3 Detection of ADP copurification with Eg5-513

Eg5-513 or an equimolar amount of ADP (2 μM) was incubated with 0.1 U/ml apyrase (Grade VII, Sigma-Aldrich Co.) for 2 hrs to convert all ADP that might be present to AMP + P_i. The apyrase treated solution was then rapidly mixed in the KinTek SF-2003 stopped-flow (KinTek Corp.) with a coumarin labeled phosphate binding protein (MDCC-PBP) [143, 299] as previously described [246]. Briefly, an initial 10 μM MDCC-PBP solution was treated with a "P_i

mop" (0.05 U/ml purine nucleotide phosphorylase (Sigma-Aldrich Co.), 75 μM 7-methylguanosine (MEG)) and mixed with the "unmopped" apyrase solutions so that any P_i released would be rapidly and tightly bound by the MDCC-PBP and cause a fluorescence enhancement (λ_{ex} = 425 nm, λem = 464 nm, 450 nm cutoff filter).

3.2.4 ADP release from Eg5-513 free in solution

The release of ADP from Eg5-513 was measured as described in [306]. Eg5-513 was incubated with trace [α-^{32}P]ATP for 90 minutes to convert all [α-^{32}P]ATP to [α-^{32}P]ADP. The solution was then mixed with a creatine kinase / phosphocreatine ATP regeneration system (Sigma-Aldrich Co.) with or without a nonradiolabeled MgATP chase (Final: 0.15 mg/ml creatine kinase, 2 mM phosphocreatine, 5 mM MgATP). In this system, all [α-^{32}P]ADP tightly bound to an active site should be protected from the ATP regeneration system. However, in the presence of the ATP chase, when [α-^{32}P]ADP is released from the active site, the cold ATP will outcompete it for rebinding allowing the regeneration system to phosphorolate it back to [α-^{32}P]ATP. [α-^{32}P]ATP was separated from [α-^{32}P]ADP by thin layer chromatography and quantified using Image Guage V4.0 software (Fuji Photo Film U.S.A). The regeneration of ADP to ATP was fit to a single exponential function.

3.2.5 Cosedimentation assays

The cosedimentation assays using μM amounts of Eg-513 were performed as previously described [250]. Eg5-513 (2 μM) was incubated with varying concentrations of microtubules for 10 min before the addition of nucleotide. The MT•Eg5•AXP complex was incubated at room

temperature for 30 min to reach equilibrium and centrifuged (100,000 X g / 30 min / 25°C). In the apyrase-treated experiments, the MT•Eg5 complex was incubated with 0.1 U/ml apyrase (Grade VII, Sigma-Aldrich Co.) for 1 hr prior to centrifugation. For each reaction the supernatant was collected, and the microtubule pellet was resuspended to an equal volume with ATPase buffer. Laemmli 5X sample buffer was added to both supernatant and pellet samples and subjected to SDS-PAGE followed by staining with Coomassie Brilliant Blue R-250. The gels were digitized using the Fuji LAS-3000 (Fuji Photo Film USA), and the fraction of motor partitioning with the microtubule pellet was determined by comparing the intensity of the Eg5 bands in the supernatant and pellet fractions for each microtubule concentration using Fuji Image Guage 4.0 software. For Eg5-513 (Figure 3.5E-H, 3.6B) where sigmoid data were obtained, the Hill equation was used to estimate the degree of cooperativity:

$$Y_s = [MT]^n / (K_h + [MT]^n) \qquad \text{Eq. 3}$$

where Y_s is the fraction of motor sedimenting with the microtubules, [MT] is the tubulin concentration as microtubule polymer, n is the Hill coefficient, and K_h is the product of the K_d values for the cooperative sites.

To more accurately determine the dissociation constants for the MT•Eg5-513 complex under varying nucleotide conditions, cosedimentation experiments were performed using 100 nM motor. There were several complications to this experiment. At such low motor concentrations Coomassie Brilliant Blue is not able to detect the protein necessitating the use of SYPRO® Ruby dye (Invitrogen Corp.) to stain the gels. Digitization was performed using a laser scanner (FLA-5100, Fuji Photo Film USA) and the data were analyzed using Image Guage V4.0.

Supernatant and pellet fractions could not be compared because if tubulin was present in the gel, no other protein was detectable. Therefore, the amount of motor in the microtubule pellet was inferred by comparing the intensity of the motor in the supernatant with the intensity of soluble motor centrifuged in the absence of microtubules. Also, at low motor concentrations, Eg5-513 was found to significantly interact with the centrifuge tubes such that soluble protein could not be detected. Addition of 50 µg/ml ovalbumin to the reaction prior to addition of Eg5-513 minimized motor from adhering to the walls of the tube (Figure 3.1).

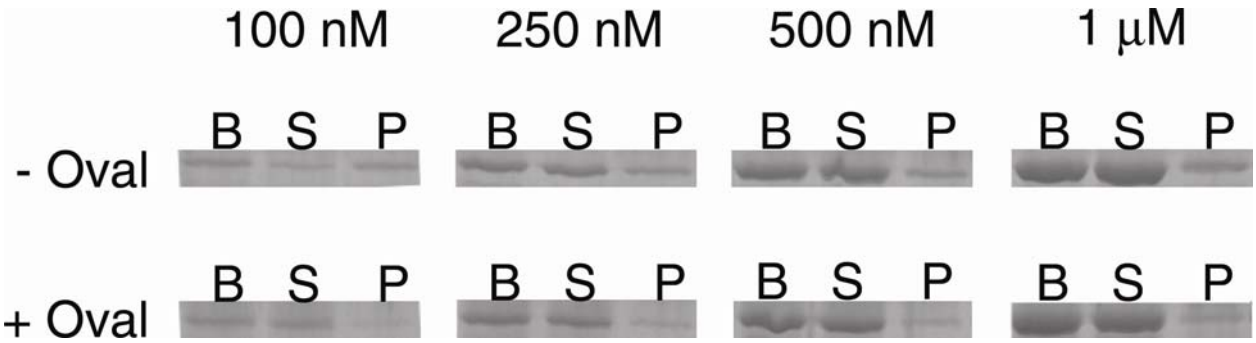

Figure 3.1 Staining with SYPRO® Ruby

Figure 3.1 indicates that any Eg5-513 that pellets in the absence of microtubules is probably due to nonspecific interactions with the centrifuge tube walls. Eg5-513 ± ovalbumin was centrifuged at 100,000 X g; the supernatant was collected, and the tube was washed with an equal volume of buffer. The supernatants and pellets were subjected to SDS-PAGE and the gels were stained with SYPRO® Ruby. As the Eg5-513 concentration was increased the amount of motor pelleting does not continually increase. Addition of ovalbumin prevents or minimizes the amount of motor found in the pellet. B = before spin, S = supernatant, P = pellet.

3.3 RESULTS

3.3.1 Eg5-513 is dimeric

A series of Eg5 constructs were engineered for protein expression (Figure 3.2A, B). Each was expressed, purified, and evaluated by analytical gel filtration to determine its oligomeric state. Out of all of the motors, only Eg5-513 appeared to produce a single species at an elution time expected for a potential dimer. Eg5-464 was seen to undergo proteolysis throughout the purification (data not shown) while Eg5-474, Eg5-488, and Eg5-495 were seen to elute as multiple species (Figure 3.2B). Eg5-513 was compared to dimeric conventional kinesin K401 [301, 307] and monomeric Eg5-367 [224, 243, 244, 250]. As shown in Figure 3.2C, Eg5-513 and Eg5-513-5His elute from the gel filtration column at similar retention times, preceding dimeric K401 and monomeric Eg5-367. A plot of K_{av} *versus* log M_r yielded an apparent molecular mass of 189,688 for Eg5-513 and 181,036 for Eg5-513-5His. The predicted M_r for dimeric motors based on amino acid sequence was 91,062 Da for K401, 115,288 Da for Eg5-513, and 117,594 for Eg5-513-5His. On the basis of this comparison alone, it could be argued that Eg5-513 was monomeric but appeared to elute with a larger apparent molecular mass because the protein is elongated rather than globular. A comparison of two other human Eg5 motors, Eg5-474 (blue trace) and Eg5-488 (black trace), argues against this possibility (Figure 3.2B). The faster elution peak for both motors elutes at about the same time as Eg5-513, and the contribution of the faster peak to the overall motor population increases with the increasing size of the motor. Gel filtration of this series of motors has apparently captured the shift of the equilibrium from monomeric Eg5-367 to dimeric Eg5-513. Gel filtration of Eg5-495 also appears to contain two species as a leading hill is attached to the main elution peak.

Furthermore, the elution profiles of varying concentrations of Eg5-513 overlap without the presence of a preceding or trailing peak (Figure 3.2D). The proposed dimeric state of Eg5-513 remains stable over a range of protein concentrations commonly used experimentally (0.5–4 μM).

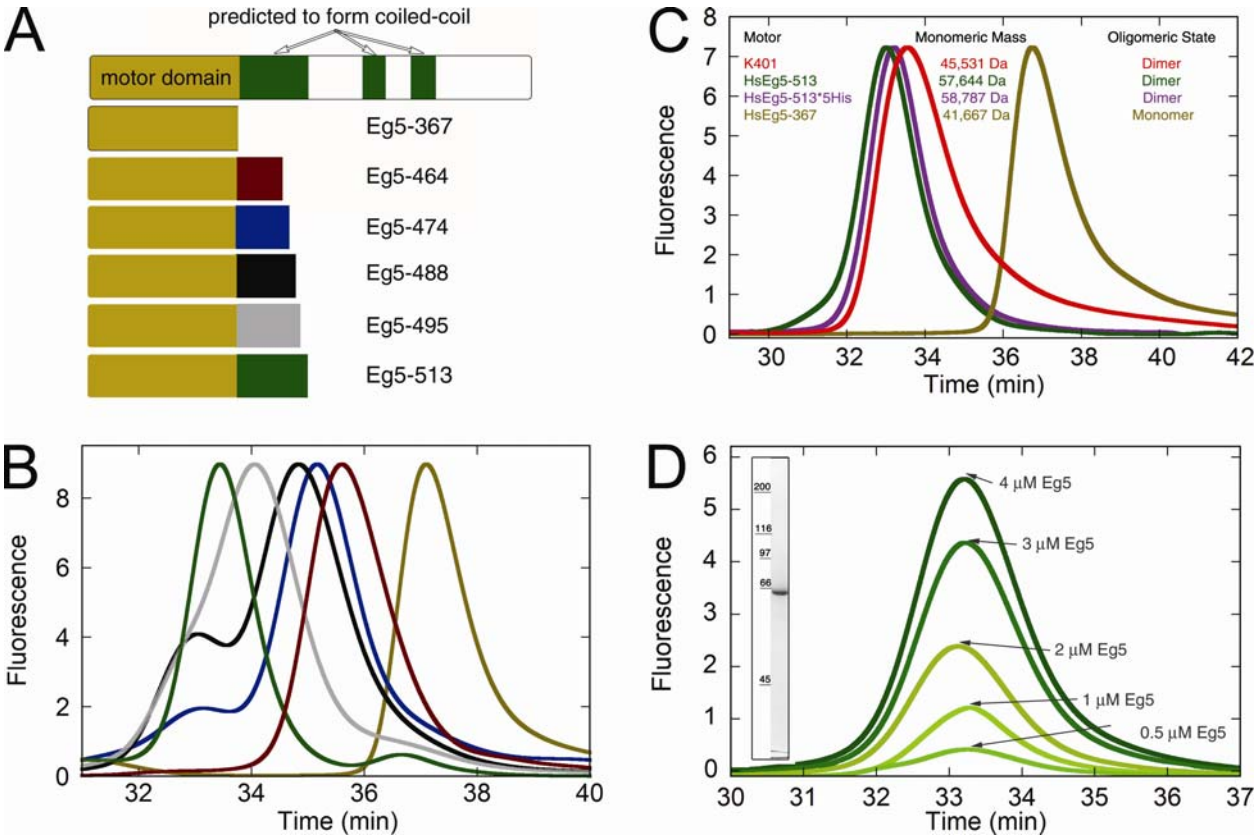

Figure 3.2 Gel Filtration of Eg5 Motors

Analytical gel filtration was used to determine the oligomeric state of various Eg5 motors through a comparison to known standards (not shown). The void volume eluted at 16 min and the included volume eluted at 51.5 min. *A*, Cartoon highlighting the motor domain and regions predicted to form a coiled-coil. The various truncated human Eg5 motors are also drawn with the color coding serving as the legend for *B*. *B*, Representative gel filtration traces of each human Eg5 motor with the retention time indicated. *C*, A comparison of the elution profiles of Eg5-513, Eg5-513-5His, dimeric kinesin K401, and monomeric Eg5-367. *D*, Gel filtration of Eg5-513 in the protein concentration range most commonly used for the presented kinetic and equilibrium studies. The inset shows an SDS-Coomassie Blue stained gel of Eg5-513.

Additional evidence for the oligomeric state of Eg5-513 was provided by Andreas Hoenger and colleagues, through their unidirectional shadowing of both monomeric Eg5-367 and the prospective dimeric Eg5-513 on microtubules and tubulin sheets [205]. Using a 1:8 ratio of Eg5-367 to tubulin, individual motor domains were visible and spaced stochastically along the microtubule lattice. The same ratio of Eg5-513 to tubulin also produced a stochastic distribution of motors. However, the density of a motor domain was predominantly accompanied by a companion. In most cases, the second density was located in the axial direction 8 nm apart to the next tubulin dimer on the same protofilament, indicative of a physical attachment expected for a dimeric motor. A few isolated motor domains were also seen, but it was not apparent whether they represent the overlay of two motor domains or are monomeric motors. These electron microscopy results provide additional evidence that purified Eg5-513 is a stable dimer.

3.3.2 ADP copurifies with Eg5-513

To initially characterize dimeric Eg5, the nucleotide state of the purified motor was determined. All previously studied kinesins have been purified with ADP at their active sites. To examine whether dimeric Eg5 was purified with ADP on its active sites, Eg5-513 was first incubated with apyrase to allow for the cleavage of the β-phosphate, and then the solution was mixed with MDCC-PBP in the stopped-flow (Figure 3.3A). The fluorescence enhancement observed from mixing Eg5-513 treated with apyrase with MDCC-PBP was much larger than that observed when untreated Eg5-513 was mixed with MDCC-PBP, indicating that dimeric Eg5 like other kinesins was purified with ADP. The fluorescence enhancement was ~65% of that obtained when an equimolar amount of ADP treated with apyrase was mixed with MDCC-PBP, suggesting that not all Eg5-513 active sites might be purified with ADP.

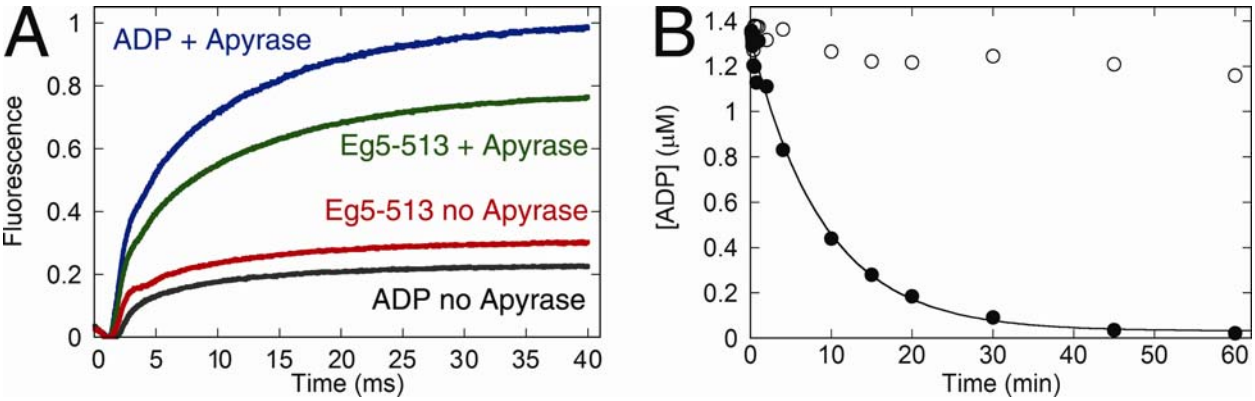

Figure 3.3 ADP Copurifies with Eg5-513

A, Either 2 μM ADP or 2 μM Eg5-513 was treated with apyrase to cleave off the β-phosphate from any ADP that is present. The reaction was then mixed in the stopped-flow instrument with MDCC-PBP. Treatment of Eg5-513 with apyrase elicits a fluorescence response greater than background P_i contamination (black and red traces) suggesting that ADP copurifies with the motor. *B*, To examine the rate of ADP release by Eg5-513 while free is solution, a Eg5-513•[α-^{32}P]ADP solution was mixed with a creatine kinase / phosphocreatine ATP regeneration system in the presence (●) or absence (○) of 10 μM cold MgATP. The conversion of ADP to ATP was fit to an exponential function giving k_{obs} = 0.002 ± 0.0002 s^{-1}.

In order to measure the release rate of bound ADP while the motor is free in solution, Eg5-513 was first incubated with [α-^{32}P]ATP for a sufficient time to allow for the conversion of all [α-^{32}P]ATP to [α-^{32}P]ADP. The Eg5-513•[α-^{32}P]ADP was then mixed with a creatine kinase / phosphocreatine ATP regeneration system ± 10 μM MgATP [306]. In the presence of the regeneration system and additional MgATP, [α-^{32}P]ADP was phosphorylated to ATP very slowly k_{obs} = 0.002 s^{-1} (Figure 3.3B).

3.3.3 Eg5-513 exhibits slow steady-state ATP turnover

The steady-state ATPase kinetics for Eg5-513 (Figure 3.4) were pursued as a function of either ATP concentration at 20 μM microtubules or microtubule concentration at 400 μM MgATP in

the presence or absence of 150 μM monastrol. In comparison to monomeric Eg5-367, Eg5-513 was 10-fold slower (k_{cat} = 0.48 s^{-1} *vs.* 5.5 s^{-1} for Eg5-367), exhibited an apparent 3-fold tighter affinity for ATP ($K_{m,ATP}$ = 7.9 μM *vs.* 25 μM for Eg5-367), yet ~3-fold weaker apparent affinity for microtubules ($K_{½,MT}$ = 1.8 μM *vs.* 0.7 μM for Eg5-367). The slower ATPase kinetics observed for the dimer in comparison to the monomer are consistent with the interpretation of cooperative interactions between the motor domains of the dimer to slow the overall rate of the reaction. This behavior has been well documented for Kinesin-1, Myosin-V, and Myosin-VI [145, 181, 249, 308-310].

In the presence of monastrol, the steady-state k_{cat} of Eg5-513 was reduced 10-fold to 0.046 s^{-1} with the affinity for *S*-monastrol at $K_{d\text{-}Mon}$ = 4.8 μM (Figure 3.4C). The apparent $K_{d\text{-}Mon}$ determined for dimeric Eg5-513 was 2-fold tighter than reported for monomeric Eg5-367 [224, 248], which also evaluated the more potent *S*-monastrol enantiomer. Surprisingly, the $K_{½,MT}$ was not altered ($K_{½,MT\text{-}M}$ = 2 μM) whereas a 10-fold increase was seen for the monomer.

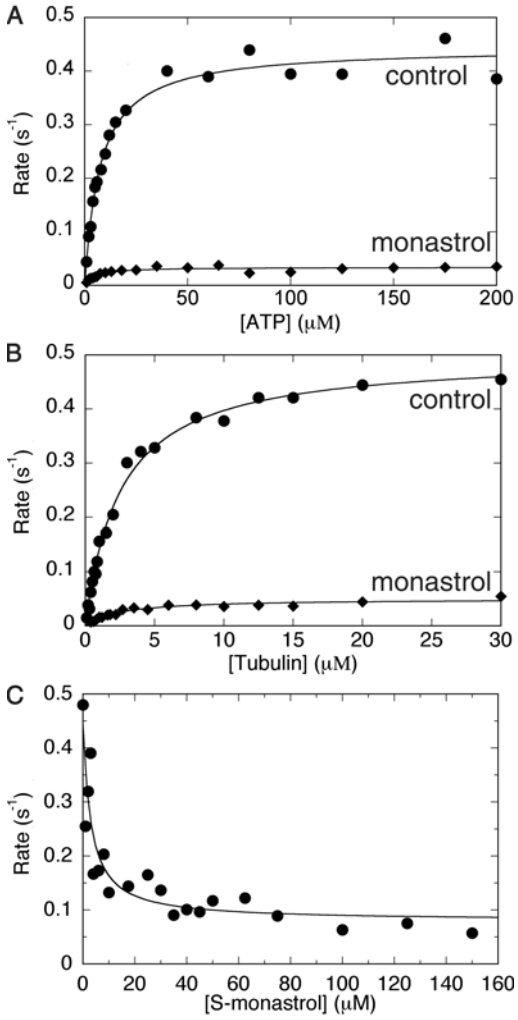

Figure 3.4 Steady-State ATP Turnover

A preformed MT•Eg5 (●) or MT•Eg5-monastrol (◆) complex was rapidly mixed with [α-^{32}P]ATP. *A,* Final concentrations: 0.5 μM Eg5-513 motor domain, 20 μM tubulin, 20 μM Taxol, 150 μM *S*-monastrol, 1-200 μM MgATP. The fit of the data to the Michaelis-Menten equation provided the steady-state parameters: k_{cat} = 0.44 ± 0.01 s^{-1}, $K_{m,ATP}$ = 7.5 ± 0.7 μM and $k_{cat\text{-}Mon}$ = 0.034 ± 0.001 s^{-1}, $K_{m,ATP\text{-}Mon}$ = 4.5 ± 0.9 μM. *B*, Final concentrations: 1 μM Eg5-513 motor domains, 0.1-40 μM tubulin, 20 μM Taxol, 150 μM *S*-monastrol, 400 μM MgATP. The data were fit to Equation 1: k_{cat} = 0.48 ± 0.01 s^{-1}, $K_{½,MT}$ = 1.8 ± 0.1 μM and $k_{cat\text{-}Mon}$ = 0.048 ± 0.002 s^{-1}, $K_{½,MT\text{-}Mon}$ = 1.7 ± 0.3 μM. *C*, Final concentrations: 0.5 μM Eg5-513 motor domain, 20 μM tubulin, 20 μM Taxol, 150 μM MgATP, 0-150 μM *S*-monastrol. The data were fit to Equation 2: $K_{d\text{-}Mon}$ = 2.88 ± 0.04 μM.

3.3.4 Monastrol disrupts the microtubule binding properties of dimeric Eg5-513 but not monomeric Eg5-367

The effect of a second motor domain could also be seen using equilibrium cosedimentation assays to analyze the affinity of Eg5-513 for the microtubule in the presence of various nucleotides. For these assays, either 2 μM Eg5-513 or 100 nM Eg5-513 was incubated with varying concentrations of microtubules plus nucleotide, allowed to come to equilibrium, and then centrifuged. The supernatant and pellet for each reaction were analyzed by SDS-PAGE to determine the fraction of Eg5 motor that partitioned with the supernatant or the microtubules in the pellet (Figure 3.5). In these assays, a dimeric motor would cosediment with the microtubules as long as one motor domain of the dimer was bound to the microtubule. When no additional nucleotide was added to the MT•Eg5 complex (Figure 3.5A, B), only ~70-80% of the motor partitioned to the microtubule pellet with the $K_{d,MT}$ = 0.6 μM. Incomplete binding was seen using both Eg5-513 concentrations.

This observation that ~20-30% of the Eg5 motor remained in the supernatant came as somewhat of a surprise because monomeric Eg5-367 showed stoichiometric binding to microtubules under these conditions [250]. Eg5-513, like other kinesin motors, was purified with ADP bound at the active site (Figure 3.3), and the ADP could affect the microtubule affinity. To test the possibility that the ADP state was affecting the partitioning of Eg5-513 with the microtubules, cosedimentation assays were performed in the presence of 2 mM MgADP. As Figure 3.5G, H shows, the presence of additional ADP increased the partitioning of Eg5-513 to the supernatant. Only 30-50% of the motor sedimented with the microtubules, $K_{d,MT}$ = 2.2 μM. In contrast, when the MT•Eg5 complex was treated with apyrase to remove any ADP that accompanies the motor through purification, all Eg5-513 partitioned with the microtubule pellet

(Figure 3.5C, D). Incubation of the MT•Eg5-513 complex with the non-hydrolyzable ATP analogue, MgAMPPNP, also caused all Eg5-513 to partition in microtubule pellet (Figure 3.5E, F). The 2 μM data obtained from apyrase treatment as well as incubation with AMPPNP display a sigmoid profile (K_{Hill} = 1.2 μM^2, n = 1.6 and K_{Hill} = 0.5 μM^3, n = 2.9 respectively), however only a quadratic dependence is detectable at 100 nM motor. Comparison of the AMPPNP ($K_{d,MT}$ < 35 nM) results with the apyrase results ($K_{d,MT}$ = 370 nM) suggests that it is the ATP state that has the highest affinity for the microtubule (Figure 3.5F inset). Additionally, the weak binding of Eg5-513 in the presence of ADP suggests that that Eg5 motor detachment follows ATP hydrolysis.

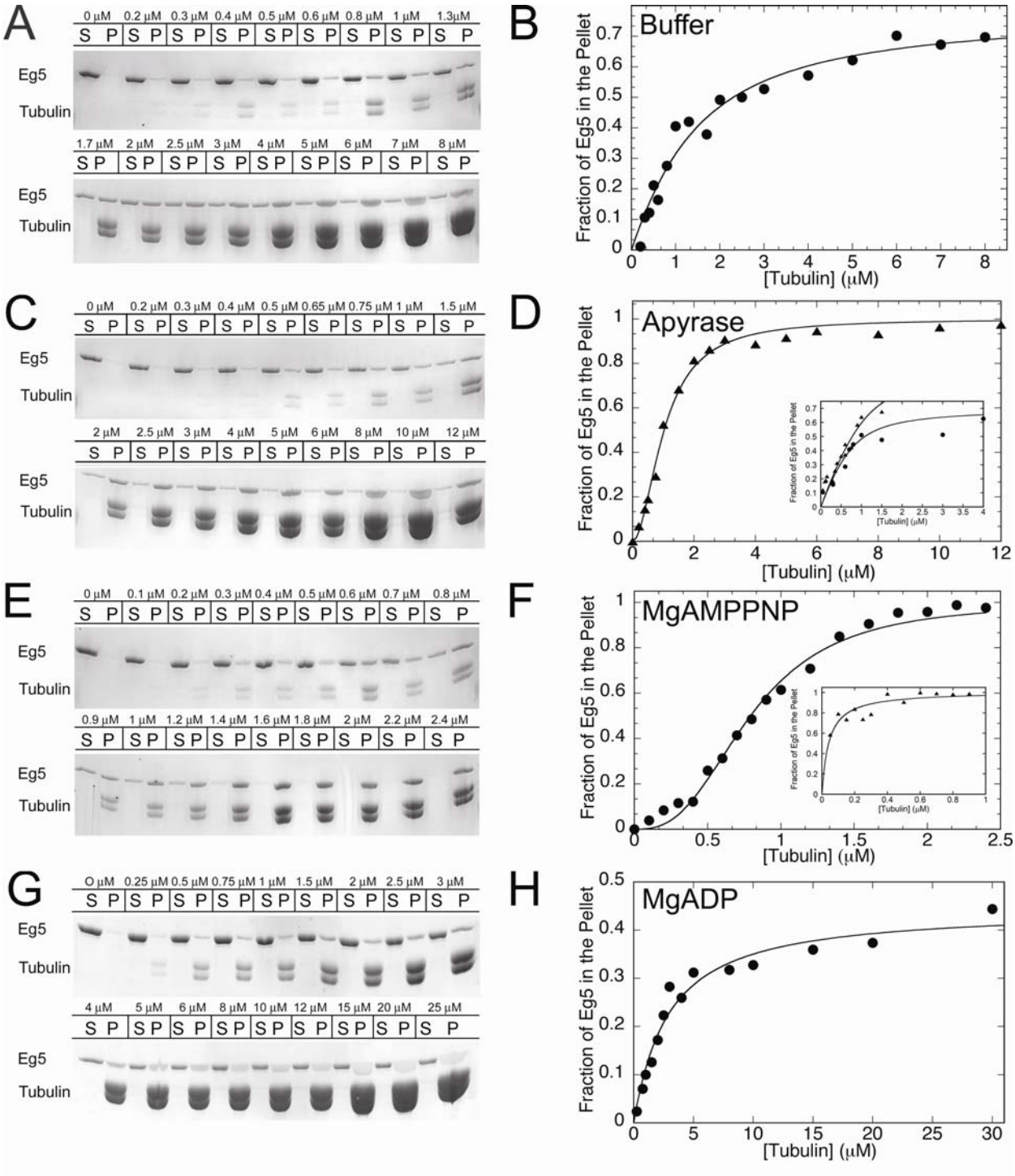

Figure 3.5 Cosedimentation of Eg5-513 with Microtubules

Eg5-513 at 2 μM (large panels) or 100 nM (insets) was incubated with microtubules (0-30 μM tubulin, 20 μM Taxol) in the *A, B* absence of added nucleotide, *i.e.*, as purified with ADP bound to the active sites, *C, D* 0.1 U/ml apyrase, *E, F* 2 mM MgAMPPNP, or *G, H* 2 mM MgADP. The fraction of Eg5-513 that sedimented with microtubules based on the Coomassie Blue-stained SDS gels was plotted as a function of microtubule concentration. *A, B* In the absence of added

nucleotide, the fit of the data provided $K_{d,MT}$ = 1.0 ± 0.2 μM with maximal fractional binding at 79 ± 0.04%. *C, D* Apyrase-treatment yields a nucleotide-free state. The sigmoid data were fit to the Hill equation: K_{Hill} = 0.93 ± 0.06 μM^2, Hill coefficient n = 1.8 ± 0.1 with maximal fractional binding at 100%. *D inset*, A comparison of microtubule binding in the absence of added nucleotide (●) and the nucleotide-free, apyrase treatment, state (▲) using 100 nM Eg5-513. In the absence of added nucleotide $K_{d,MT}$ = 561 ± 180 nM with maximal fractional binding at 70 ± 10%. In the nucleotide-free state, $K_{d,MT}$ = 553 ± 252 nM; however, the maximal fractional binding could not be experimentally observed due to the presence of microtubules in the supernatants at the higher microtubule concentrations. *E, F* MgAMPPNP was used to generate an ATP-prehydrolysis state. The fit to the Hill equation provided K_{Hill} = 0.53 ± 0.03 μM^3, Hill coefficient n = 2.7 ± 0.15 with maximal fractional binding at 100%. *F inset*, Displays Eg5-513 binding to the microtubule at nM concentrations of motor. All motor is observed to bind to the microtubule with $K_{d,MT}$ = 22 ± 6 nM. *G, H* , The MgADP data yielded $K_{d,MT}$ = 2.6 ± 0.4 μM with maximal fractional binding at 45 ± 2%. S, supernatant; P, pellet.

Cosedimentation experiments using both monomeric and dimeric motors were also perfomed under all nucleotide conditions in the presence of *S*-monastrol. Sedimentation of monomeric Eg5-367 in the presence of AMPPNP, in the nucleotide-free state achieved with apyrase treatment, and in the presence of AMPPNP + *S*-monastrol revealed stoichiometric binding of Eg5-367 to microtubules (Figure 3.6A). Cosedimentation of Eg5-513 with microtubules in the presence of *S*-monastrol did however alter the binding performance of Eg5-513 though the sigmoid profile remained (Figure 3.6B). In the absence of inhibitor AMPPNP, dimeric Eg5-513 exhibits tight, stoichiometric binding, however, in the presence of *S*-monastrol, the data became superimposable with the weaker, nucleotide-free binding curve. These results for dimeric Eg5-513 are consistent with the observation that *S*-monastrol does not abolish MT•Eg5 complex formation [217, 218, 245]. Also, consistant with monastrol stabilizing the ADP state, sedimentation in the presence of 2 mM ADP + *S*-monastrol further decreased the the fraction of Eg5-513 bound to microtubules from 45% to 19% (Figure 3.6B inset).

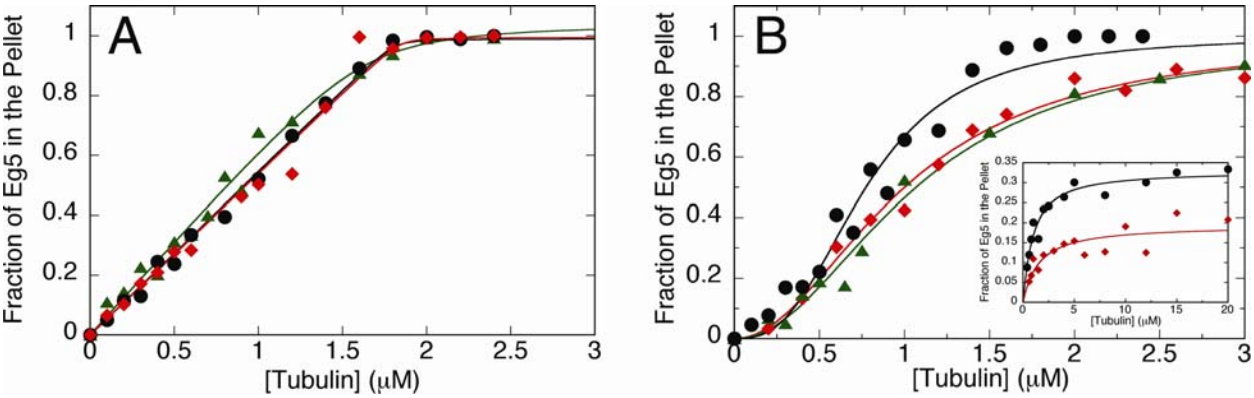

Figure 3.6 *S*-Monastrol's Effect on MT•Eg5 Complex Formation

Monomeric Eg5-367 *A* or dimeric Eg5-513 *B* (2 μM motor) was incubated with microtubules, in the presence or absence of monastrol. *A*, Eg5-367 lacking nucleotide at the active-site (▲), in the presence of 2 mM MgAMPPNP (●), and 2 mM MgAMPPNP + 150 μM *S*-monastrol (♦) displays stoichiometric binding to the microtubule. *B*, Eg5-513 lacking nucleotide at the active-site (▲), in the presence of 2 mM MgAMPPNP (●), and 2 mM MgAMPPNP + 150 μM *S*-monastrol (♦) displays a sigmoid binding profile. Notice that in the presence of *S*-monastrol the higher degree of cooperativity seen in the presence of MgAMPPNP as compared to the apyrase treated nucleotide-free state is lost. *Inset*, Comparison of Eg5-513 microtubule binding in the presence 2 mM MgADP (●) or 2 mM MgADP + 150 μM *S*-monastrol (♦). *S*-monastrol decreased the fractional binding to 19 ± 2%

3.4 DISCUSSION

3.4.1 Eg5 Dimerization

A stable Eg5 dimer was identified based on both analytical gel filtration and electron microscopy. Eg5-513, however, contains significantly more amino acid sequence than has been necessary to induce dimerization of other kinesins. For example, the Kinesin-1 motor of rat, *Drosophila melanogaster*, and *Neurospora crassa* all dimerized with 379-391 amino acids [278, 307, 311, 312]. The presence of multiple species in the gel filtration traces of Eg5-474, Eg5-488 and, though not as easily visible, Eg5-494 (Figure 3.2B, C) suggest either multiple

conformations of the motors or multiple oligomeric states. While the multiple conformations hypothesis cannot be strictly ruled out, the elution of the larger species at the same time as Eg5-513 suggests that the two species represents equilibrium between monomeric and dimeric species favoring the dimeric species in motors comprised of more amino acids. In preparation for designing the constructs, both the COILS [313] and PAIRCOIL programs [314] were used to examine the coiled-coiled probability of full length human Eg5. The coiled-coil prediction score was largely uninterrupted from amino acid 368 to 523. Interestingly, the coiled-coil prediction score decreases around amino acid 480 and depending on the program, decreases to zero either shortly before or after amino acid 513. Quite possibly, Eg5 dimerizes by using C-terminal sequence flanking regions with a propensity to form coiled-coils to set the register for stable oligomerization. A C-terminal to N-terminal dimerization of a kinesin motor has been observed with Xklp3A/B, a Kinesin-2 from *Xenopus laevis* [315, 316].

3.4.2 Intramolecular Cooperativity

In vivo, Eg5 is a homotetramer with two motor domains interacting with one microtubule and two motor domains interacting with a second microtubule [109]. This organization raises questions about the intramolecular cooperativity of the four motor domains of the homotetramer. (1) Do all four motor domains function independently of each other? (2) Do the two sets of motor domains alternate their mechanochemical cycles while the two motor domains that interact on the same microtubule function in unison? (3) Do all four motor domains alternate their mechanochemical cycles? (4) Do the two motor domains that interact with the same microtubule alternate their mechanochemical cycles but function in unison with a corresponding motor domain on the second microtubule? The steady-state ATPase kinetics strongly argue against the

first two hypotheses. In comparison to the monomer, dimeric Eg5 exhibits differences in all three kinetic parameters (Figure 3.4, Table 3). If the motor domains were independent or functioned in unison, the steady-state kinetic parameters of both monomeric and dimeric motors should be indistinguishable. With regards to cooperativity between the dimeric halves of Eg5, hypothesis 3 and 4 cannot be definitively distinguished; however, hypothesis 4 is temporarily favored. Microtubule gilding experiments performed with dimeric Eg5 display microtubule displacement at rates comparable to what has been seen for the homotetramer (see section 3.5). If all four motor domains alternated their mechanochemical cycles, the rate of microtubule displacement by the homotetramer should be half that of the dimer. Regardless of the sequence of activity by all four motor domains, at some point, the motion imparted on one microtubule will be delayed until the half of the motor interacting with the second microtubule completes its function; essentially doubling the time it takes for the motor to undergo two displacement events on the same microtubule.

Table 3 Steady-state Parameters

Kinetic Parameter	Eg5-513	Eg5-513 Monastrol	Eg5-367[a]	Eg5-367[b] Monastrol
Steady-state k_{cat}	0.48 ± 0.2 s^{-1} n = 17	0.046 ± 0.006 s^{-1} n = 6	5.5 ± 0.3 s^{-1}	1.2 ± 0.03 s^{-1}
$K_{m,ATP}$	7.9 ± 2.4 μM n = 10	4.5 ± 0.06 μM n = 3	25.1 ± 0.7 μM	3.6 ± 0.3 μM
$K_{½,MT}$	1.8 ± 0.2 μM n = 7	1.94 ± 0.2 μM n = 3	0.71 ± 0.15 μM	6.7 ± 0.4 μM
$K_{d\text{-}mon}$		4.8 ± 1.3 μM n = 3		13.8 ± 1.0 μM

[a]Cochran *et al*. [250]
[b]Cochran *et al*. [248]

3.4.3 Intermolecular Cooperativity

One of the more surprising observations was the sigmoid binding data obtained from cosedimentation of 2 μM Eg5-513 following treatment with apyrase or in the presence of MgAMPPNP (Figure 3.5C-F). Typically, one would argue that a sigmoid binding profile was indicative of intermolecular cooperativity between two or more dimers, yet the unidirectional shadowing suggests that Eg5-513, at concentrations insufficient to saturate the microtubule lattice, binds microtubules stochastically rather than cooperatively [205]. The sigmoid profile was not apparent in the cosedimentation assays using 100 nM Eg5-513, but that could be a result of inherent error in detecting such small amounts of motor using the particular experimental design. Cooperativity by a kinesin motor when binding to microtubules has been most evident in the case of dimeric Ncd [317]; cryo-EM techniques imaged fully decorated microtubules side-by-side with empty microtubules.

Intermolecular cooperativity between Eg5 dimers cannot be ruled out, though. If it were completely absent, the regularity of the surface pattern observed in the unidirectionally shadowing of Eg5 dimers on microtubules by Andreas Hoenger and colleagues [205] would most likely have been disrupted as found for dimeric Kinesin-1 [see Figure 4 in [305]]. In fact, a recent study with Kinesin-1 suggested that it also displays cooperative binding toward the plus-end of the microtubule during ATP turnover, yet absent with the addition of ADP or AMP-PNP [318]. Possibly, the interplay between the Eg5 motor domains and the microtubule causes a more subtle global effect preventing binding cooperativity from being easily detected by the cryo-EM analysis of dimeric Eg5.

3.4.4 Model for the Inhibition of Eg5-513 by Monastrol

Cosedimentation assays using monomeric Eg5-367 did not indicate an affect by *S*-monastrol on the ability of the motor to bind to microtubules in the nucleotide-free form or in the presence of AMPPNP (Figure 3.6A). Likewise, the cryo-electron microscopy (cryo-EM) performed by Andreas Hoenger and colleagues, which accompanied the cosedimentation data in [205], indicated similar binding geometries under the three conditions. A higher degree of mobility was seen in the presence of AMPPNP + *S*-monastrol, though large differences were not detected in the averaging.

To the contrary, in cosedimentation assays using dimeric Eg5-513, an enhancement in binding was seen in the AMPPNP state as compared to the nucleotide-free state (Figure 3.5F inset). In the presence of AMPPNP + *S*-monastrol the enhancement in binding caused by AMPPNP is not observed, though all motor was seen as pelleted with the microtubules in the nucleotide-free pattern (Figure 3.6B). Under the more stringent cryo-EM conditions, a more drastic difference was seen between the three conditions [205]. In the nucleotide-free state and AMPPNP state, Eg5-513 was sufficiently able to decorate the microtubules, but the motor domain density in the nucleotide-free state was only 50% that of the AMPPNP state. Decoration of the microtubule was not observed in the presence of AMPPNP + *S*-monastrol [205].

These differences in binding between monomeric and dimeric Eg5 would suggest that the inhibitory effects of monastrol on Eg5 are not merely a result of induced conformations in one motor domain alone. More likely the induced conformations in the two motor domains of the dimer or four motor domains of the *in vivo* tetramer act synergistically to impair microtubule binding and possibly force generation. Structurally, the neck-linker was seen to be "docked" along the motor domain in the Eg5•ADP•monastrol crystal structure [244] whereas the neck-

linker was seen to be "undocked" in the Eg5•ADP crystal structure [243]. In the collaborative effort with the Hoenger lab [205], it was proposed that a monastrol induced docking of the neck-linkers of both motor domains of the dimer could sterically constrict the motor and prevent the motor from engaging in its normal microtubule contacts. This idea was based off of the walking model of conventional kinesin in which the rearward motor domain is capable of docking its neck-linker but the forward motor domain cannot due to intramolecular strain [186, 191, 291, 319-321]. In the past year, the model proposed in Krzysiak *et al*. [205] has gained support from FRET studies identifying a change in the position of the neck-linker upon binding of monastrol to monomeric Eg5 motor domains [247].

3.5 CHAPTER 3 ADDENDUM: EG5-513 DRIVEN MICROTUBULE GLIDING

Finally, as a prelude to the later chapters in this dissertation, the contribution of Lisa R. Sproul, who performed the multiple motor microtubule gliding assays in reference [205], needs to be mentioned.

3.5.1 Methods

Highly fluorescent microtubules were polymerized by incubating a 1:1 ratio of rhodamine-labeled tubulin (Cytoskeleton, Inc.) to native bovine tubulin in PME buffer (10 mM Pipes, 5 mM $MgCl_2$, 1 mM EGTA) at 34 °C, and subsequently stabilized with 20 μM Taxol. The microtubules were sheared using a 23.5 gauge needle to generate seeds, and a 1:4 ratio of rhodamine-tubulin to native bovine tubulin was added. The highly fluorescent microtubule seeds

were extended with soluble tubulin at a lower concentration of rhodamine-labeled tubulin. The resulting microtubules were polarity marked with a highly fluorescent short minus end and more dim plus end. Microscopy was performed in OSM: PME supplemented with 1.5 mM MgATP or MgAMPPNP, 1.0 mg/ml BSA, 0.2 mg/ml glucose oxidase, 35 μg/ml catalase, 4.5 mg/ml glucose, 2.5 μl of β-mercaptoethanol, and 20 μM Taxol. A preformed MT•Eg5-513•AMPPNP complex (2 μM Motor, 300 nM tubulin, 20 μM Taxol, 1 mM MgAMPPNP) was flowed into an acid washed perfusion chamber and incubated for three minutes. The chamber was rinsed OSM plus 1 mM MgAMPPNP to remove unattached microtubules. Three-to-four image frames of the stationary microtubules were collected prior to reaction initiation by 1.5 mM MgATP plus an ATP regeneration system (0.3 μg/μl creatine phosphokinase, 2 mM phosphocreatine in OSM). Images were collected every 20 s over 20 min. Microtubules were analyzed using Adobe Photoshop 7 based on the following criteria for evaluation: microtubules exhibited continuous movement in one direction for $t > 1$ min, microtubules did not contact other microtubules, microtubules were ≥ 2.5 μm in length, and the microtubules were completely in the field of view. The average length of the scored microtubules was 6 μm. The motility was imaged with an Olympus BX60 epifluorescence microscope using a 100X oil immersion objective. Digital images were captured with a Hamamatsu 4742 CCD-cooled camera in conjunction with QED In Vivo™ imaging software

3.5.2 Results and Discussion

As expected for a plus-end-directed motor, polarity marked microtubules were observed to move with their brightly labeled minus-ends leading when Eg5-513 was present (Figure 3.7). Microtubule gliding was not observed in the absence of either Eg5-513 or MgATP. The average

rate at which Eg5-513 promoted microtubule gliding was 2.83 ± 0.06 μm/min with a range of 1.6 μm/min to 5.2 μm/min (Figure 3.7). The rate of Eg5-513-promoted microtubule gliding was comparable to the 2.75 μm/min observed *in vitro* for *Xenopus* homotetrameric Eg5 with translocation on microtubule asters [135] and the 2.4 μm/min observed for Baculovirus-expressed and purified Eg5 homotetramer sliding microtubules against axonemes [255]. The polarity of the microtubule seeds was confirmed using conventional kinesin, a well described plus-end directed motor (Figure 3.7). This commonality between the results for dimeric Eg5-513 and homotetrameric Eg5 motors strongly supports the idea that mechanistic data obtained using Eg5-513 will be applicable in defining the cooperative interactions and mechanistic basis of homotetrameric Eg5 function *in vivo.*

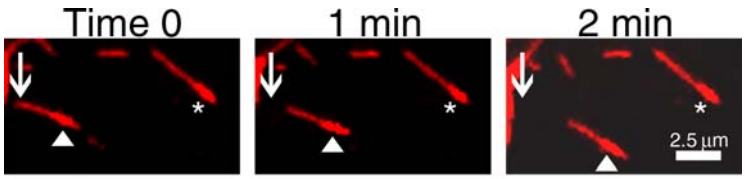

2 μM Motor	n	Rate (μm/min)	Polarity Marked Microtubules		
			n	Plus-end Lead	Minus-end Lead
No Motor	50	0.0	50	0	0
Eg5-513	144	2.83 ± 0.06	56	3	53
KHC	*57*	*0.79 ± 0.02 μm/sec*	*17*	*1*	*16*

Figure 3.7 Microtubule Gliding by Eg5-513

Eg5-513-5His promotes plus-end-directed microtubule gliding in the presence of 1.5 mM MgATP. Polarity-marked microtubules exhibit a more highly fluorescent microtubule minus-end. The ▲ indicates a microtubule that is changing its position over time in comparison to the stationary microtubule denoted by★. Conventional Kinesin-1 (KHC) was used to assess the polarity of the microtubules. The microtubule gliding assays as well as this figure are the work of Lisa R. Sproul.

4.0 THE TRANSIENT-STATE KINETICS GOVERNING PROCESSIVE MOTION BY EG5-513

Eg5/KSP is a homotetrameric, Kinesin-5 family member whose ability to cross-link microtubules has associated it with mitotic spindle assembly and dynamics for chromosome segregation. Transient-state kinetic methodologies have been used to dissect the mechanochemical cycle of a dimeric motor, Eg5-513, to better understand the cooperative interactions that modulate processive stepping. Microtubule association, ADP release, and ATP binding are all fast steps in the pathway. However, the acid-quench analysis of the kinetics of ATP hydrolysis with substrate in excess of motor was unable to resolve a burst of product formation during the first ATP turnover event. In addition, the kinetics of P_i release and ATP-promoted microtubule-Eg5 dissociation were observed to be no faster than the rate of ATP hydrolysis. In combination the data suggest that dimeric Eg5 is the first kinesin motor identified to have a rate-limiting ATP hydrolysis step. Furthermore several lines of evidence implicate alternating-site catalysis as the molecular mechanism underlying dimeric Eg5 processivity. Both mantATP binding and mantADP release transients are biphasic. Analysis of ATP hydrolysis through single turnover assays indicates a surprising substrate concentration dependence, where

the observed rate is reduced by half when substrate concentration is sufficiently high to require both motor domains of the dimer to participate in the reaction.[2]

4.1 INTRODUCTION

Eg5 is member of the homotetrameric, BimC/Kinesin-5 family. Members of this family function during mitosis and provide a plus-end directed force that has become associated with bipolar spindle assembly, spindle maintenance, and microtubule flux [104, 106, 109, 219, 322-327]. The function of Eg5 in the mitotic spindle has been shown to be indispensable. Perturbation of its function prior to anaphase B by either antibody [104, 328] or small molecule inhibitors [217, 218, 223, 225, 226, 231-233, 236, 238, 329, 330] causes collapse of the bipolar spindle into a monoaster and leads to apoptosis in cells with intact spindle checkpoint machinery [8, 331]. As a result Eg5 has garnered substantial interest as a potential chemotherapeutic target in cancer treatment.

Mechanistically, the ATPase cycle of monomeric Eg5 motor domains are fairly well understood both free in solution and bound to microtubules [245-248, 250, 251, 332]. Off the microtubule, monomeric Eg5 demonstrates weak ATP binding and has a propensity to form a nonproductive Eg5•ATP complex [246]. However, on the microtubule, ATP binding is tight, substrate productively proceeds through ATP hydrolysis, and the rates of all the individual steps

[2] The data presented in this chapter is reprinted with permission from the American Society for Biochemistry and Molecular Biology, Inc. The original form of this data is by Krzysiak *et al*. and can be found in J. Biol. Chem. 281: 39444-39454.

in the mechanochemical cycle are accelerated [250]. The microtubule-activated ATPase cycle concludes with a conformational change of the motor domain in relation to the microtubule, termed "rolling" [251], followed by the rate-limiting event in the cycle, the coupled action of phosphate release, and motor detachment from the microtubule [250, 251].

In vivo the individual Eg5 motor domains probably do not function independently, therefore analysis of a higher order oligomeric structure is necessitated. Indeed, previous analysis of dimeric Eg5, Eg5-513, has indicated that two conjoined motor domains exhibit cooperativity *in vitro* [205, 333]. In comparison to a single Eg5 motor domain, the steady-state ATPase of Eg5-513 is reduced 10-fold suggesting the physical attachment of two motor domains causes a reciprocal modulation of each enzymatic cycle [205]. Also, a His_5-tagged form of Eg5-513 has displayed processivity in single molecule studies [333], strongly suggesting that dimeric Eg5, like other kinetically characterized dimeric kinesins, is able to maintain the ATPase cycles of its motor domains out of phase to facilitate processive stepping. To begin to dissect the nature of these cooperative interactions, a mechanistic analysis of the individual steps in the ATPase cycle has been employed. Like conventional kinesin [143, 162, 168, 172], dimeric Eg5 alternates the catalysis of its motor domains to allow for processive movement along the microtubule. However, dimeric Eg5 is the first kinesin motor found to have its ATPase cycle limited by ATP hydrolysis during a processive run.

4.2 MATERIALS AND METHODS

The biochemical analysis of Eg5-513 was performed in ATPase buffer at room temperature (25°C). Paclitaxel in DMSO was used throughout to stabilize the microtubule polymer. The concentrations reported are final concentrations after mixing. For the cloning and purification off all motors see chapter 2.

4.2.1 Generation of Nucleotide-Free MT•Eg5-513 Complexes

For experiments in which a MT•Eg5-513 complex was treated with apyrase, the complex was incubated with 0.02 U/ml apyrase (Grade VII, Sigma-Aldrich Co.) for 20 min. Apyrase treatment was performed for 1 hr when Eg5-513 was free in solution because ADP release is slowed significantly in the absence of microtubules. Apyrase converts free ADP to AMP + P_i. However, the affinity of Eg5-513 for AMP is so weak that apyrase treatment effectively generates a nucleotide-free state for Eg5 (data not shown). Apyrase treated Eg5-513 was fully active based on microtubule binding (Figure 3.5, [205]) and steady-state ATP turnover (k_{cat} = 0.67 s^{-1}).

4.2.2 MantATP Binding

The MT•Eg5 complex was first treated with apyrase to produce the nucleotide-free state of the motor. After treatment the complex was rapidly mixed with mantATP in the Kin-Tek SF2003 stopped-flow (Kin-Tek Corp.), and an increase in fluorescence was monitored (λ_{ex} = 360 nm, λ_{em}

= 460 nm, 400 nm longpass filter). Experiments were performed using either racemic mantATP (Invitrogen Corp.) or the 3′-mant-2′-dATP isomer. Differences in the data produced using the pure isomer as compared to the racemate were not apparent (Figure 4.1D). The data were best fit by a double exponential function. The rate of the initial exponential phase was plotted as a function of mantATP concentration and fit both hyperbolically and to Equation 4,

$$k_{obs} = K_1 k_{+1}'[\text{ATP}]/(K_1[\text{ATP}] + 1) + k_{-1}' \qquad \text{(Eq. 4)}$$

where K_1 represents the equilibrium association constant for the collision complex ($K_d = 1/K_1$) and k_{+1}' is the maximum rate of the first-order isomerization. The second-order rate constant for mantATP binding is defined by $K_1 k_{+1}'$, and the y-intercept defines the dissociation rate, k_{-1}'.

The second phase of the fluorescence enhancement displayed a linear dependence on mantATP concentration. The observed exponential rates of second phase as well as the first phase, at low concentrations of mantATP, where the data approximate a line, were fit to the linear function,

$$k_{obs} = k_{on}*[\text{ATP}] + k_{off} \qquad \text{(Eq. 5)}$$

where k_{obs} is the observed exponential rate of fluorescence enhancement, k_{on} is the second-order rate constant of nucleotide binding, and k_{off} is the dissociation rate obtained from the y-intercept.

4.2.3 Pulse-Chase Measurement of ATP Binding

Preformed MT•Eg5 complexes were rapidly mixed with MgATP + trace [α^{32}P]ATP in the KinTek chemical quench-flow instrument for a set time and chased with an excess of unlabeled MgATP (10 mM final). The reaction was allowed to proceed for 10 half-lives and quenched with formic acid. [α^{32}P]ADP and P_i were separated from ATP using thin layer chromatography and quantified using Image Guage V4.0 software (Fuji Photo Film U.S.A.). The individual transients were fit to the burst equation,

$$[\text{ADP}] = A*[1-\exp(-k_b t)] + k_{slow} t \qquad \text{(Eq. 6)}$$

where A is the amplitude of the initial burst of product formation on the active site during the first turnover, t is the time in seconds, k_b is the rate constant of the exponential burst, and k_{slow} is the rate of subsequent ATP binding events.

4.2.4 Acid-Quench Experiments

A preformed MT•Eg5 complex was rapidly mixed with MgATP + trace [α^{32}P]ATP in the quench-flow. At varying times of incubation, reactions were quenched with 5 M formic acid, and product formation was both resolved and quantified in the same manner as described for the pulse-chase experiments. Single turnover experiments were performed with Eg5-513 active sites in excess of MgATP concentration. The data from these experiments were fit to a single exponential function.

4.2.5 Phosphate Release

A solution containing a preformed MT•Eg5 complex and the MDCC labeled phosphate binding protein from *E. coli* (MDCC-PBP) [143, 299] was rapidly mixed with MgATP in the stopped-flow instrument (λ_{ex} = 425 nm, λ_{em} = 466 nm, 450 nm longpass filter). Final concentrations: 0.5 μM Eg5-513, 4 μM microtubules, 20 μM Taxol, 5 μM MDCC-PBP, varying MgATP. In this assay, P_i liberated from the hydrolysis of ATP to ADP•P_i will be rapidly and tightly bound by the MDCC-PBP, eliciting a fluorescence increase [299]. To remove any P_i present in the buffer that is not a result of an enzymatic event, all solutions were supplemented with a "P_i Mop" (0.05 U/ml PNPase + 0.5 mM MEG) and incubated at 25 °C for at least 30 min prior to experimentation. The fluorescence amplitude was converted to P_i concentration using a KH_2PO_4 standard curve generated the day of the experiment [334]. Single turnover experiments were also performed with Eg5-513 active sites in excess of MgATP concentration. A MT•Eg5-513 complex (30 μM Eg5-513, 40 μM microtubules, 40 μM Taxol) was treated with apyrase, and the complex was sedimented (100,000 X g for 30 min) to remove the apyrase, AMP, and P_i that partitioned to the supernatant. The microtubule pellet was then resuspended in ATPase buffer supplemented with the "P_i Mop" and incubated at 25 °C for 20 min. The solution was adjusted to 40 μM MDCC-PBP and incubated at 25 °C for 1 hr. During resuspension, recovery of the MT•Eg5-513 complex was assumed to be 100%. To determine the concentration of Eg5-513 present following centrifugation, SDS-PAGE was performed to compare the experimental sample with an Eg5-513 standard curve.

4.2.6 Dissociation of the MT•Eg5-513 Complex

MT•Eg5-513 complex dissociation was observed by monitoring a decrease in turbidity (λ = 340 nm) in the stopped-flow instrument. A preformed MT•Eg5-513 complex was rapidly mixed with MgAXP (ATP, ADP, ATPγS, or AMPPNP). Kinetic measurements of the rate of MT•Eg5 complex dissociation were performed as a function of MgATP. The observed exponential rates were plotted and hyperbolically fit. For dissociation experiments, an additional 200 mM KCl (100 mM final) was added to the nucleotide syringe to weaken ionic interactions between the motor domains and the microtubule, therefore, slowing motor rebinding to the microtubule. Dissocation of the MT•Eg5-513 complex was also pursued by mixing motor with microtubules + MgATP without additional salt.

4.2.7 Formation of the MT•Eg5-513 Complex

The presteady-state kinetics of MT•Eg5-513 association were determined by monitoring an increase in turbidity (λ = 340 nm) in the stopped-flow instrument. Apyrase-treated or untreated Eg5-513 was mixed with increasing microtubule concentrations. The rates of the exponential phase of each transient were plotted as a function of microtubule concentration and fit to the following linear equation,

$$k_{obs} = k_{assoc}*[MT] + k_{off} \quad \text{(Eq. 7)}$$

where k_{obs} is the rate of the exponential change in turbidity, k_{assoc} is the second-order rate constant of complex formation (k_{+4}), and k_{off} is defined by the y-intercept.

4.2.8 MantADP Release

Measurements of the rate of ADP release from Eg5-513 triggered by the formation of the MT•Eg5-513 complex were performed by first incubating Eg5-513 with mantADP racemate at a 1:1 stoichiometry. The Eg5-513•MantADP complexes were subsequently mixed with increasing amounts of microtubules + 1 mM MgATP, and a decrease in mantADP fluorescence was monitored (λ_{ex} = 360 nm, λ_{em} = 460 nm, 400 nm longpass filter). The observed exponential rate constants were then fit to a hyperbola.

4.3 RESULTS

4.3.1 MantATP Binding

The rate of substrate binding by dimeric Eg5 was pursued by two methods: monitoring the fluorescence enhancement of mantATP binding to Eg5-513 (Figure 4.1) and pulse-chase analysis (Figure 4.2). A preformed MT•Eg5-513 complex was treated with apyrase to remove any ADP that accompanied Eg5-513 through purification, and the resultant nucleotide-free complex was rapidly mixed with mantATP in the stopped-flow instrument. A nucleotide-free MT•Eg5-513 complex was used in these experiments because ADP copurified with Eg5-513 [205], has been observed to cause Eg5-513 to partition off of the microtubule [[205], and Figure 4.2C inset] , and in essence reduce the number of Eg5-513 active-sites that participate in the first mantATP binding event. The resultant mantATP transients were best fit by a double exponential function

with both phases showing a mantATP concentration dependence. This is in contrast to the monophasic transients obtained from mantATP binding to monomeric Eg5-367 [250].

At low concentrations of mantATP, the data from the initial phase can be linearly fit with the slope of the line providing a second-order rate constant of mantATP binding at 3 $\mu M^{-1}s^{-1}$ (Figure 4.1B inset). However, a plot of the observed rate as a function of mantATP concentration over the entire concentration range examined was hyperbolic with k_{max} = 54 s^{-1} and $K_{½,mantATP}$ = 11.3 μM (Figure 4.1B, Table 4). Deviation from linearity indicates that ATP binding is at least a two step process with the initial collision (K_1) followed by a rate-limiting conformational change ($k_{+1'}$). As such, the data in Figure 4.1B were also fit to Equation 4, the mathematical representation of two-step substrate binding. The fit of the data provided a second-order rate constant of mantATP binding $K_1k_{+1'}$ = 5.8 $\mu M^{-1}s^{-1}$, the maximal rate of the isomerization to tight ATP binding $k_{+1'}$ = 54 s^{-1}, and an apparent $K_{d,mantATP}$ = 9.4 μM.

Data from the second, slower exponential phase can also be fit to a linear function providing a second-order rate constant for mantATP binding of 0.14 $\mu M^{-1}s^{-1}$ (Figure 4.1C). The concentration dependence of both phases suggests that this assay is monitoring two separate nucleotide binding events by two distinct populations, presumably Head-1 *versus* Head-2 of the dimeric molecule.

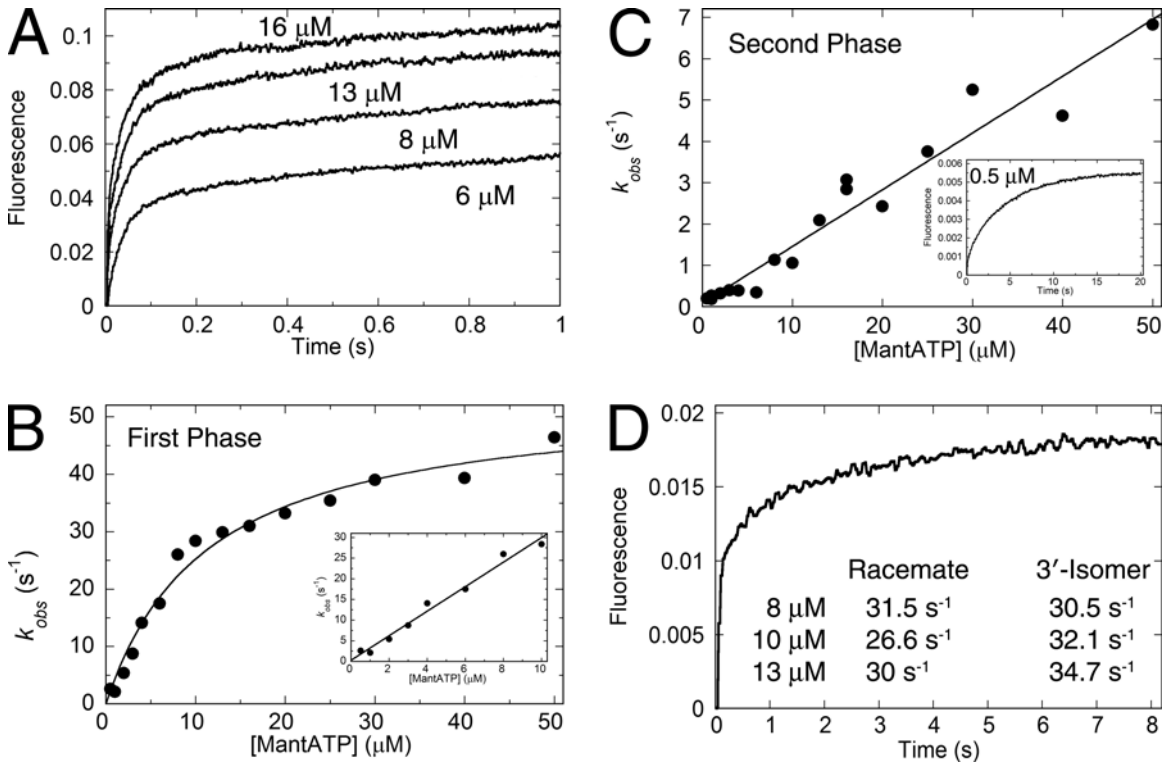

Figure 4.1 MantATP Binding

A MT•Eg5-513 complex was first treated with apyrase and then rapidly mixed with MgMantATP in the stopped-flow instrument. Final concentrations after mixing were 0.5 μM Eg5-513/8 μM microtubules for 0.5-4 μM MgMantATP and 2.5 μM Eg5-513/8 μM microtubules for 4-50 μM MgMantATP. *A*, The averaged fluorescence transients for the listed MgMantATP concentrations are displayed. *B*, Each transient was fit to a double exponential function, and the observed rate of fluorescence enhancement for the first exponential is plotted as a function of MgMantATP concentration. The data display a hyperbolic dependence and were fit to Equation 4 with $K_1 = 0.11 \pm 0.02\ \mu M^{-1}$, $k_{+1'} = 54 \pm 2\ s^{-1}$ and $K_{d,mantATP} = 9.4\ \mu M$. *B inset,* At low substrate concentrations, the observed rates of the initial exponential phase were linear providing the second-order rate constant of MantATP binding, $k_{+1} = 3 \pm 0.2\ \mu M^{-1}s^{-1}$. *C*, The observed rates of the second exponential phase also display a linear dependence with respect to the MantATP concentration range examined. The apparent second-order rate constant of substrate binding defined by this phase is $0.14 \pm 0.01\ \mu M^{-1}s^{-1}$. *C inset*, A representative transient, 0.5 μM Eg5-513/8 μM microtubules and 0.5 μM MgMantATP, displaying the completion of both phases. The amplitudes of both phases of this transient are equal with corresponding rates of 0.41 s^{-1} and 0.12 s^{-1} respectively. *D*, A representative transient obtained from mixing a MT•Eg5-513 complex with the 3′-mant-2′-dATP isomer only. The inset table compares k_{obs} for a few mantATP concentrations.

4.3.2 ATP Binding by Pulse-Chase

To determine the kinetics of Eg5-513 binding the natural substrate, MgATP, pulse-chase experiments were performed (Figure. 4.2). A preformed MT•Eg5-513 complex was rapidly mixed with MgATP + trace [α^{32}P]ATP and chased with an excess of unlabeled MgATP. This experimental design ensures that any weakly bound radiolabeled substrate from collision complex formation will be effectively outcompeted by unlabeled substrate, and only the formation of an MT•Eg5-513•ATP complex that proceeds through ATP hydrolysis will be monitored. The individual transients were fit to the burst equation (Equation 6) (Figure 4.2A). A plot of the observed rates of the exponential burst of product formation as a function of ATP concentration can be fit to a hyperbolic function providing $k_{+1'}$ = 50 s^{-1} and $K_{d,ATP}$ = 35 μM (Figure 4.2D). At low ATP concentrations, where the data can be fit linearly, the slope of the line provides a second-order rate constant of ATP binding, k_{+1} = 1.2 $\mu M^{-1}s^{-1}$ and an off-rate determined by the y-intercept of 1.4 s^{-1} (Figure 4.2D inset). As with the mantATP binding experiment, deviation from linearity indicates multistep process with substrate binding limited by a conformational change. The observed rates from both the pulse-chase and mantATP experiments (50 s^{-1} and 54 s^{-1} respectively) are in good agreement with each other, suggesting that the experimental approaches were monitoring the same event. Furthermore, the fact that product formation during the first ATP turnover was visible as well as the $k_{+1'}$ being 100-fold faster than steady-state ATP turnover (Figure 3.4, [205]), indicates that ATP binding is a rapid event in the cycle.

Additional information can also be gained from the amplitude of the transients as well as from the rate of the linear phase of the transients. From the burst amplitude data, the percentage of the motor population that is participating in the first ATP turnover can be determined. In

these experiments, the effective motor population is represented only by motor bound to the microtubule. When Eg5 is free in solution, the ATPase cycle is limited by ADP release at 0.002 s^{-1} (Figure 3.3B) and will not significantly contribute to the observed signal. As evidenced by the inset SDS-polyacrylamide gel in Figure 4.2C, not all motor is bound to the microtubule at the start of the experiment and the effective motor population needs to be corrected for the motor that is free in solution. After normalizing for the percentage of the motor population that is bound to the microtubule and therefore able to bind and hydrolyze ATP at the microtubule-activated rate, 97 ± 5% of motor active sites were competent to bind and hydrolyze ATP during the first turnover. The $K_{d,ATP}$ determined from the burst amplitude data at 57 μM (Figure 4.2F) is higher than the $K_{d,ATP}$ determined from the rate of the burst in Figure 4.2D at 35 μM. The $K_{d,ATP}$ difference is suggestive that the burst rate is monitoring Head-1 while the burst amplitude data represent both Head-1 and Head-2.

The rate of the linear phase represents subsequent ATP turnovers and is therefore enzyme concentration dependent. Like the amplitude data, the rate of the linear phase must be corrected for the fraction of motor that is not bound to the microtubule at the start of the experiment. The observed rate of the linear phase approached k_{max} = 5.7 μM ADP•s^{-1} with a $K_{d,ATP}$ = 26.7 μM. Considering that only 85-90% of the motor (4.25-4.5 μM out of 5 μM) was bound to the microtubule under the experimental conditions (Figure 4.2C, inset), the predicted slow step governing subsequent ATP turnover events was 1.27-1.34 s^{-1} per μM Eg5-513.

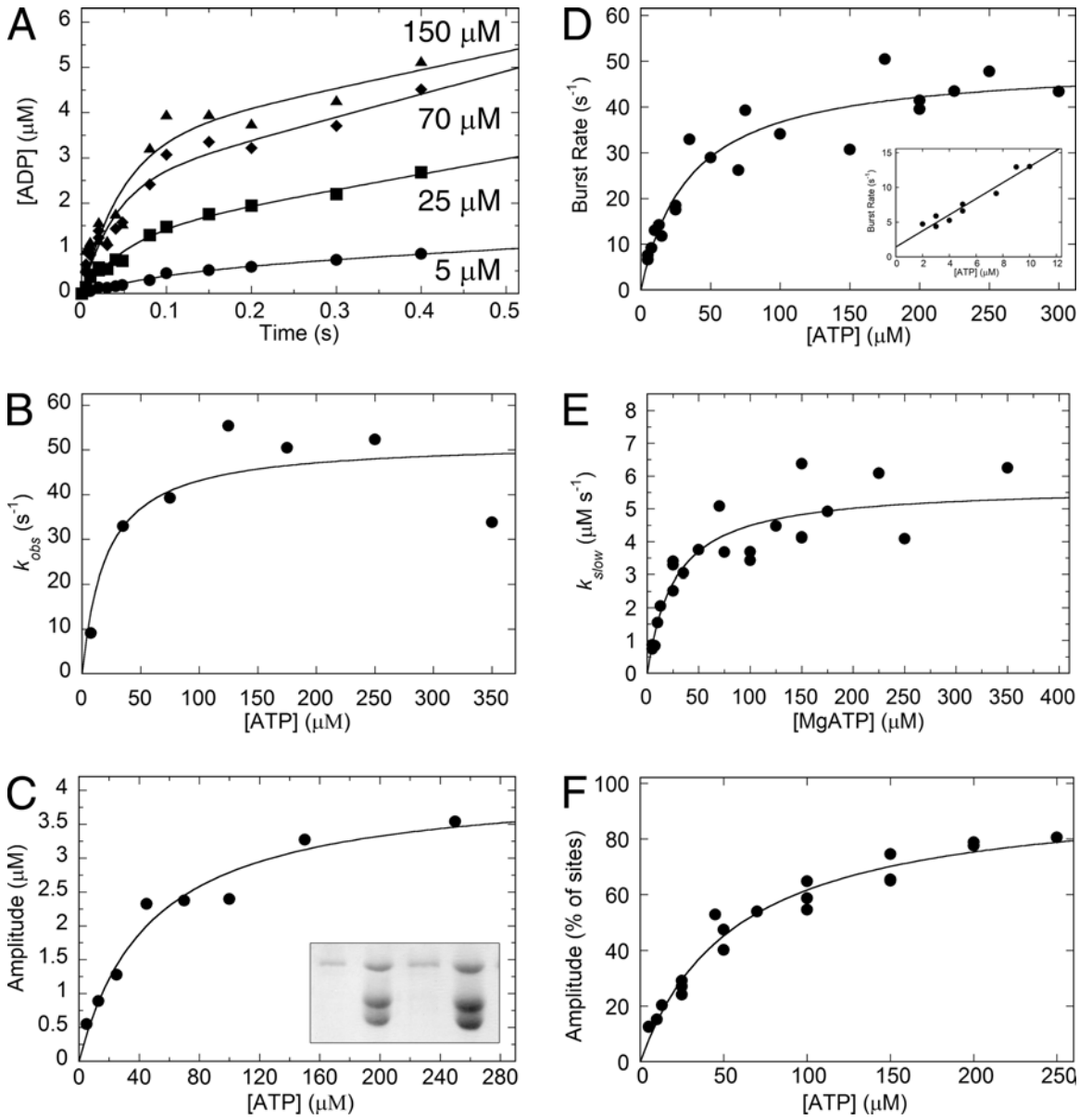

Figure 4.2 Pulse Chase Kinetics of ATP Binding

A preformed MT•Eg5 complex was rapidly mixed with Mg[α^{32}P]ATP and chased with 10 mM unlabeled MgATP. *A*, Individual transients displaying an ATP concentration-dependent presteady-state burst of product formation followed by a linear phase of product formation. *B*, The observed exponential rates were plotted as a function of MgATP concentration and fit to a hyperbola: k_{max} = 52 ± 7 s^{-1} and $K_{d,ATP}$ = 20.4 ± 14.5 μM. *C inset gel*, Not all Eg5 was bound to the microtubules at the start of the experiment. Displayed are two load volumes of the supernatant and pellet fractions of centrifuged MT•Eg5 complexes. *C*, The burst amplitude as μM ADP formed is plotted. The hyperbola extrapolates to 4.1 μM of possible 4.5 μM maximal amplitude based on the fraction of motor that was bound to the microtubules at the start of the experiment. While *B* and *C* display the data from individual experiments, *D-F* represent data from multiple experiments. *D*, the hyperbolic fit of the observed burst rates providing $k_{+1'}$ = 50

± 3 s^{-1} and $K_{d,ATP}$ = 35.3 ± 7.4 μM. The inset displays ATP binding at low ATP concentrations where the data can be linearly fit to Equation 5. The second-order rate constant for ATP binding given by the slope is k_{+1} = 1.15 ± 0.1 $\mu M^{-1}s^{-1}$ and the off-rate provided by the y-intercept is 1.4 ± 0.6 s^{-1}. *E*, The observed rates for subsequent ATP binding events obtained from the linear phase of the transients were plotted and fit to a hyperbola: k_{slow} = 5.7 ± 0.4 μM ADP•s^{-1}, $K_{d,ATP}$ = 27 ± 7 μM. *F*, The burst amplitudes from multiple experiments have been normalized according to the amount of Eg5 sites that partition with the microtubule pellet on the day of the experiment, and were plotted as function of MgATP concentration. The hyperbolic fit extrapolates to 97 ± 5 % of Eg5 active sites with $K_{d,ATP}$ = 57 ± 8 μM. Final concentrations of the MT•Eg5 complexes: 1 μM Eg5-513/6 μM MTs for 1-3 μM ATP, 2 μM Eg5-513/6 μM MTs for 2-6 μM ATP, and 5 μM Eg5-513/6 μM MTs for 5-300 μM.

4.3.3 Acid-Quench Analysis of ATP Hydrolysis

The kinetics of ATP hydrolysis were originally pursued by rapidly mixing a preformed MT•Eg5-513 complex (5 μM Eg5-513, 6 μM microtubules) with Mg[α^{32}P]ATP in excess of enzyme concentration in the quench-flow instrument. Surprisingly, a burst of product formation during the first ATP turnover was not observed as compared to the pulse-chase transients at the same ATP concentration (Figure 4.3). There are several possibilities that can account for this result: *(1)* ATP binding is rate limiting, *(2)* steady-state ATP turnover is fast enough to significantly obscure visualization of the burst phase, *(3)* copurifying ADP is occupying the active sites, *(4)* ATP hydrolysis is the rate limiting step in the mechanism. The first hypothesis, that the ATP hydrolysis step is limited by rate limiting substrate binding, must be rejected because ATP binding is a fast step (Figures 4.1-4.3).

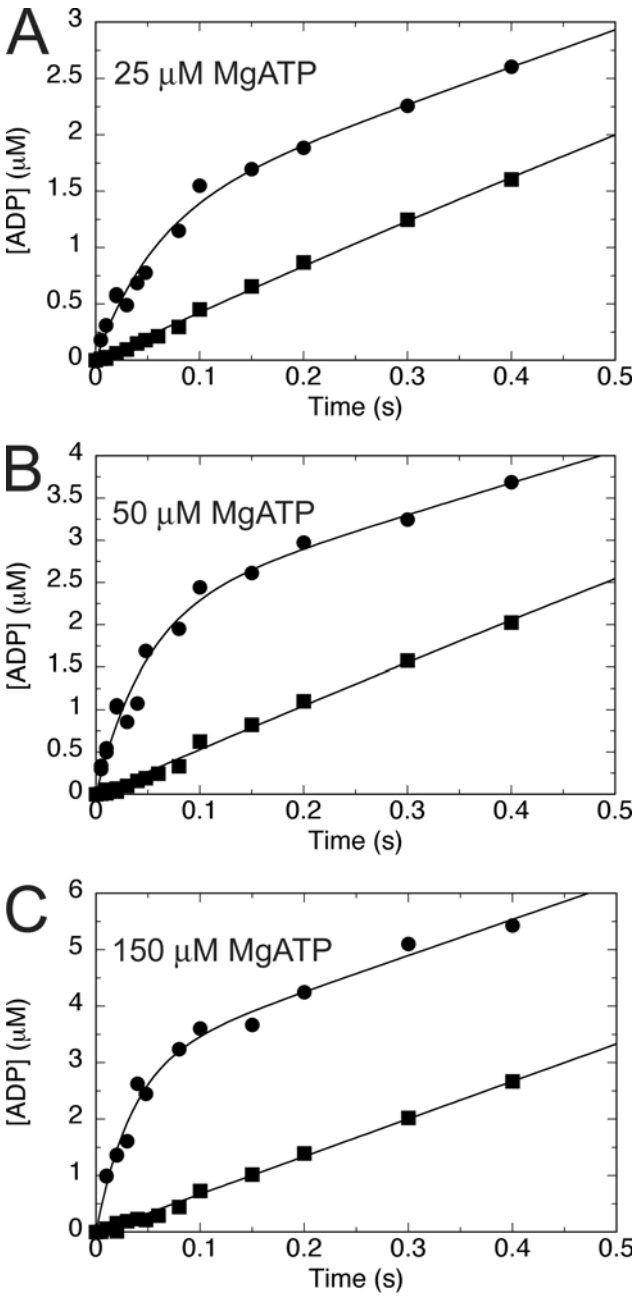

Figure 4.3 Comparison of Pulse Chase and Acid Quench Transients

Pulse-chase (●) and acid-quench (■) experiments were performed on the same day at the specified MgATP concentrations. Note the absence of a presteady-state burst in the acid-quench transients, yet present in each pulse-chase transient.

To address the hypothesis that steady-state ATP turnover is obscuring the burst phase, additional KCl was added to the nucleotide syringe. In the case of conventional kinesin [143,

181, 335] and monomeric Eg5 [250], additional salt was added to the nucleotide syringe to better visualize the burst phase. The additional salt did not have an affect on the first ATP turnover, but was able to lower steady-state by weakening ionic interactions between the motor domains and the microtubule. In this design, dissociation of the MT•motor complex is favored following the initial ATP hydrolysis event: effectively disrupting the microtubule's ability to enhance ATP turnover and revealing the burst phase. Incorporation of an additional 100 mM KCl (final after mixing) into the MgATP syringe did not permit resolution of a burst of product formation in the case of Eg5-513 (Figure 4.4A).

ADP has been demonstrated to have an affect on the equilibrium of the MT•Eg5-513 complex [Figures 3.5, 4.2C inset, [205]], and there was the possibility that it could be influencing the experimental readout. Removal of copurifying ADP by apyrase treatment was done to ensure that all motor was bound to the microtubule [Figure 3.5, [205]], and there would be no nucleotide to compete with ATP for binding sites at the start of the experiment. A burst of product formation was not observed when the MT•Eg5-513 complex was pretreated with apyrase prior to performing the acid quench experiment (Figure 4.4B). The failure to resolve product formation during the first turnover event from subsequent ATP turnovers using several experimental designs, in conjunction with ATP binding being a rapid event, implied that ATP hydrolysis may be the rate-limiting step in the cycle.

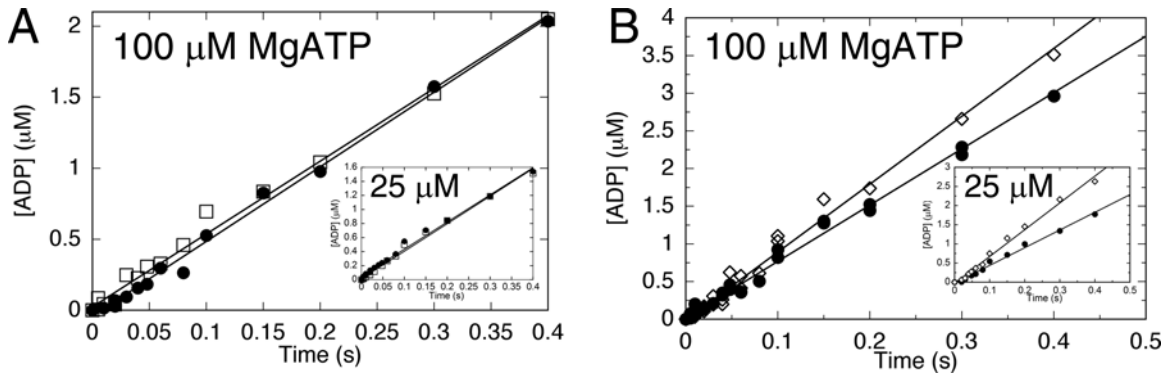

Figure 4.4 Inability to Resolve First Hydrolysis Event

A preformed MT•Eg5 complex was rapidly mixed in the quench-flow with Mg[α^{32}P]ATP, and the reaction was quenched with formic acid. Final concentrations: 5 μM Eg5-513, 6 μM microtubules, varying MgATP. *A*, Subsequent ATP turnovers were slowed by the addition of KCl to the MgATP syringe. The data in the presence (□) and absence (●) of 100 mM KCl are similar and appear linear. *B*, Treatment of the MT•Eg5 complex with 0.1 U/ml apyrase (◊) does not resolve of a presteady-state burst.

4.3.4 Single Turnover Analysis of ATP Hydrolysis

A series of single turnover experiments were pursued to test this hypothesis and to determine the intrinsic rate constant of the ATP hydrolysis step (Figure 4.5). With Eg5-513 active sites present in excess of ATP, the observed exponential conversion of ATP to ADP•P_i would reflect the intrinsic rate of ATP hydrolysis as long as the rate of substrate binding governed by [E]*k_b is faster than the intrinsic rate of ATP hydrolysis. Experimental conditions at which the observed rate of ATP hydrolysis saturated were not able to be met due to technical difficulties in combining high concentrations of motor and microtubules. At the highest concentration of MT•Eg5-513 used (45 μM Eg5-513, 50 μM microtubules, 1 μM MgATP), the observed rate was 3.3 s^{-1} with the hyperbolic fit of the data providing k_{+2} = 5.4 s^{-1} (Figure 4.5B).

With the high motor concentration used in these experiments, it was a concern that the amount of ADP copurifying with Eg5-513 was effectively competing with the low concentration of ATP at 1 μM. To examine if this hypothesis were true, the MT•Eg5-513 complex was treated with apyrase to remove the copurifying ADP. The observed rate after apyrase treatment increased slightly for most of the motor concentrations tested, suggesting that co-purifying ADP did have an impact on this experiment (Figure 4.5B). A hyperbolic fit to the data produced a k_{+2} = 9.6 ± 1.7 s^{-1}. This range of 5-10 s^{-1} for the rate of ATP hydrolysis, appears to be suitable based off of motility experiments and the MT•Eg5 dissociation kinetics (Figure 4.7) which will be discussed later.

If both Eg5-513 active sites of the dimer bound and hydrolyzed ATP independently of each other, the observed rate should be independent of ATP concentration. An ATP concentration dependence was pursued using single turnover experiments to test for cooperativity between the two motor domains. If the MT•Eg5-513 complexes were mixed with a substrate concentration greater than half the active site concentration such that both Head-1 and Head-2 bind and hydrolyze ATP, the observed rate of ATP hydrolysis was reduced by almost half (Figure 4.5C). These results provide compelling evidence that the two motor domains hydrolyze ATP in a sequential fashion in these single turnover experiments.

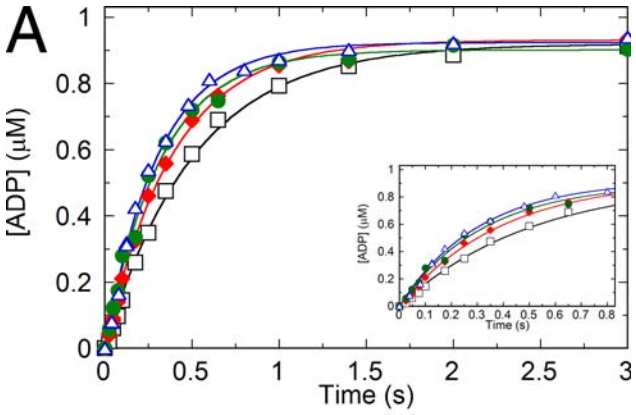

C

Single Turnover Rate as a Function of Eg5 Site Participation

[Eg5]	Apyrase	k_{obs} [ATP]<50% Eg5 Sites	k_{obs} [ATP]>50% Eg5 Sites
15 μM	+	2.7-2.8 s^{-1} 2.7 ± 0.1 s^{-1} n = 2	1.6-1.8 s^{-1} 1.7 ± 0.1 s^{-1} n = 2
20 μM	-	2.3-2.6 s^{-1} 2.5 ± 0.1 s^{-1} n = 4	1.2-1.7 s^{-1} 1.4 ± 0.1 s^{-1} n = 4

Figure 4.5 Single Turnover Acid Quench Kinetics of ATP Hydrolysis

A, A prefomed MT•Eg5 complex was rapidly mixed with Mg[α^{32}P]ATP in the quench-flow. Final concentrations were 15 μM Eg5-513/20 μM microtubules (□), 20 μM Eg5-513/25 μM microtubules (♦), 30 μM Eg5-513/35 μM microtubules (●), 45 μM Eg5-513/50 μM microtubules (Δ) and 1 μM MgATP. Each transient was fit to a single exponential function. *B*, The observed exponential rates were plotted as a function of Eg5-513 concentration and hyperbolically fit; k_{+2} = 5.4 ± 1 s^{-1}. The (♦) represents data from a MT•Eg5 complex that was pretreated with apyrase, k_{+2} = 9.6 ± 1.7 s^{-1}. *Inset,* Transients obtained on the same day from a MT•Eg5 complex (45 μM Eg5-513, 50 μM microtubules final concentrations after mixing) in the absence of apyrase pretreatment (●) and treated with apyrase (♦). No treatment, k_{obs} = 3.3 ± 0.1 s^{-1} compared to 4.8 ±

0.2 s^{-1} with apyrase treatment. *C*, The rate of ATP hydrolysis was examined by varying the MgATP concentration to evaluate ATP hydrolysis for one head *versus* two heads of the dimer at single turnover conditions.

4.3.5 Phosphate Release

If the kinetic step of ATP hydrolysis were the slowest step in the enzymatic cycle, then any step following ATP hydrolysis, such as phosphate release, should be limited by ATP hydrolysis. The rate of phosphate release was first examined by mixing an MT•Eg5-513 complex and MDCC-PBP with ATP in excess of motor concentration (Figure 4.6A). Under these conditions, product formed in the first turnover could not be separated from subsequent ATP hydrolysis events. As an example (Figure 4.6A), when the MT•Eg5-513 complex was mixed with MgATP (0.5 μM Eg5-513, 2 μM MTs, 10 μM MgATP), k_{obs} = 0.22 s^{-1} with the burst amplitude equal to 3 μM phosphate based on the KH_2PO_4 standard curve (Figure 4.6A). These results at 0.5 μM Eg5-513 indicate that the slow exponential phase of phosphate release represents six ATP turnovers.

Single turnover experiments were also performed to monitor the first phosphate release event. An apyrase treated MT•Eg5-513 complex plus MDCC-PBP was rapidly mixed in the stopped-flow with MgATP (Final: 11 μM Eg5-513, 20 μM microtubules, 20 μM MDCC-PBP, 1 μM MgATP). The resultant single exponential function displayed k_{obs} = 1.9 s^{-1} with an amplitude corresponding to 0.98 μM phosphate (Figure 4.6B). The observed amplitude is in good agreement with the expected amplitude of 1 μM phosphate released from 1 μM ATP. Furthermore, single turnover ATP hydrolysis data of an apyrase-treated MT•Eg5-513 complex at 11 μM Eg5-513 predicts ATP hydrolysis at 1.85 s^{-1} (Figure 4.5B). The observed rate of

phosphate release at 1.9 s^{-1} supports the hypothesis that phosphate release is limited by ATP hydrolysis.

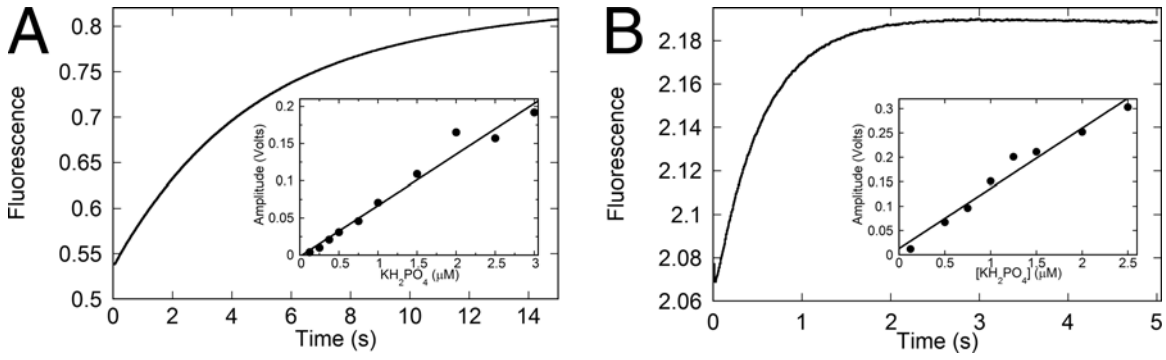

Figure 4.6 Phosphate Release

A, A preformed MT•Eg5-513 complex plus MDCC-PBP was mixed in the stopped-flow with MgATP. Final concentrations: 0.5 μM Eg5-513, 2 μM microtubules, 5 μM MDCC-PBP, 10 μM MgATP. The transient displays an amplitude corresponding to 3 μM P_i with k_{obs} = 0.22 ± 0.0002 s^{-1}. *B*, A preformed MT•Eg5-513 complex plus MDCC-PBP was mixed in the stopped-flow with MgATP at single turnover conditions. Final concentrations: 15 μM Eg5-513, 20 μM microtubules, 20 μM MDCC-PBP, 1 μM MgATP). The data were fit to a single exponential function with k_{obs} = 1.9 ± .002 s^{-1} with the amplitude of 0.98 μM. *A, B insets*, The KH_2PO_4 standard curves used to convert fluorescence voltage to μM P_i released for the corresponding experiments.

4.3.6 Dissociation of the MT•Eg5-513 Complex

To evaluate whether Eg5 detachment from the microtubule occurred following ATP hydrolysis as has been observed for conventional kinesin, Ncd, Kar3, and monomeric Eg5, dissociation of the MT•Eg5-513 complex was explored as a function of various nucleotides and nucleotide analogues [250, 336, 337]. A preformed MT•Eg5-513 complex was rapidly mixed in the stopped-flow with 2 mM MgAXP (ATP, ADP, AMPPNP, or ATPγS) or buffer supplemented with salt (100 mM KCl final concentration). Again, the presence of additional salt does not

affect the first ATP turnover but weakens MT•motor interactions such that the dissociated state becomes more predominant [143, 181, 250, 335] . A slight decrease in turbidity was seen in the presence of the nonhydrolyzable ATP analogue AMPPNP and the slowly hydrolysable analogue ATPγS. However, the amplitudes of the transients were quite small and similar to that of buffer, suggesting that the decrease was caused by the presence of the additional KCl and not the nucleotide (Figure 4.7A). In contrast, if the MT•Eg5-513 complex were mixed with either MgATP or MgADP, a dramatic decrease in turbidity was detected. In conjunction, these results further support Eg5-513•ADP as a weak microtubule binding state and suggest that dissociation occurs, as observed for other kinesin family members, after ATP hydrolysis.

Since dissociation follows ATP hydrolysis, the observed rate of dissociation should not exceed the rate of ATP hydrolysis if hydrolysis were rate-limiting in the pathway. The kinetics of dissociation were explored as a function of MgATP concentration. The individual transients were biphasic with the rate of the initial fast phase extrapolating to 6.6 s^{-1} with a $K_{½,ATP}$ = 5.4 μM (Figure 4.7). The slow rate of the second phase did not display an ATP concentration dependence (average k_{obs} = 0.7 s^{-1}).

Another expectation as a result of dissociation following ATP hydrolysis would be that the dissociation transients would display a lag before the decrease in turbidity because of the time required for ATP binding, ATP hydrolysis, and phosphate release. The presence of such a lag was not always detected in experiments with additional salt in the nucleotide syringe. Therefore, to verify that the dissociation data were indeed measuring a signal attributable to dissociation of the MT•Eg5-513 complex following ATP hydrolysis, Eg5-513 was mixed with microtubules + MgATP in the stopped-flow. There was an initial increase in turbidity as expected for motor association with the microtubule, followed by a lag of ~100 ms, and a

biphasic decrease in turbidity. This profile is consistent with MT•Eg5-513 complex formation followed by a lag representing at least one slow intermediate preceding detachment from the microtubule.

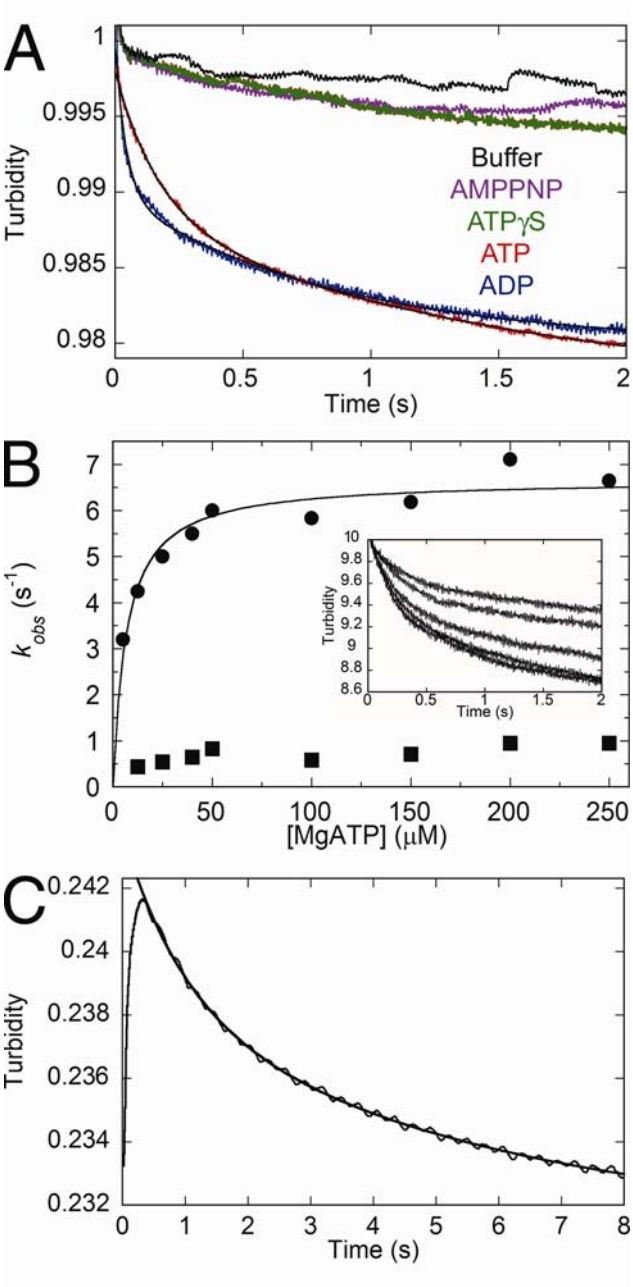

Figure 4.7 Dissociation of the MT•Eg5-513 Complex

A, A preformed MT•Eg5 complex was rapidly mixed in the stopped-flow with either buffer, MgAMPPNP, MgATPγS, MgADP, or MgATP. In each case the nucleotide syringe contained an additional 200 mM KCl resulting in final concentrations of 100 mM KCl, 1 mM MgAXP, 4 μM Eg5-513, 6 μM tubulin. The average of 4-6 transients for each condition is displayed. The ATP and ADP transients were fit to a double exponential function yielding the initial fast k_{obs} = 6.2 ± 0.2 s^{-1} and 23.9 ± 0.6 s^{-1} and the slower second phase k_{obs} = 0.76 ± 0.02 s^{-1} and 1.2 ± 0.02 s^{-1}, respectively. The amplitudes associated with the fast and slow phases were approximately equal for both the ATP and ADP transients. *B*, The observed rates of both the fast (●) and slow (■) exponential phases were plotted as a function of MgATP concentration. A hyperbolic fit to data from the initial rapid phase produces a k_{max} = 6.7 ± 0.2 s^{-1} and $K_{½,ATP}$ = 6.9 ± 1.2 s^{-1}. The data from the slower exponential phase does not vary as a function of MgATP concentration (average k_{obs} = 0.7 ± 0.1 s^{-1}). *C*, Dissociation of the MT•Eg5-513 complex was examined in the absence of additional KCl. Eg5-513 was mixed with microtubules + MgATP. Final concentrations: 5 μM Eg5, 5 μM microtubules, 1 mM ATP. The resultant transient exhibits an increase in turbidity at 14.4 ± 0.3 s^{-1} followed by a 100 ms lag, and a biphasic decrease in turbidity of equal amplitude (phase 1 k_{obs} = 1.05 ± 0.05 s^{-1}, phase 2 k_{obs} =0.19 ± 0.01 s^{-1}).

4.3.7 Microtubule•Eg5-513 Association

Besides examining steps in the mechanochemical cycle of Eg5-513 while it is associated with the microtubule, experiments were performed to address steps in the cycle leading to MT•Eg5-513 complex formation. Formation of the MT•Eg5-513 complex was measured by monitoring an increase in turbidity when Eg5-513 and microtubules were mixed in the stopped-flow. The second-order rate constant of association was measured at k_{assoc} = 2.8 $\mu M^{-1}s^{-1}$, with an off-rate of k_{off} = 9.7 s^{-1} (Figure 4.8). These kinetic constants provide a $K_{d,MT}$ = 3.5 μM which is similar to the steady-state $K_{½,MT}$ = 1.8 μM [Figure 3.4, [205]]. To address the contribution that copurifying ADP might have on the association kinetics, Eg5-513 was treated with apyrase prior to mixing with microtubules in the stopped-flow. After apyrase treatment the second-order rate constant for complex formation is k_{assoc} = 3.2 $\mu M^{-1}s^{-1}$ with an off-rate k_{off} = 7.7 s^{-1}, and $K_{d,MT}$ = 2.4 μM . These kinetic constants are similar, and the results indicate that the magnitude of k_{off} was not due to the presence of copurifying ADP.

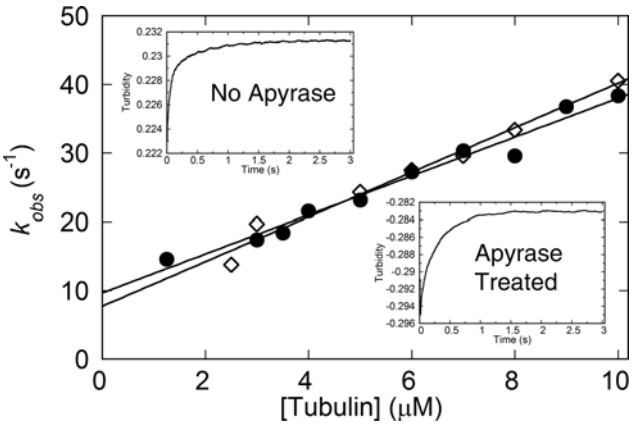

Figure 4.8 Association of Eg5-513 with Microtubules

Eg5-513 ± apyrase treatment was rapidly mixed with microtubules in the stopped-flow instrument, and the increase in turbidity was monitored. Final concentrations are 1.25 μM Eg5-513 for 1.25-2.5 μM microtubules, 2.5 μM Eg5-513 for 2.5-5 μM microtubules, 5 μM Eg5-513 for 5-10 μM microtubules. The individual transients were fit to a double exponential function, and the observed rate of the initial fast phase was plotted as a function of microtubule concentration. The data were fit to Equation 7, yielding a second-order rate constant for complex formation in the absence of apyrase treatment (●) of 2.8 ± 0.2 $\mu M^{-1}s^{-1}$ and 3.2 ± 0.2 s^{-1} with apyrase treatment (◊), and an off-rate provided by the y-intercept of 9.7 ± 1 s^{-1} (no apyrase treatment) and 7.7 ± 1.4 $\mu M^{-1}s^{-1}$ with apyrase treatment. *Insets*, representative MT•Eg5 association transients with and without apyrase treatment (*upper left*: 5 μM Eg5-513, 8 μM microtubules final) or with apyrase treatment (*lower right*: 5 μM Eg5-513, 5 μM microtubules final concentrations).

4.3.8 MantADP Release from Eg5-513

To measure the rate of ADP release with motor collision with the microtubule, Eg5-513 was first incubated with an equimolar amount of mantADP to exchange bound ADP with the fluorescent analogue. Eg5-513•mantADP was then rapidly mixed with microtubules plus 1 mM MgATP in the stopped-flow, and the decrease in fluorescence upon mantADP release from the active site was monitored. The addition of non-fluorescent MgATP to the reaction served to diminish the probability that mantADP released to the solution would rebind the motor domain. The resultant

fluorescence decrease was biphasic with the initial fast phase producing k_{+4} = 28 s^{-1} with a $K_{½,MTs}$ = 3.7 μM (Figure 4.9). The slower phase was also microtubule concentration dependent with k_{max} = 0.5 s^{-1} and a $K_{½,MTs}$ = 13 μM.

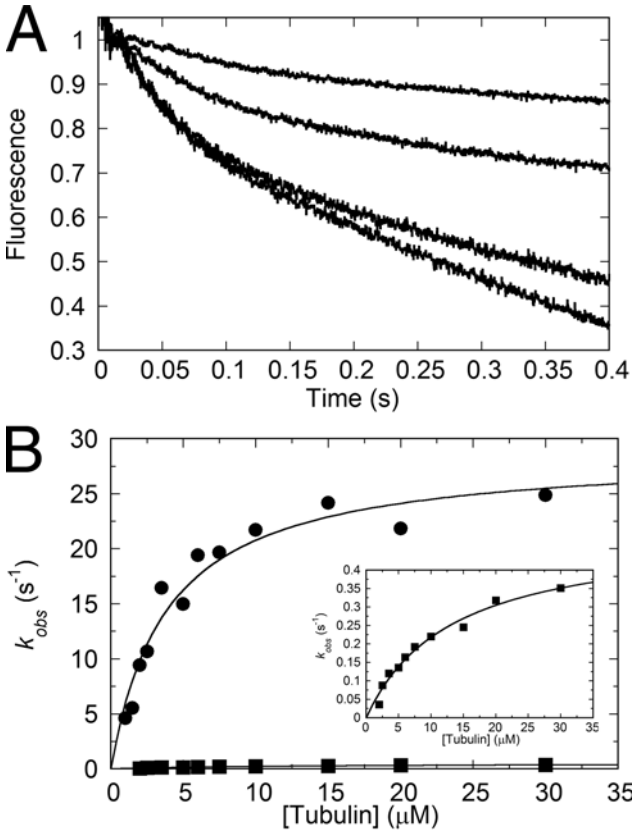

Figure 4.9 MantADP Release

The Eg5•MantADP complex was rapidly mixed with microtubules + MgATP in the stopped-flow and the decrease in MantADP fluorescence emission was monitored. Final concentrations were 2 μM Eg5-513•mantADP, 1 mM MgATP, 2-30 μM microtubules. *A*, The individual transients were biphasic. *B*, the observed rates of both phases were plotted as a function of microtubules concentration and hyperbolically fit. The fits for the first (●) and second (■) phases extrapolate to k_{+4} = 29 ± 2 s^{-1}, $K_{½,MT}$ = 3.8 ± 0.7 μM, and k_{max} = 0.5 ± .04 s^{-1}, $K_{½,MT}$ = 13 ± 2 μM respectively. *Inset*, the observed rates of the second phase.

4.4 DISCUSSION

This study provides kinetic evidence for the observed processive stepping of dimeric Eg5 [333]. Dimeric Eg5-513 like conventional Kinesin-1 alternates the enzymatic cycles of its motor domains to ensure that one motor domain is tightly bound to the microtubule while the other detaches to rebind at its next microtubule site 16 nm away and toward the microtubule plus-end. Dimeric Eg5 also has the striking characteristic of having a rate-limiting catalytic step while microtubule associated. This result is in direct contrast to what has been observed for the Eg5 monomer [250] and unlike any other kinesin we have examined to date. Therefore, Eg5 is not simply a slower version of conventional Kinesin-1 although both motors step toward microtubule plus-ends, are processive, and exhibit cooperative interactions.

4.4.1 ATP Hydrolysis is Rate Limiting for Eg5-513

For monomeric Eg5, the rate-limiting step in the ATPase cycle was proposed to be the coupled step of phosphate release and detachment from the microtubule [250]. The data presented here suggest that the rate-limiting step for dimeric Eg5 is altered from that of the monomer. A presteady-state burst of product formation was not observed for MT•Eg5-513 for the step of ATP hydrolysis using acid-quench techniques with ATP in excess of Eg5-513 active sites (Figure 4.3, 4.4). This result was surprising because all other kinetically characterized kinesin motors have displayed a presteady-state burst of product formation under these conditions [143, 156, 158, 172, 175, 179, 180, 182, 250, 338]. The analysis of ATP binding by pulse-chase or with mantATP indicates that ATP binding is a rapid step in the cycle with the ATP-dependent

isomerization, $k_{+1'}$ *at* 50 s^{-1} (Figure 4.1, 4.2, Table 4). In addition, the single turnover acid quench experiments measured ATP hydrolysis at 5-10 s^{-1} (Figure 4.5, Table 4),

Table 4 Comparison of Monomeric and Dimeric Eg5 Constants

	Eg5-513	[2,3]Eg5-367
MantATP Binding	K_1k_{+1} = 5.8 $\mu M^{-1}s^{-1}$	k_{+1} = 3.4 ± 0.3 $\mu M^{-1}s^{-1}$
		k_{-1} = 16.3 ± 0.6 s^{-1}
	$k_{+1'}$ = 54 ± 3 s^{-1}	$k_{+1'}$ = 21.2 ± 1.3 s^{-1}
	$K_{d,mantATP}$ = 9.4 μM	$K_{½,mantATP}$ = 4.4 ± 1.1 μM
ATP Binding	k_{+1} = 1.2 ± 0.1 $\mu M^{-1}s^{-1}$	NA
(Pulse Chase)	k_{-1} = 1.4 ± 0.6 s^{-1}	NA
	$k_{+1'}$ = 50 ± 3 s^{-1}	$k_{+1'}$ = 19.7 ± 1.1 s^{-1}
	$K_{d,ATP}$ = 35.3 ± 7.4 μM	$K_{d,ATP}$ = 14.2 ± 4.1 μM
	A_{max} = 97 ± 5%	A_{max} = 75 ± 2%
	$K_{d,ATP}$ = 57 ± 8 μM	NA
ATP Hydrolysis	k_{max} = 5-10 s^{-1}	$k_{b,max}$ =10.2 ± 0.7 s^{-1}
MT•Eg5-513 Dissociation	k_{max} = 6.6 ± 0.1 s^{-1}	k_{max} = 7.7 ± 0.2 s^{-1}
	$K_{½,ATP}$ = 5.4 ± 1.3 μM	$K_{½,ATP}$ = 4.2 ± 0.3 μM
MantADP Release	k_{max} = 28.2 ± 0.5 s^{-1}	k_{max} = 43.3 ± 0.2 s^{-1}
	$K_{½,MTs}$ = 3.7 ± 0.2 μM	$K_{½,MTs}$ = 2.5 ± 0.1 μM
MT•Eg5-513 Association	k_{on} = 2.8 ± 0.2 $\mu M^{-1}s^{-1}$	k_{on} = 17 ± 2.2 $\mu M^{-1}s^{-1}$
	k_{off} = 9.7 ± 1 s^{-1}	NA
Steady-State	[1]k_{cat} = 0.48 ± 0.2 s^{-1}	k_{cat} =5.4 ± 0.1 s^{-1}
	[1]$K_{M,ATP}$ = 7.9 ± 2.4 μM	$K_{M,ATP}$ = 7.0 ± 0.4 μM
	[1]$K_{½,MTs}$ = 1.8 ± 0.2 μM	$K_{½,MTs}$ = 0.29 ± 0.02 μM

[1]Krzysiak *et al*. (34)
[2,3]Cochran *et al*. (30)

1 1′ 2 3′ 5

$$M{\bullet}E + ATP \leftrightarrows M{\bullet}E{\bullet}ATP \leftrightarrows M{\bullet}E^{*}{\bullet}ATP \leftrightarrows M{\bullet}E{\bullet}ADP{\bullet}P_i \leftrightarrows M{\bullet}E{\bullet}ADP \leftrightarrows M{\bullet}E + ADP$$

4 ⇓↑
E•ADP

suggesting that ATP hydrolysis was intrinsically slower and no faster than other steps in the ATPase cycle. This interpretation was supported by the phosphate release kinetics as well as the ATP-promoted dissociation kinetics of the MT•Eg5 complex (Figure 4.6, 4.7, Table 4). In both cases, the observed rates were no faster than ATP hydrolysis. These results in combination also indicate that phosphate release occurs as a fast step and while the motor is still associated with the microtubule.

Steps in the mechanochemical cycle not directly involved with catalysis were also examined. Both Eg5 association with the microtubule and the subsequent release of mantADP were rapid steps in the cycle (Figure 4.8, 4.9, Table 4). At present, dimeric Eg5 is the only microtubule-based motor to have its ATPase cycle slowed at the catalytic step although myosin IXb has been reported to have a rate-limiting ATP hydrolysis step as well [339, 340].

4.4.2 Eg5-513 Displays Alternating-Site Catalysis

For a processive motor, it would be logical to expect an alternating-site mechanism for ATP hydrolysis as observed previously for conventional Kinesin-1 [143, 162, 168, 172], and there are multiple lines of evidence that provide support for such a model for Eg5-513. The kinetics of mantATP binding, and mantADP release were biphasic (Figure 4.1, 4.9), suggesting that the second phase of each was gated by a slower structural transition. In addition, the single turnover experiments for ATP hydrolysis show that the observed rate decreases by approximately half when both heads of the Eg5 dimer bind and hydrolyze ATP as compared to an experiment in which only one head of the dimer can bind and hydrolyze ATP (Figure 4.5C). Lastly, two dissociation constants for ATP have been observed with one being ~5-10-fold tighter than the

other (Table 4). The higher affinity for ATP was seen in the mantATP binding experiments (~9 μM), the ATP promoted dissociation of the MT•Eg5-513 complex (~6 μM), and in the steady-state $K_{m,ATP}$ (~8 μM). The pulse-chase analysis of ATP binding however produced a $K_{d,ATP}$ of ~60 μM. Because the higher $K_{d,ATP}$ in the pulse-chase experiments was obtained from a plot of the burst amplitude, which is a reflection all of the Eg5-513 sites, and the tighter affinity for ATP only require substrate binding by one motor domain, these different ATP affinities suggest a biochemical asymmetry between the two motor domains favoring ATP binding to one motor domain only. Although these results taken together are consistent with an alternating-site mechanism for catalysis, they do not address the nature of the gating between the two motor domains (see Chapter 6)

4.4.3 Establishing the Processive Run

The kinetic data presented in this chapter argue for a rate-limiting step of ATP hydrolysis between 5-10 s^{-1}. This range is acceptable with relation to the predicted steady-state rate of 11.9 s^{-1} obtained from single molecule studies [333], but it cannot account for the steady-state k_{cat} of 0.48 s^{-1} determined by our solution studies [205]. Could the solution steady-state measurements just be inaccurate? This is not likely as the rate of the linear phase from the pulse-chase transients (Figure 4.2E) was measured at ~1.3 s^{-1}. If steady-state ATP turnover was in fact the 12 s^{-1} suggested by the motility studies, the rate of the linear phase governed by the slowest step in the ATPase cycle should be measured to be near 12 s^{-1}. Furthermore, a kinetic event that could correspond to the solution k_{cat} was observed in the second phase of mantADP release transients with k_{obs} = 0.5 s^{-1} (Figure 4.9).

So, where does this steady-state limiting event fit in the ATPase cycle of dimeric Eg5? This event does not appear to occur during the first ATP turnover. If ATP hydrolysis at 5-10 s^{-1} were followed by a slow step at 0.5 s^{-1}, a presteady-state exponential burst phase followed the linear phase at 0.5 s^{-1}, once enzyme concentration was considered, would have been easily detected in the acid quench experiments. Furthermore, the single molecule results from Valentine and Fordyce et al. [333] indicate that the rate-limiting step during a processive run must occur significantly faster than 0.5 s^{-1} and at ~10 s^{-1}. Therefore, the steady-state governing slow step cannot occur while the motor is converting chemical energy to mechanical energy, i.e. stepping along the microtubule. Also, the experiments to determine the kinetics of ATP binding, ATP hydrolysis, P_i release, and motor detachment from the microtubule were all begun with a preformed MT•Eg5 complex. These events were not seen to be limited by the steady-state governing step, indicating that it is possible for this event to be completed by the mere incubation of dimeric Eg5 and microtubules. This slow step must occur upon formation of the MT•Eg5-513 complex because the event tied to this slow step was visualized as a second phase in the mantADP release experiments.

Dimeric Eg5 is proposed to rapidly associate with the microtubule and couple release of ADP from at least one of its motor domains to a slow structural transition occurring only after the initial contact of the motor with the microtuble. Once this transition has occurred, then each additional step is limited by ATP hydrolysis until the processive run is ended with the Eg5 motor falling off the microtubule. Dimeric Eg5 exhibits very short processive runs of approximately 8 steps [333], while Kinesin-1 can continue for > 100 steps [148-151]. Because of the short processive run length of dimeric Eg5, the steady-state solution studies would be more sensitive

to the slow transition that begins the processive run rather than the ATP hydrolysis step within the processive run.

Based on their fluorescence resonance energy transfer (FRET) studies with monomeric Eg5, Rosenfeld et al. proposed that neck-linker docking occurred upon collision with the microtubule [251]. The FRET results in combination with the single molecule studies and the kinetics presented here suggest a model in which there is a structural transition, possibly neck-linker docking, that occurs at ~0.5-1 s^{-1}, yet once the Eg5 motor begins stepping, then its movement is limited by ATP hydrolysis at ~5-10 s^{-1}. From the work presented in this chapter, the communication from Head-1 to Head-2 that maintains the two heads out-of-phase and controls the processive stepping is unknown. These cooperativity questions will be addressed in Chapter 6 where experiments that examine the nucleotide state of the motor domains of dimeric Eg5 both before the steady-state rate-limiting conformational change and during processive stepping are presented.

5.0 CHARACTERIZATION OF R234K

The R210K mutation in *Drosophila* conventional kinesin resulted in a motor that displayed severely inhibited ATP hydrolysis, though otherwise a wild-type kinetic profile. The homologous mutation, R234K, was made in dimeric human Eg5, Eg5-513. The R234K mutant displayed a 20-fold reduction in steady-state ATP turnover and > 100-fold reduction in the rate of ATP hydrolysis. Microtubule association, which is a rapid event for the Eg5-513, was surprisingly enhanced 9-fold. ATP binding was at least a two step process with a comparable maximal rate to that of Eg5-513. Most importantly, ADP release was biphasic with the rates of both phases being comparable to that of Eg5-513.

5.1 INTRODUCTION

Point mutations have been an important tool for the dissection of the mechanochemical cycle of conventional kinesin [190, 262, 263, 265, 335, 341]. Several mutations have been made in the Switch -I and Switch-II clusters to analyze the communication pathway between the nucleotide binding pocket and the microtubule interface. A conserved arginine, R210 according to the Kinesin-1 heavy chain gene in *Drosophila melanogaster*, located in the Switch-I region has been proposed to form a salt bridge with a glutamic acid, E243, in the Switch-II cluster. When ATP is bound at the active-site, these two residues come into proximity of each other and form a salt

bridge that positions a water molecule for a nucleophylic attack on the γ-phosphate of ATP [58, 73, 74, 139, 140, 142, 258, 259]. Mutations of R210 to both an alanine and a lysine have resulted in motors that hydrolyzed ATP 1000-fold slower than wild-type [263, 265]. The R210A mutation also had the additional effect of inhibiting motor association with the microtubule whereas the R210K mutation displayed wild-type microtubule interactions.

Eg5 is a homotetrameric Kinesin-5 family member that crossbridges microtubules in the mitotic spindle and slides them relative to each other in order to assemble the bipolar spindle and maintain spindle bipolarity prior to Anaphase B [104, 106, 109, 111, 135, 137, 206, 219, 255, 342, 343]. An analysis of a truncation of the human gene resulting in a dimeric Eg5 motor, Eg5-513, has indicated that the two motor domains that interact with the same microtubule display cooperative interactions [Chapter 3, 4 and [205, 344]]. The cooperativity between these motor domains is novel with respect to previously studied kinesins. Eg5-513 has a two stage microtubule associated mechanochemical cycle: there is a period in which the motor is bound to the microtubule but presumably not turning over ATP, and a period in which the motor is turning over ATP as it steps along the microtubule [Chapter 4 and [344]]. Mechanistically, dimeric Eg5 is believed to associate with the microtubule rapidly and release bound ADP from one of its motor domains. A slow structural transition follows that is kinetically coupled to a second round of ADP release. After completion of this slow structural transition, the motor is thought to be able to convert chemical energy to mechanical energy and take multiple steps along the microtubule.

The fact that the steady-state rate-limiting transition is not detected when experiments are performed using a preformed MT•Eg5-513 complex, as well as the rate of processive stepping being 20-fold faster than steady-state ATP turnover, suggests that ATP does not affect the slow

transition. However, it does not rule out the possibility that events such as ATP binding and hydrolysis could occur on one of the motor domains of the Eg5 dimer prior to the steady-state limiting transition. If this were to happen, it would suggest that movement, force generation, and ATP turnover could be uncoupled.

To address the connection of ATP hydrolysis to the steady-state rate-limiting transition, the homologous mutation of the conventional kinesin mutant R210K was made in human dimeric Eg5, Eg5-513*R234K. As expected the R234K mutation resulted in a motor with impaired ATP hydrolysis.

5.2 MATERIALS AND METHODS

The biochemical analysis of R234K was performed in ATPase buffer at room temperature (25°C). Paclitaxel in DMSO was used throughout to stabilize the microtubule polymer. The concentrations reported are final concentrations after mixing. For the cloning and purification off R234K see, Chapter 2. Experiments were performed with the assistance of Yuan Yuan Duan.

5.2.1 Steady-State ATPase Measurements

Steady-state kinetics were determined by monitoring the hydrolysis of [α-^{32}P]ATP [306]. The rate of ATP turnover, in the presence of saturating microtubules, was measured at various ATP concentrations that produce the maximal rate for Eg5-513.

5.2.2 Microtubule Association Kinetics

The presteady-state kinetics of MT•R234K association were determined by monitoring an increase in turbidity (λ = 340 nm) in the stopped-flow instrument. The rates of the exponential phase of each transient were plotted as a function of microtubule concentration and fit to Equation 7 (see 4.2.7).

5.2.3 MantADP Release from R234K

Measurements of the rate of ADP release from R234K triggered by the formation of the MT•R234K complex were performed by first incubating R234K with a 5-fold excess of mantADP. The solution was then passed over a Bio Spin-30 gel filtration column (Bio-Rad Laboratories, Inc.) to remove any unbound nucleotide. R234K, like Eg5-513, only contains ADP on ~60% of its active sites following gel filtration (see section 6.3.1 and Table 6). The R234K•MantADP complexes were then supplemented with additional mantADP, half the active site concentration, generating at 1:1 stoichiometry of R234K active-sites to mantADP. The R234K•mantADP complexes were subsequently mixed with increasing amounts of microtubules + 1 mM MgATP, and a decrease in mantADP fluorescence was monitored (λ_{ex} = 360 nm, λ_{em} = 460 nm, 400 nm longpass filter). The observed exponential rate constants were then fit to a hyperbola.

5.2.4 MantATP Binding

The MT•R234K complex was first treated with apyrase to produce the nucleotide-free state of the motor. After treatment the complex was rapidly mixed with racemic mantATP (Invitrogen Corp.) in the Kin-Tek SF2003 stopped-flow (Kin-Tek Corp.), and an increase in fluorescence was monitored (λ_{ex} = 360 nm, λ_{em} = 460 nm, 400 nm longpass filter). The data were best fit by a double exponential function. The rate of the initial exponential phase was plotted as a function of mantATP concentration and fit to Equation 4 (see 4.2.2). At low mantATP concentrations, the data could be fit linearly, Equation 5 (see 4.2.2), to determine the second-order rate constant of substrate binding.

5.2.5 Single Turnover Measurements of ATP Hydrolysis

Preformed MT•R234K and MT•Eg5-513 complexes were rapidly mixed with MgATP + trace [α^{32}P]ATP in the quench-flow with motor active sites in excess of substrate. At varying times of incubation, reactions were quenched with 5 M formic acid, and product formation was both resolved and quantified as described in section 4.2.3. The Eg5-513 data were fit to a single exponential function, whereas the R234K data were fit linearly due to the incompletion of the enzymatic process on the time scale used.

5.3 RESULTS

The kinetic analyses of the R210A and R210K *Drosophila* conventional kinesin mutants indicated that the mutations severely limit ATP turnover, $k_{cat\text{-}R210A}$ = 0.08 s^{-1}, $k_{cat\text{-}R210K}$ = 0.03 s^{-1}, as compared to wild-type, $k_{cat\text{-}K401}$ = 20 s^{-1} [263, 265]. To see if the R234K mutation in Eg5-513 produced a similar result, the steady-state ATPase kinetics were measured at microtubule and MgATP concentrations demonstrated to saturate steady-state ATP turnover for Eg5-513. R234K, like the *Drosophila* mutants, displays an inhibited rate of ATP turnover, k_{cat} = 0.02 s^{-1}.

5.3.1 Initial Interactions of R234K with the Microtubule

To verify that the reduction in the rate of steady-state ATP turnover is due to defects in ATP hydrolysis, the transient kinetics of events leading up to (microtubule association, ADP release, and ATP binding) and including ATP hydrolysis were examined. The rate of the formation of the MT•R234K complex was pursued by mixing R234K with microtubules in the stopped-flow. Suprisingly, the arginine to lysine mutation, which displayed wild-type kinetics in the context of conventional kinesin, caused an enhancement in the second-order rate constant of microtubule binding: $k_{on\text{-}R234K}$ = 26 $\mu M^{-1}s^{-1}$, $k_{on\text{-}513}$ = 3 $\mu M^{-1}s^{-1}$ (Figure 5.1). The enhancement in microtubule binding can also be seen in the apparent dissociation constant ($K_d = k_{off}/k_{on}$): $K_{d,R234K}$ =0.9 μM, $K_{d,513}$ = 3 μM.

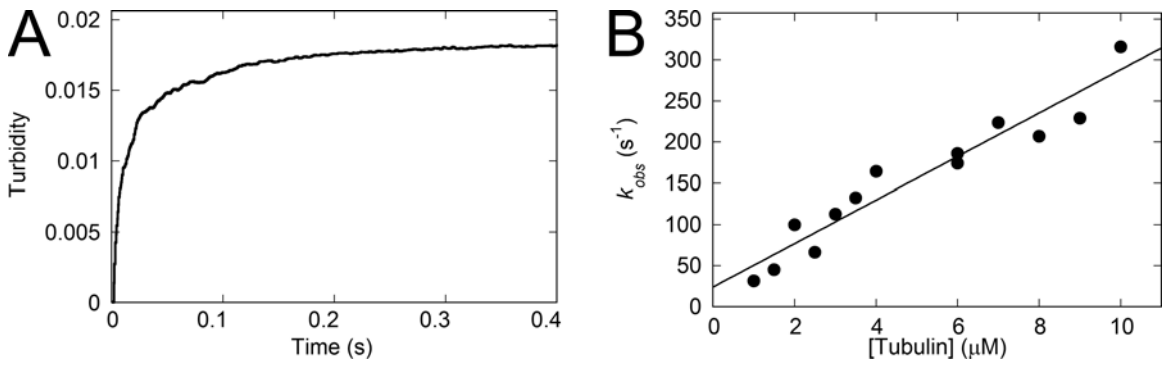

Figure 5.1 R234K Microtubule Association

R234K was rapidly mixed with microtubules in the stopped-flow instrument, and the increase in turbidity was monitored. Final concentrations: 1 μM R234K for 1-2.5 μM microtubules, 2.5 μM R234K for 2.5-6 μM microtubules, and 5 μM R234K for 6-10 μM microtubules. *A*, A representative transient at 5 μM R234K and 6 μM microtubules. *B*, Individual transients were fit to two exponentials, and the rate of the initial fast phase was plotted as a function of microtubule concentration. The data were linearly fit yielding a second-order rate constant for complex formation of 26.4 ± 2.3 $\mu M^{-1}s^{-1}$, with an off-rate provided by the y-intercept of 24.1 ± 13 s^{-1}.

After kinesins associate with the microtubule, they release any ADP that is present at their active-sites as the motor shifts from a weak to a strong microtubule binding state. Since R234K associates more rapidly with microtubules than Eg5-513, was the isomerization leading to ADP release more rapid for R234K than Eg5-513? A R234K•mantADP complex in a 1:1 stoichiometry was mixed with microtubules and ATP in the stopped-flow. As was the case with Eg5-513, the resultant transients were biphasic and best fit to a two exponential function (Figure 5.2A). The initial fast phase was comparable to what has been observed for mantADP release form Eg5-513: R234K k_{max}= 20 s^{-1}, $K_{½,MTs}$ = 3.9 μM (Figure 5.2B); Eg5-513 k_{max} = 29 s^{-1}, $K_{½,MTs}$ = 3.8 μM (Figure 4.9).

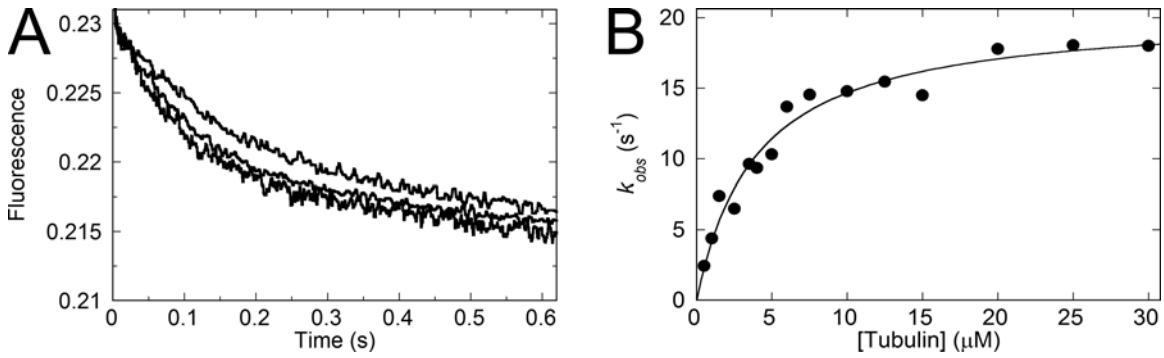

Figure 5.2 MantADP Release from R234K

R234K•mantADP in a 1:1 stoichiometry was rapidly mixed in the stopped-flow instrument with microtubules + MgATP. *A*, Representative averaged transients (Final: 2.5, 5, and 10 μM microtubules). *B*, The observed rate of the initial, fast fluorescence decrease is plotted as a function of microtubule concentration: k_{max} = 20.4 ± 0.9 s^{-1}, $K_{½,MTs}$ = 3.9 ± 0.5 μM.

5.3.2 Substrate Binding and Catalysis by R234K

Measurements of ATP binding were pursued by mixing an apyrase treated MT•R234K complex with mantATP in the stopped-flow. The resultant transients were biphasic and best fit to a double exponential function (Figure 5.3A). Like Eg5-513, the observed rate of mantATP binding by R234K does not display a linear dependence on the mantATP concentration. The hyperbolic dependence of the rate on the substrate concentration indicated that the multistep nature of ATP binding, an initial collision complex followed by an isomerization of the motor domain leading to the enhanced fluorescence, had been preserved in the R234K mutant. Fit of the data to Equation 5 gave a maximal rate for the isomerization to tight ATP binding k_{max} = 77 s^{-1}, an equilibrium association constant K_a = 0.11 μM^{-1}, an apparent $K_{d,mantATP}$ = 9.1 μM, and a second-order rate constant for the initial collision complex $K_a k_{max}$ = 8.4 $\mu M^{-1}s^{-1}$.

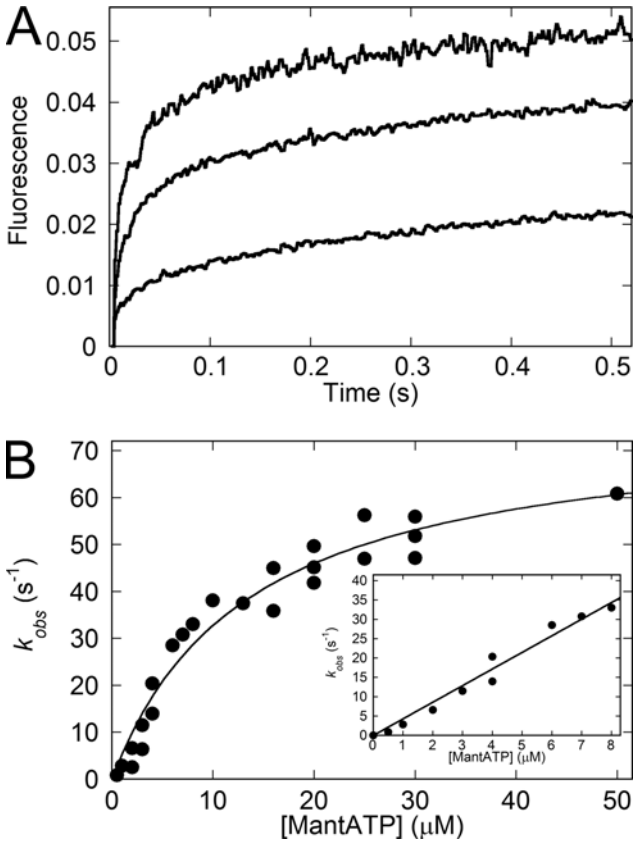

Figure 5.3 MantATP Binding by R234K

A MT•R234K complex was first treated with apyrase and then rapidly mixed with MgMantATP in the stopped-flow instrument. Final concentrations after mixing were 0.5 μM R234K/8 μM microtubules for 0.5-4 μM MgMantATP and 2 μM R234K/8 μM microtubules for 4-50 μM MgMantATP. *A*, Representative averaged transients are displayed (Final: 2 μM R234K, 2, 6, and 8 μM MgMantATP). *B*, Each transient was fit to a two exponential function, and the observed rate of fluorescent enhancement of the first phase was plotted as a function of MgMantATP concentration. As with Eg5-513, the data display a hyperbolic dependence. Fit of the data to Equation 5 yields a k_{max} = 77 ± 3 s^{-1}, K_a = 0.11 ± 0.02 μM^{-1}, a second-order rate constant of substrate binding $K_a k_{max}$ = 8.4 $\mu M^{-1}s^{-1}$, and $K_{d,MantATP}$ = 9.1 μM. *Inset*, at low MgMantATP concentrations, the data can be linearly fit providing a second-order rate constant of substrate binding of 4.3 ± 0.2 $\mu M^{-1}s^{-1}$.

With all of the events prior to ATP hydrolysis remaining rapid in the cycle, single turnover experiments to compare the rate of ATP hydrolysis of Eg5-513 with that of R234K were performed (Figure 5.4). Either an apyrase treated MT•Eg5-513 or a MT•R234K complex was mixed with limiting MgATP (Final: 20 μM motor/25 μM microtubules, 1 μM ATP). The

MT•Eg5-513 complex converted all substrate to product at a rate expected for the given conditions (see Figure 4.5). R234K was capable of hydrolyzing ATP to ADP•P_i but does so 100-fold slower than Eg5-513. The Eg5-513 data were fit to a single exponential function providing k_{obs} = 2.9 s^{-1}. Due to the incompletion of the enzymatic process by R234K on the time scale used, the data were fit linearly, k_{obs} = 0.08 s^{-1}.

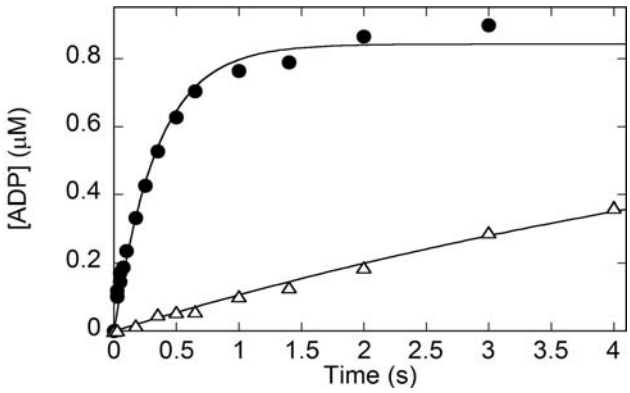

Figure 5.4 R234K has Impaired ATP Hydrolysis

An apyrase treated MT•R234K (△) or a MT•Eg5-513 (●) complex was rapidly mixed with Mg[α^{32}P]ATP in the rapid quench-flow instrument. Final concentrations: 20 μM motor, 25 μM microtubules, and 0.8 μM MgATP. The Eg5-513 data was fit to a single exponential function, k_{obs} = 2.9 ± 0.2 s^{-1}, while the R234K data was fit to a line k_{obs} = 0.08 ± 0.003 s^{-1}.

5.4 DISCUSSION

The purpose of generating Eg5-513 with an R234K mutation was to engineer a dimeric Eg5 motor that functions comparable to wild-type but has significantly impaired ATP hydrolysis such that the contribution of ATP hydrolysis to various stages in the dimerc Eg5 mechanochemical cycle can be examined. The primary step of interest was the release of ADP upon MT•Eg5

complex formation that is kinetically coupled to the steady-state rate-limiting transition. This stage in the mechanochemical cycle was of particular interest because of its implications for Eg5 processivity. MantADP release experiments using Eg5-513 (Figure 4.9) were biphasic with one rapid phase and one slow phase. The traditional interpretation of this result, based on the mechanochemical cycles of conventional kinesin and Ncd, would be that each phase of mantADP release from Eg5-513 represents ADP being released from a specific motor domain. The rate of the initial rapid phase of ADP release is ~50-fold faster than the rate of the secondary phase (Figure 4.9). Therefore, one motor domain will be nucleotide-free and potentially capable of binding and hydrolyzing ATP before the second motor domain could release its ADP. This would result in the motor containing ADP on both motor domains and dissociation of the MT•Eg5-513 complex should be favored, (Figure 4.7) inhibiting the motors ability to move processively.

The use of R234K in addressing the contribution of ATP hydrolysis to various transitions in the mechanochemical cycle of dimeric Eg5 seems reasonable (Table 5). As expected ATP hydrolysis was severely inhibited, > 100-fold, in comparison to wild-type. Release of ADP upon formation of the MT•R234K complex displayed two phases and comparable rates to what has been observed for wild-type. ATP was found to bind to R234K with the same affinity and at a comparable rate. The only other significant difference, beside the rate of ATP hydrolysis, between R234K and Eg5-513 was in the association of the motor with microtubules. R234K displays a second-order rate constant of microtubule association that is ~9-fold faster than what has been measured for Eg5-513. This result was unexpected as the arginine to lysine mutation was not seen to have this effect on conventional kinesin [265]. Helix-α4, a part of the Switch-II cluster containing the glutamic acid that forms a salt bridge with the arginine in question,

effectively relaying the nucleotide state to the microtubule binding interface, has been observed to be 1.5 turns longer and rotated in comparison with conventional kinesin [243]. Conventional kinesin normally displays a second-order rate constant of microtubule association between 10-20 $\mu M^{-1}s^{-1}$. Possibly, rearrangements caused by the R234K mutation allow Helix-α4 to adopt a more conventional kinesin-like appearance to account for the enhancement in microtubule binding. Regardless, enhancing the rate of a fast step in the ATPase cycle should not impact the mechanistic interpretations based on work with this mutant.

One possible complication that could arise based off of enhanced microtubule interactions would be if the kinetics of ADP release following microtubule association should also be enhanced. If the ADP release kinetics were different, this mutant could not be used to address the importance, if any, of ATP hydrolysis on the second phase of ADP release. Fortunately, the ADP release kinetics of both R234K and Eg5-513 are identical (Table 5). Along those lines, the presence of two phases of ADP release for both mutant and wild-type indicate that ATP hydrolysis does not cause the second phase of ADP release. This will be expounded upon in Chapter 6.

Table 5 Comparison of Eg5-513 and R234K Constants

	R234K	[a,b]Eg5-513
MT•R234K Association k_{on}	26.4 ± 2.3 $\mu M^{-1}s^{-1}$	2.8 ± 0.2 $\mu M^{-1}s^{-1}$
k_{off}	24.1 ± 13 s^{-1}	9.7 ± 1 s^{-1}
ADP Release	20.4 ± 0.9 s^{-1}	28.2 ± 0.5 s^{-1}
MantATP Binding k_{max}	77 ± 3 s^{-1}	54 ± 3 s^{-1}
$K_a k_{max}$	8.4 $\mu M^{-1}s^{-1}$	5.8 $\mu M^{-1}s^{-1}$
$K_{d, app}$	9.1 μM	9.4 μM
ATP Hydrolysis	0.08 s^{-1}	5-10 s^{-1}
Steady-State k_{cat}	0.02 ± 0.005 s^{-1}	0.48 ± 0.2 s^{-1}

[a]Krzysiak *et al*.[205]
[b]Krzysiak *et al*. [344]

6.0 EG5-513 MOTOR DOMAIN COORDINATION

Eg5/KSP is the major plus-end directed force for the assembly and maintenance of the mitotic spindle. Recent work using a dimeric Eg5 motor has found it to be processive; however, its mechanochemical cycle appears different from that of conventional kinesin. Dimeric Eg5 appears to undergo a conformational change shortly after collision with the microtubule that primes the motor for its characteristically short processive runs. To better understand this conformational change as well as head-head communication during processive stepping, equilibrium and transient kinetic approaches have been used to examine specific intermediates tied to these events. Unlike conventional kinesin, microtubule association is sufficient to trigger ADP release from both motor domains. One motor domain releases ADP rapidly while ADP release from the other is limited by a slow conformational change at ~1 s^{-1}. Essentially, dimeric Eg5 begins its processive run with both motor domains associated with the microtubule. However, during processive stepping, ADP release is controlled by a different mechanism. One motor domain can proceed through its mechanochemical cycle, ATP binding-ATP hydrolysis-P_i release; however, ATP must bind to its partner motor domain and be potentially hydrolyzed for the motor to release ADP and complete its 8 nm (center of mass displacement) advance.

6.1 INTRODUCTION

Eg5 is a homotetrameric, Bim C/Kinesin-5 family member that plays a vital role in the mitotic spindle, and has attracted substantial interest as a potential target for chemotherapeutic agents in cancer treatment. Eg5, as with other members of this kinesin subfamily, has been demonstrated to provide a plus-end directed force necessary to both assemble and maintain the mitotic spindle and contribute to microtubule flux within the mitotic spindle [104, 106, 109, 111, 135, 137, 206, 219, 255, 342, 343]. If Eg5 function is disrupted prior to anaphase B, the bipolar spindle will collapse into a monoaster from which the cell can no longer divide [104, 210, 217, 218, 223, 225, 226, 231-234, 236, 238, 329]. In fact, a cell that loses functional Eg5 will apoptose if the spindle checkpoint machinery is intact [7, 8].

A reductionist agenda has been heavily pursued in order to discern how a homotetrameric kinesin is able to function. Through comparison of the kinetics of monomeric and dimeric truncations of Eg5, it is evident that the two motor domains of dimeric Eg5 are able to substantially modulate each others function. The microtubule association kinetics of the dimer indicate that it is less efficient than the monomer in binding the microtubule [Chapters 3, 4 and [205, 250, 344, 345]]. More strikingly, the catalytic step, which is a rapid event in the mechanochemical cycle of monomeric Eg5, is a rate-limiting step for dimeric Eg5 [250, 251, 344, 345].

To some extent, dimeric Eg5 appears like conventional kinesin in that it alternates catalysis on its motor domains to move processively along a microtubule [333, 344]. In contrast, dimeric Eg5 takes 8-10 steps before dissociating [333], whereas conventional kinesin can take more than one hundred steps before detaching [148, 150, 196, 197]. The mechanochemical cycle of conventional kinesin is tuned such that it can step processively as soon as the first motor

domain touches its track. In contrast, Eg5 requires a slow conformational change to occur shortly after MT•Eg5 complex formation before it can begin a processive run [Chapter 4 and [344]]. These differences indicate that the Kinesin-5s have additional functional requirements requiring further investigation.

In this chapter, equilibrium and transient kinetic approaches have been used to specifically address what mechanistic events occur prior to the steady-state rate-limiting conformational change that precedes processive stepping. These experiments have also revealed the mechanism of head-head communication during a processive run. Ultimately, dimeric Eg5 begins a processive run from a transitory nucleotide-free state with both motor domains associated with the microtubule. Processivity will terminate after a few steps because the motor is unable to sufficiently prevent both motor domains from entering the same nucleotide bound state.

6.2 MATERIALS AND METHODS

All experiments were performed at room temperature, 25°C, in ATPase buffer. All microtubules were stabilized with Paclitaxel in DMSO. For all mantAXP experiments, a racemate (Invitrogen Corp.) was used. Unless otherwise noted, mantAXP was excited at λ_{ex} = 360 nm and the emission was monitored using a 400 nm long pass filter.

6.2.1 Nucleotide-free Eg5-513

Two methods were used to generate nucleotide-free Eg5-513. In most experiments, the motor was treated with apyrase (Grade VII, Sigma-Aldrich Co.) as described [Chapter 3 and [344]] unless otherwise noted. Nucleotide-free Eg5-513 was also obtained by supplementing existing protein stocks with 6 mM EDTA and performing gel filtration using a Bio-Spin P-30 column (Bio-Rad Laboratories) equilibrated in ATPase buffer lacking magnesium acetate and supplemented with 6 mM EDTA. A second round of gel filtration was performed to adjust the solution back to standard buffer conditions.

6.2.2 Quantitation of Bound ADP by Gel Filtration

Eg5-513, dimeric conventional kinesin K401, and ovalbumin were incubated with trace [α^{32}P]ATP for 90 min and subjected to gel filtration to quantitate the amount of tightly bound ADP. Protein concentration was determined pre and post gel filtration by Bio-Rad Protein Assay. For Eg5-513 and K401, nucleotide concentration prior to gel filtration was determined spectrophotometrically at A_{259}. Since ovalbumin lacks nucleotide, it was incubated with MgADP prior to gel filtration to give a reference point. The amount of ADP bound to the proteins post-column was determined by spotting equal volumes of the column void on thin-layer chromatography plates and comparing the radioactive signal pre and post gel filtration using Image Guage V4.0 software (Fuji Photo Film U.S.A.).

6.2.3 MantADP Titration of Eg5-513 Free in Solution

An equilibrium titration of nucleotide-free Eg5-513 (EDTA treatment) and Eg5-367 (0.3-4 μM motor) with mantADP was performed using a FluoroMax-2 spectrofluorometer with magnetic stirring capability (Figure 6.1). Data was collected using the DataMax software program (Jobin Yvon-Spex Instruments S.A., Inc). The sample was excited at 290 nm and mantADP emission was monitored at 445 nm. For each mantADP concentration, three trials with an integration time of one second were collected and averaged. Both the volume of the sample and the motor active site concentration were constant. The total mantADP concentration was determined for each point *i*:

$$((V\text{-}v)*M_{i\text{-}1} + v*m)/V \qquad \text{(Eq. 8)}$$

where, V is the total volume of the sample, M_{i-1} is the concentration of the sample at the previous point, v is the volume being added and m is the concentration of the mantADP stock being added. The measured fluorescence intensity was corrected for the inner filter effect [346]:

$$F_{i,c} = F_{i,obs} * 10^{0.5(Abs_{i,ex} + Abs_{i,em})} \qquad \text{(Eq. 9)}$$

where, $F_{i,c}$ is the corrected fluorescence intensity, $F_{i,obs}$ is the observed fluorescence intensity, and $Abs_{i,ex}$ and $Abs_{i,em}$ are the absorbance of the sample at point i at the excitation and emission wavelengths. The contributions of mantADP and buffer were subtracted, and the data were fit to either a hyperbola or sum of hyperbolas.

6.2.4 MantADP Release from the motor domain with a higher ADP affinity

Eg5-513 or R234K was incubated with a 5-fold molar excess of mantADP for 4 hours and then subjected to gel filtration. The motor•mantADP complex that passes through the column in the void, which should contain a motor active-site to mantADP ratio of 0.6 (see Table 6), is then mixed in the stopped-flow with varying microtubules plus 1 mM MgATP (Figure 6.2A-C). To assess the contribution of the ATP chase in the microtubule syringe to the second, slower phase of mantADP release, a motor•mantADP complex was mixed with microtubules (Final: 25 μM) and varying MgATP (Figure 6.2D).

6.2.5 MantATP Binding to Eg5-513 in the Absence of Microtubules

Eg5-513 or Eg5-513 that had been treated with 0.001 Units/ml apyrase for 5 hrs to achieve a nucleotide-free state was mixed with mantATP in the stopped-flow (Final: 0.5μM Eg5-513, 0.0005 U/ml apyrase). The observed rates of the fluorescence increase (λ_{ex} = 290 nm, 400 nm long pass filter) were fit to a hyperbola (Figure 6.3A, B).

6.2.6 MantATP Binding to Eg5 following MT•Eg5 Complex Formation

Eg5-513, apyrase treated Eg5-513, or Eg5-367_{NF} was mixed in the stopped-flow with varying microtubules and mantATP (Final: 3 μM motor, 30 μM mantATP). The observed rates of the fluorescence increase were fit to a hyperbola (Figure 6.3C-F).

6.2.7 MantATP Binding to the MT•Eg5-513 Complex under Single Turnover Conditions

A MT•Eg5-513 complex was treated with apyrase and mixed in the stopped-flow with limiting mantATP (Final: 15 μM Eg5-513/25 μM microtubules, 1 μM mantATP). A rapid fluorescence increase was observed on a short time scale; however the fluorescence decayed very slowly over hundreds of seconds (Figure 6.4).

6.2.8 MantADP Release during Motor Stepping

An apyrase treated MT•Eg5-513 complex was supplemented with mantATP immediately prior to loading the complex in the stopped-flow (Figure 6.5). The time required to load the stopped-flow instrument is sufficient for Eg5-513 to bind the mantATP, hydrolyze the nucleotide to mantADP•P_i, and release P_i [Chapter 4 and [344]]. The resultant MT•Eg5-513•mantADP complex was then rapidly mixed (Final: 15 μM Eg5-513/25 μM microtubules, 1 μM mantADP) with varying MgATP, or 500 μM final MgAXP (ATPγs, or AMPPNP). The observed rates of the ATP induced, exponential fluorescence decrease were fit to a hyperbola.

6.3 RESULTS

6.3.1 Eg5-513 has an Asymmetric ADP Affinity while free in Solution

A kinetic characterization of Eg5-513 presented in Chapter 4 suggested that steady-state ATP turnover by dimeric Eg5 is governed by a slow conformational change that occurs only once in

the mechanochemical cycle, after association with the microtubule, and prior to processive motion [344]. To dissect the behavior of the motor both before and after this conformational change, Eg5-513 was examined in the absence of microtubules. On the microtubule, there is a biochemical asymmetry in the motor: it demonstrates a sequential release of ADP upon association with the microtubule as well as alternates catalysis on its motor domains [Chapter 4 and [344]]. To test whether there is a biochemical asymmetry in the molecule prior to association with the microtubule, the ADP affinity of the two motor domains was examined by gel filtration and a mantADP active-site titration.

Eg5-513 was incubated with trace [α^{32}P]ATP to exchange the ADP that copurifies with the motor with radiolabeled ADP and subjected to gel filtration. Only ADP that is tightly bound to an active-site will accompany the motor through the column. As a result of gel filtration, ADP was found to be bound to 64% of Eg5 active sites whereas dimeric conventional kinesin, K401, maintained ADP bound at almost all of its sites (92%) and ovalbumin proceeded through the column without any bound nucleotide (Table 6). Furthermore, when Eg5-513 was incubated with an additional 1 mM MgADP prior to gel filtration, additional active-sites were not observed to contain ADP suggestive of a distinct difference in affinity for ADP between the two motor domains of the dimer (Table 6).

Table 6 ADP Affinity by Gel Filtration

Protein	ADP (μM) / Active Site (μM)	Range
Eg5-513	0.64 ± 0.01	0.62-0.66
K401	0.92 ± 0.02	0.83-1
Ovalbumin	0.01 ± 0.002	0.001-0.013
Eg5-513 + 1 mM MgADP	0.59 ± 0.04	0.44-0.74

Another possible interpretation of the gel filtration data is that there is not a difference in the affinity for ADP among the two active-sites. The amount of ADP bound is merely a coincidental result due to experimental conditions and a shared ADP affinity by both motor domains. To address this possibility, a mantADP titration was performed comparing monomeric and dimeric Eg5 motors (Figure 6.1). A mantADP titration of monomeric Eg5 motor domains (nM motor concentrations) yielded a monophasic curve with an apparent $K_{d,mantADP}$ = 1.6 μM (Figure 6.1A). Titration of dimeric Eg5 at the same enzyme concentration displays a biphasic curve with an apparent $K_{d,mantADP}$ for the tighter phase of 0.5 μM (Figure 6.1B). In order to better measure the apparent $K_{d,mantADP}$ for the weaker phase, titrations were performed with motor active-sites in the micromolar range yielding a $K_{d,mantADP}$ = 3.3 μM (Figure 6.1C). The data indicate that the two motor domains of dimeric Eg5-513 are biochemically different prior to motor interaction with the microtubule

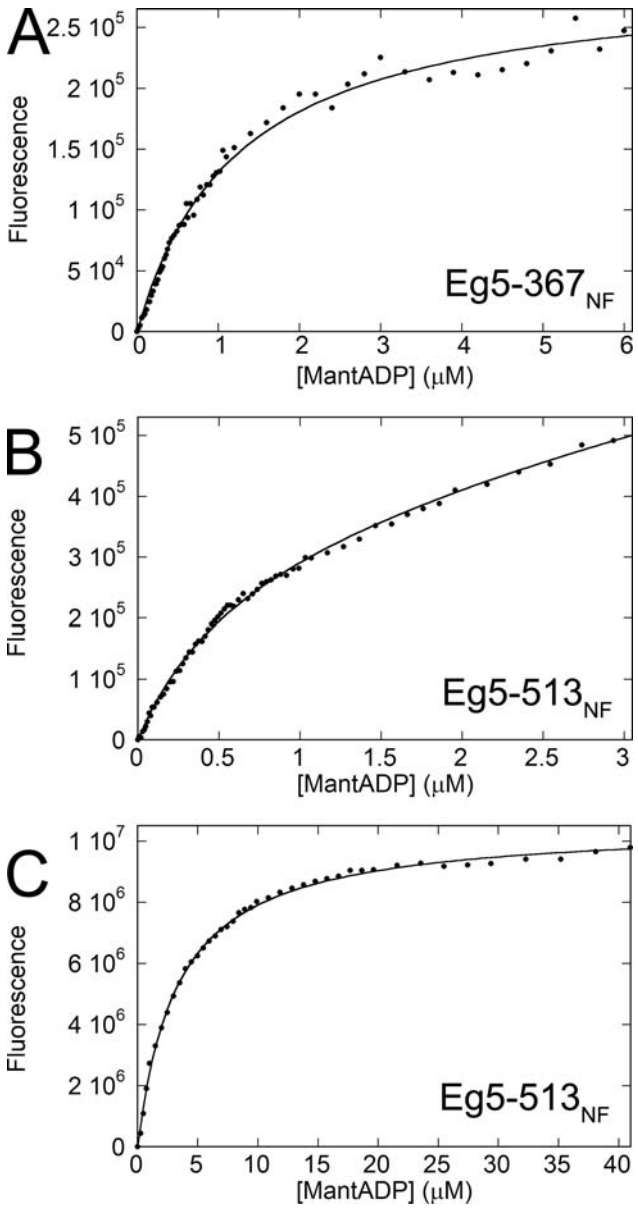

Figure 6.1 MantADP Titration of Monomeric and Dimeric Eg5

Titrations of both monomeric and dimeric Eg5 motors were performed at constant volume and motor concentration. *A*, 300 nM monomeric Eg5-367 was titrated with mantADP. The resultant increase in fluorescence was best fit by a single hyperbola yielding an apparent $K_{d,mantADP} = 1.2 \pm 0.1$ μM. *B*, 300 nM dimeric Eg5-513 was titrated with mantADP. The resultant increase in fluorescence was best fit by a sum a two hyperbolas yielding an apparent $K_{d,mantADP} = 0.62 \pm 0.14$ μM for the initial phase. The error on the apparent $K_{d,mantADP}$ for the second weaker phase was too large at this motor concentration so additional experiments were performed using higher motor active site concentrations. *C*, 4 μM dimeric Eg5-513 was titrated with mantADP. The resultant increase in fluorescence was best fit by a single hyperbola yielding an apparent $K_{d,mantADP} = 3.3 \pm 0.1$ μM.

6.3.2 Biphasic ADP Release

The work detailed in Chapter 4 [344] identified the steady-state governing, slow conformational change as being kinetically coupled to the second slower phase of ADP release upon microtubule association. Conventional kinesin has been demonstrated to release ADP from its two motor domains in a sequential fashion upon collision with the microtubule (Figure 1.4). One motor domain will release bound ADP following collision with the microtubule [162, 168, 172]; however, release of ADP from the second motor domain occurs following ATP binding to the motor domain associated with the microtubule [162, 168, 172]. Potentially, the two phases of ADP release by dimeric Eg5 could also represent ADP being sequentially released from specific motor domains as is the case for conventional kinesin. In support of this possibility, a biochemical asymmetry is present in dimeric Eg5 prior to interaction with the microtubule (Figure 6.1) and is maintained during processive stepping along the microtubule [Chapter 4 and [344]].

What then triggers the second phase of ADP release from dimeric Eg5? A caveat to the experimental design used in Chapter 4 [344] was the presence of ATP. Being that ATP binding causes the second phase of ADP release in the case of conventional kinesin, the event that triggers the second phase of ADP release from Eg5-513 could not be discerned from the ADP release experiments in Chapter 4 [see Figure 4.9 and [344]]. Three possibilities exist: (1) both phases of ADP release could simply be caused by association of Eg5-513 with microtubules; (2) Eg5-513 could have an identical mechanism to conventional kinesin where the ATP binding triggers the second slower phase of ADP release; (3) the mechanism could be more complicated in that ATP binding followed by ATP hydrolysis is necessary to trigger the second slower phase. The two scenarios that implicate ATP as influencing the second phase of ADP release would

prove problematic for Eg5-513 processivity. In both scenarios, the requirement for ATP to be bound before the release of ADP from the second motor domain could occur would lead to the rapid formation of an ADP state, the weakest known microtubule binding state for dimeric Eg5 [Chapter 3 and [205]], on both motor domains; most likely resulting in detachment of the motor from the microtubule before processive motion could ensue.

To test the possibility that ATP binding followed by ATP hydrolysis is the trigger for the slower phase of ADP release from Eg5-513, a mutant motor was generated (detailed in Chapter 5), referred to as R234K. The R234K mutation was chosen because it is the homologous mutation of a Switch-I mutation in *Drosophila* conventional kinesin (R210K) that caused the motor to display severely inhibited ATP hydrolysis while maintaining otherwise normal kinetic behavior [265]. R234K displayed inhibited steady-state ATP turnover, >10-fold slower ATP hydrolysis, and a surprising enhancement in the microtubule association kinetics (Table 5). Importantly, the kinetics of ADP release were comparable between Eg5-513 and R234K (Table 5), and the biphasic nature of the fluorescence transients representing ADP release was maintained (Figure 5.2). The presence of both phases indicates that the second phase of ADP release cannot be caused by ATP binding followed by ATP hydrolysis.

Because dimeric Eg5 possesses a differential affinity for ADP off of the microtubule (Figure 6.1, Table 6), it might be possible to solely monitor the second slower phase of ADP release if the motor domain with the higher affinity for ADP off the microtubule also released ADP more slowly on the microtubule. To experimentally test this, mantADP was not added back to the Eg5-513•mantADP or R234K•mantADP complexes that eluted from the gel filtration column (see Methods). In Figure 6.2A, B, it is evident that the contribution of the initial fast phase of mantADP release to the overall response is diminished under this experimental setup.

The observed kinetics (Eg5-513 k_{max} = 0.6 s^{-1}, $K_{½,MTs}$ = 14.6 μM; R234K k_{max} = 0.79 s^{-1}, $K_{½,MTs}$ = 9.1 μM) from mixing either a Eg5-513•60%mantADP or a R234K•60%mantADP complex with microtubules and ATP in the stopped-flow, (Figure 6.2) are in good agreement with what has been previously published concerning the slower phase of mantADP release from Eg5-513 [k_{max} = 0.5 s^{-1}, $K_{½MTs}$ = 13 μM (Chapter 4 and [344])]. These data argue that the motor domain with the higher nucleotide affinity off the microtubule is directly responsible for the second slower phase of the mantADP release transients (Figure 6.6 states 1-3).

To address whether ATP binding to the motor domain that releases ADP more rapidly causes the slower phase of ADP release, the ATP concentration dependence on the observed rate of the dominant, slow fluorescence decrease from both an Eg5-513•60%mantADP and a R234K•60%mantADP complex was examined. An ATP concentration dependence was not observed (Figure 6.2D) suggesting that binding of a dimeric Eg5 motor to the microtubule is sufficient to cause ADP release from both motor domains.

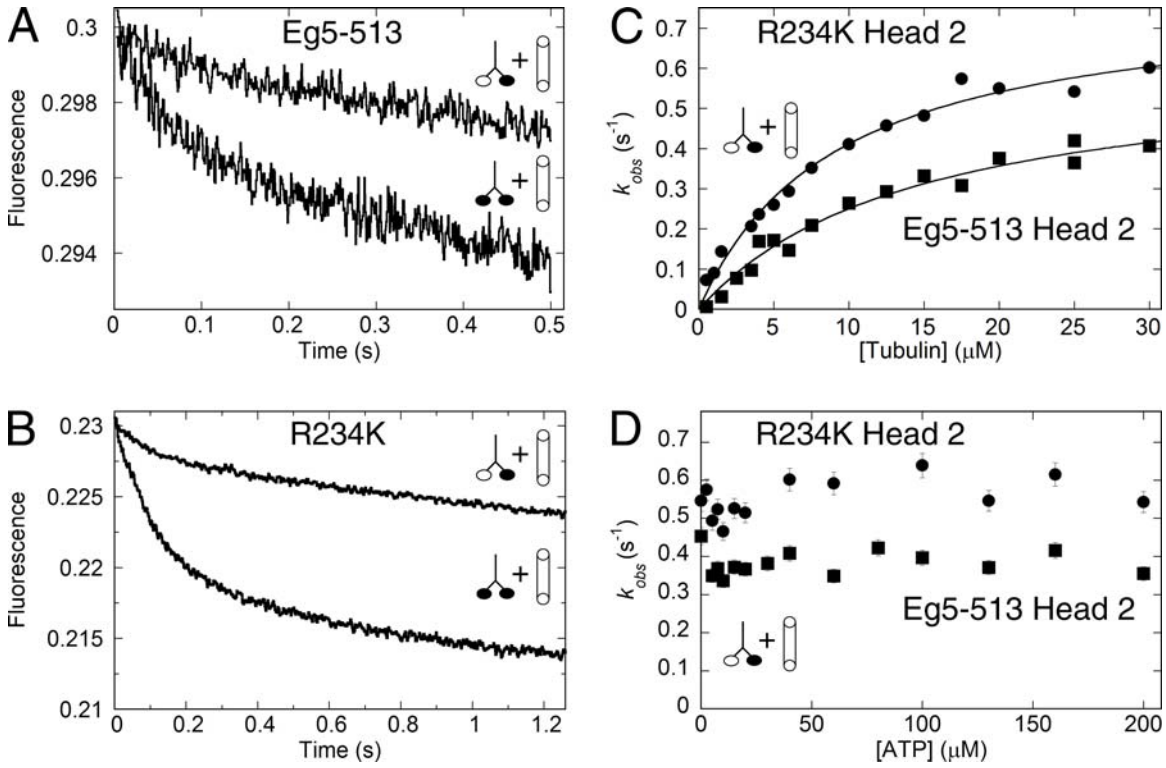

Figure 6.2 ADP Release from Head-2

R234K•mantADP or Eg5-513•mantADP in either a 1:1 or 1:0.6 stoichiometry was rapidly mixed in the stopped-flow instrument with microtubules + MgATP. *A*, Averaged transients (Final: 2.5 μM Eg5-513, 10 μM microtubules, 500 μM MgATP) representing the observed fluorescence decrease if Eg5-513 was supplemented with additional mantADP post gelfiltration column (a 1;1 stoichiometry) or not supplemented with additional mantADP (a 1:0.6 stoichiometry). *B*, Averaged transients (Final: 2.5 μM R234K, 4 μM microtubules, 500 μM MgATP) representing the observed fluorescence decrease if R234K was supplemented with additional mantADP post gel filtration column (a 1:1 stoichiometry) or not supplemented with additional mantADP (a 1:0.6 stoichiometry). *C,* The observed rate of the more prominent, second, slower fluorescence decrease is plotted as a function of microtubule concentration: R234K (●) k_{max} = 0.79 ± 0.04 s^{-1}, $K_{½,MTs}$ = 9.1 ± 1 μM, Eg5-513 (■) k_{max} = 0.62 ± 0.04 s^{-1}, $K_{½,MTs}$ = 14.6 ± 2.3 μM. *D,* R234K•mantADP or Eg5-513•mantADP in the 1:0.6 stoichiometry was mixed with microtubules and varying MgATP (Final: 2.5 μM motor, 25 μM microtubules). The observed rate (R234K (●), Eg5-513 (■)) did not change as a function of MgATP concentration.

6.3.3 MantATP Binding to Eg5-513 Following Association with the Microtubule

Even though ATP binding does not act as the trigger for ADP release from the second Eg5-513 motor domain, there was still the possibility that ATP could bind to the motor domain that released ADP rapidly irrespective of having any influence on the actions of the second motor domain. With the isomerization to tight ATP binding at ~50 s^{-1} and the rate of ATP hydrolysis at 5-10 s^{-1} (Chapter 4 and [344]), the possibility of the motor entering a dual ADP bound state before processive motion could begin was kinetically viable. To see if ATP was capable of binding before the motor completes ADP release from both motor domains, Eg5-513, apyrase treated Eg5-513, or nucleotide-free Eg5-367 was mixed with varying microtubules and a final of 30 μM mantATP. Under this experimental design, the second-order microtubule binding constants for the motors ($k_{on\text{-}513}$ = 3 $\mu M^{-1}s^{-1}$ [Chapter 4 and [344]], $k_{on\text{-}367}$ = 10-20 $\mu M^{-1}s^{-1}$ [250, 345]) are sufficiently rapid such that association with the microtubule should not limit the assay. ATP binding by both Eg5-513 and Eg5-367 is very slow off the microtubule ($k_{max\text{-}513}$ = 0.23 s^{-1} (Figure 6.3B), $k_{max\text{-}367}$ = 0.5-0.9 s^{-1} [246]); therefore, mantATP binding should occur after the motor has associated with the microtubule. Unless there is a kinetically detectable conformational change occurring on the microtubule but preceeding substrate binding, the rate of the observed fluorescence increase from the motor binding mantATP should approach what has been observed when a preformed MT•Eg5 complex is mixed with mantATP.

When Eg5-367_{NF} is mixed with microtubules and mantATP in the stopped-flow, a biphasic fluorescence enhancement of approximately equal amplitude is observed. The maximal observed rate of the initial fast phase (k_{max} = 27 s^{-1}, $K_{½,MT}$ = 5.1 μM) is nearly identical to what has been observed for mantATP binding to a preformed MT•Eg5-367 complex (compare Figure 6.3D with Figure 4 in [250] and Table 1 in [345]). At this point the second slower phase

(k_{max} = 4.2 s^{-1}, $K_{½,MTs}$ = 4 μM) cannot be attributed to a particular step or structural transition in the Eg5-367 pathway. A second phase of mantATP fluorescence has not been previously seen when a preformed complex has been mixed with mantATP [250, 344]. At lower microtubule concentrations there was a very short lag which quickly disappeared as microtubule concentration was increased, suggesting that the lag resulted from association of Eg5-367_{NF} with the microtubule.

Like Eg5-367_{NF}, both Eg5-513 and apyrase treated Eg5-513 also displayed a lag followed by a biphasic fluorescence enhancement when mixed with microtubules and mantATP. Corresponding turbidity measurements observing MT•Eg5-513 complex formation indicated that the lag also represented motor association with the microtubule. However, the initial fast phase (Eg5-513 k_{max} = 1.2 s^{-1}, $K_{½,MTs}$ = 2.1 μM; Eg5-$513_{apyrase}$ k_{max} = 1.6 s^{-1}, $K_{½,MTs}$ = 3.8 μM) was over 30-fold slower than if a preformed apyrase treated MT•Eg5-513 complex is mixed with mantATP [Figure 4.1 and [344]]. The second slower phase (Eg5-$513_{apyrase}$ k_{max} = 0.5 s^{-1}, $K_{½,MTs}$ = 6.7 μM) also shows a microtubule dependence, however, as with Eg5-367, the nature of the second phase is unknown. In this experimental setup, the observed rate of the fluorescence enhancement corresponding to dimeric Eg5 binding mantATP was comparable to the rate of the slow structural transition limiting steady-state ATP turnover. These results suggest that ATP cannot bind to the nucleotide-free motor domain until the structural transition limiting ADP release from the partner motor domain has occurred. The amplitude difference between apyrase treated and untreated Eg5-513 likely the result of copurifying ADP preventing all motor from binding the microtubules [Chapter 3 and [205]].

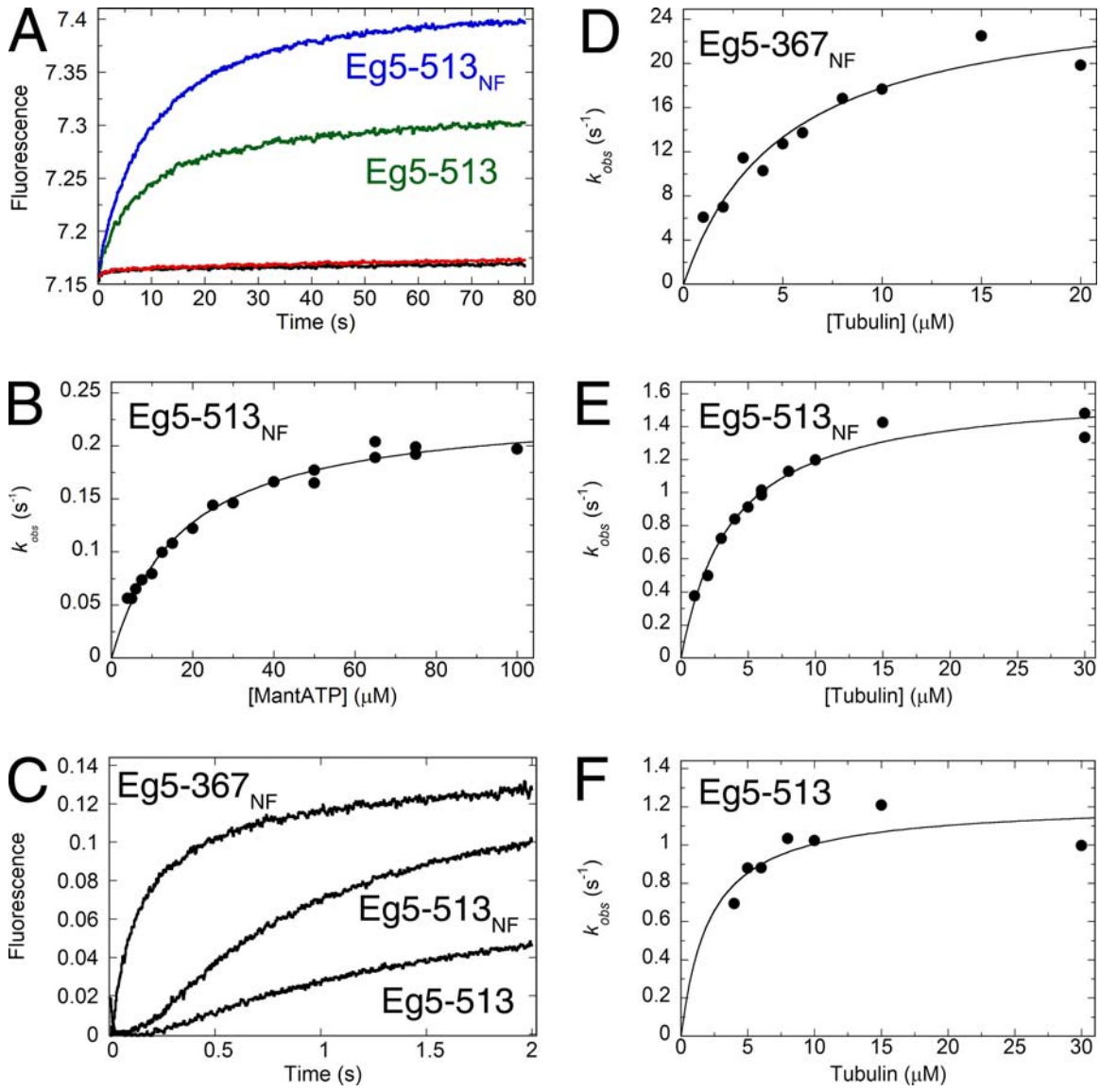

Figure 6.3 ATP Binding Following Microtubule Association

Eg5-513 was rapidly mixed in the stopped-flow instrument with mantATP (*A, B*). *A*, averaged transients representing the fluorescence enhancement upon mixing nucleotide-free Eg5-513 (apyrase treated), Eg5-513 as purified, apyrase, or buffer with mantATP in the absence of microtubules. Final: 0.5μM Eg5-513, 0.005 U/ml apyrase, 75 μM mantATP. *B,* the observed rate of the initial phase is plotted, k_{max} = 0.23 ± 0.12 s^{-1}, $K_{½,MantATP}$ = 14.5 ± 2.4 μM. Nucleotide-free Eg5-367_{NF}, Eg5-513_{NF}, or Eg5-513 was mixed in the stopped flow with microtubules plus mantATP *(C-F)*. Final: 3 μM motor, 30 μM mantATP. *C*, Comparison of averaged transients of the fluorescence enhancement upon mantATP binding to each motor. Final: 8 μM microtubules. *D*, the observed rate of the initial fast phase for mantATP binding by Eg5-367NF is plotted as a function of microtubule concentration: k_{max} = 26.8 ± 2.3 s^{-1}, $K_{½,MT}$ = 5.1 ± 1.1 μM. *E*, The observed rate of the fast phase of fluorescent enhancement of mantATP binding by apyrase treated Eg5-513 is plotted as a function of microtubule concentration: k_{max} = 1.6 ± 0.06 s^{-1}, $K_{½,MT}$ = 3.8 ± 0.4 μM. *F*, The observed rate of the fast phase of fluorescent enhancement of

mantATP binding by Eg5-513 is plotted as a function of microtubule concentration: k_{max} = 1.2 ± 0.1 s^{-1}, $K_{½,MT}$ = 2.1 ± 1 μM.

6.3.4 ADP Release During Processive Motion

In the model proposed in Chapter 4 [344], ATP hydrolysis at 5-10 s^{-1} is the rate-limiting step while Eg5-513 is stepping along the microtubule. For this to be accurate, the steady-state rate-limiting conformational change limiting ADP release from one of the motor domains cannot occur during the processive run. This then begets the question: how fast is ADP release while the motor is processively stepping? To address this question, an apyrase treated MT•Eg5-513 complex was mixed with mantATP in the stopped-flow under single turnover conditions (Final: 15 μM Eg5-513/25 μM microtubules, 1 μM mantATP). In this experimental setup, an initial rapid phase of fluorescence enhancement corresponding to motor binding the substrate is expected followed by a decrease in fluorescence corresponding to release of mantADP from the active-site. The initial fluorescence enhancement was observed (k_{obs} = 33 s^{-1} Figure 6.4A) but the fluorescence did not begin to decrease until 50 s elapsed. The observed fluorescence decrease was very slow, k_{obs} = 0.001 s^{-1} (Figure 6.4B), and comparable to the rate of fluorescence decay seen when mantATP was mixed with buffer (k_{obs} = 0.0014 s^{-1} data not shown). This suggested that a kinetically stable Eg-513•mantADP intermediate was being formed, and there was a nucleotide-gated mechanism preventing ADP release.

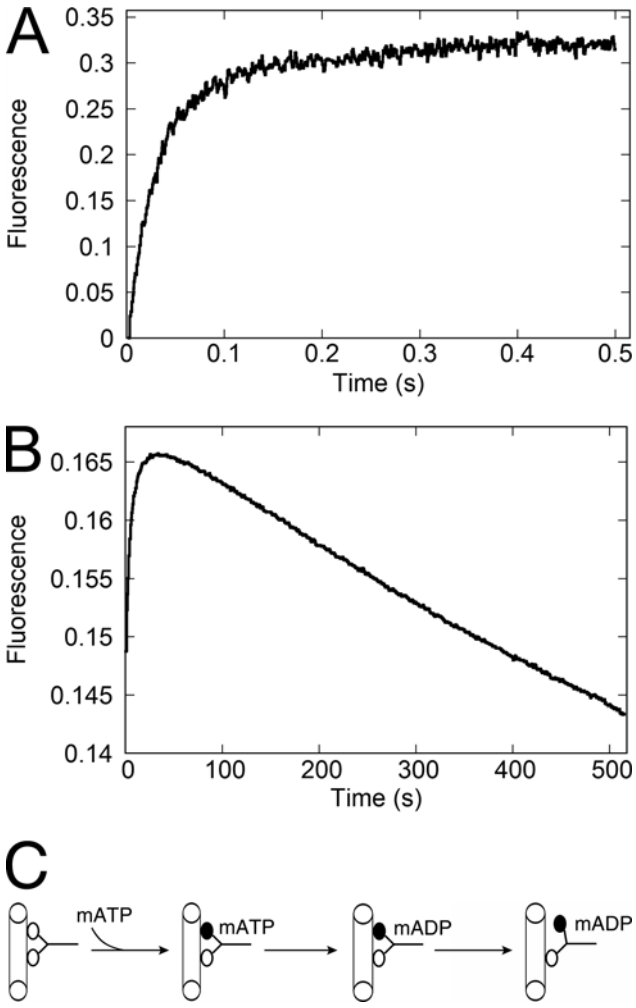

Figure 6.4 Single Turnover ATP Binding

A preformed apyrase treated MT•Eg5-513 complex was rapidly mixed in the stopped-flow with mantATP. Final: 15 µM Eg5-513/25 µM microtubules, 1 µM mantATP (*A*) or 0.25 µM mantATP (*B*). *A*, a representative transient reflecting initial rapid mantATP binding by Eg5-513: Phase 1 k_{obs} = 33 ± 0.3 s^{-1}, Phase 2 k_{obs} = 2.1 ± 0.06 s^{-1}. *B*, Rapid mantATP binding to the MT•Eg5-513 complex followed by fluorescence decay, k_{obs} = 0.0008 ± 0.00002 s^{-1}. *C*, A cartoon depicting a likely pathway that Eg5-513 can take in response to mantATP binding.

In order to determine the signal for mantADP release following the first ATP hydrolysis event, a MT•Eg5-513•mantADP intermediate was formed by adding mantATP to an apyrase treated MT•Eg5-513 complex just prior to loading in the stopped-flow (Final: 15 µM Eg5-513/25 µM microtubules, 1 µM mantATP). Mixing with MgATP produced an ATP concentration dependent fluorescence decrease (Figure 6.5A). The transients were biphasic with an initial fast

phase k_{max} = 8.4 s^{-1}, $K_{½,\ ATP}$ = 4 μM, and a second slower phase that did not vary with ATP concentration, $k_{obs} \cong 1\ s^{-1}$ (Figure 6.5B).

To try and assess whether ATP binding was sufficient to cause this fluorescence decrease, the MT•Eg5-513•mantADP complex was mixed with the slowly hydrolyzable analogue, ATPγS, and the nonhydrolyzable analogue, AMPPNP (Final: 1 mM AXP). For both analogues, there was a small (amplitudes were 24-32% of the initial amplitude from mixing with ATP) initial rapid fluorescence decrease (k_{obs} = 20-30 s^{-1} for both analogues) followed by a larger slow (k_{obs}= 0.5-0.8 s^{-1}) phase of comparable amplitude to the ATP transient (Figure 6.5C). The same experiment was also performed using the ATP hydrolysis defective mutant R234K (Figure 6.5C). Essentially all transients from R234K mimicked the results of mixing Eg5-513 with an ATP analogue. These results indicate that ATP binding is sufficient to induce the release of the ADP produced from the enzymatic cycle of one motor domain.

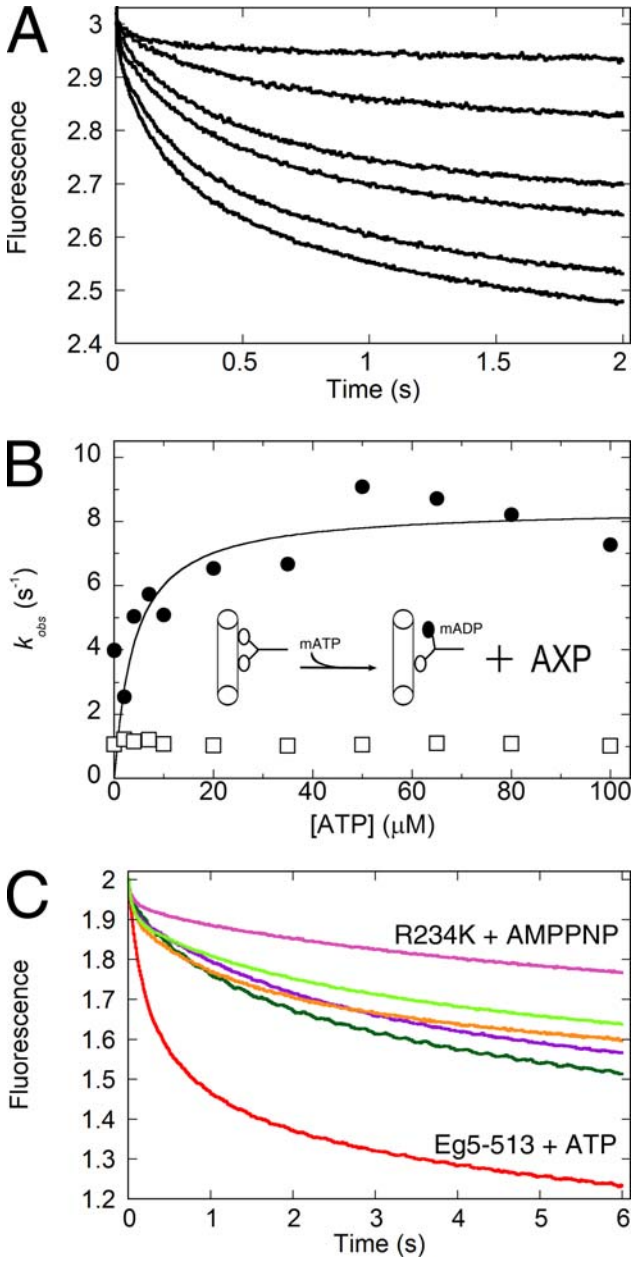

Figure 6.5 ATP Triggered Eg5-513 Stepping

A preformed MT•Eg5-513•mantADP or MT•R234K•mantADP complex was mixed in the stopped-flow with MgATP. Final: 15 μM motor/25 μM MTs, 1 μM mantATP). *A*, Fluorescence transients of mantADP release from Eg5-513 following mixing with MgATP. Final MgATP from top to bottom: 0, 2, 4, 10, 20, and 65 μM. *B*, The observed rate of the initial phase of fluorescence decrease (•) is plotted as a function of ATP concentration: k_{max} = 8.4 ± 0.8 s^{-1}, $K_{½, ATP}$ = 4 ± 1.8 μM^{-1}. The second phase (□) at ~1 s^{-1} does not show an ATP concentration-dependence. *C*, a comparison of the fluorescence response when either a MT•Eg5-513•mantADP or a MT•R234K•mantADP complex was mixed with ATP, ATPγS, or AMPPNP: Eg5-513+ATP, Eg5-513+ATPγS, Eg5-513+AMPPNP, R234K+ATP, R234K+ATPγS, and R234K+AMPPNP.

6.4 DISCUSSION

6.4.1 The Mechanochemical Cycle of Eg5-513

Off the microtubule, the motor domains of dimeric Eg5 have different affinities for ADP (Figure 6.1), with one motor domain binding ADP 10-fold more tightly. Association with the microtubule, while slowed compared to monomeric Eg5 and conventional kinesin, is fast relative to steady-state ATP turnover. It is followed by sequential release of ADP from both motor domains. The motor domain with the weaker affinity for ADP off the microtubule is proposed to initiate productive microtubule interactions and lead to the rapid release of ADP. ATP cannot bind to this motor domain until the motor domain with the tighter affinity for ADP off the microtubule releases its ADP kinetically coupled with the steady-state rate-limiting structural change (Figure 6.2). Following this conformational change, both motor domains of the dimer are interacting with the microtubule. In the model, (Figure 6.6) this state, state 3, has been drawn with two nucleotide-free motor domains. This has been done in order to graphically segregate the time in which ATP cannot bind to the motor from the time in which ATP is capable of binding to the motor. However, at high ATP concentrations, ATP binding most likely occurs as soon as the second molecule of ADP dissociates from its motor domain: effectively transitioning the motor from a nucleotide-free/ADP situation to an ATP/nucleotide-free situation. The processive run is proposed to begin as soon as ATP binds. ATP is proposed to bind to the rearward motor domain because steric constraints would imply that only its neck-linker can be oriented along the length of the motor domain parallel to the microtubule [205]. ATP hydrolysis occurs, facilitating the weakening of the interaction of the rearward motor domain with the microtubule. ATP will then bind to the second, forward motor domain, triggering the structural

change that leads to ADP release from the rearward motor domain and the 8 nm advance of the motor (Figure 6.5). From this point of the cycle on, the motor resembles conventional kinesin in that catalysis of ATP is alternated between the two motor domains [Chapter 4 and [344]] and ATP binding is required for the motor to take successive steps along the microtubule.

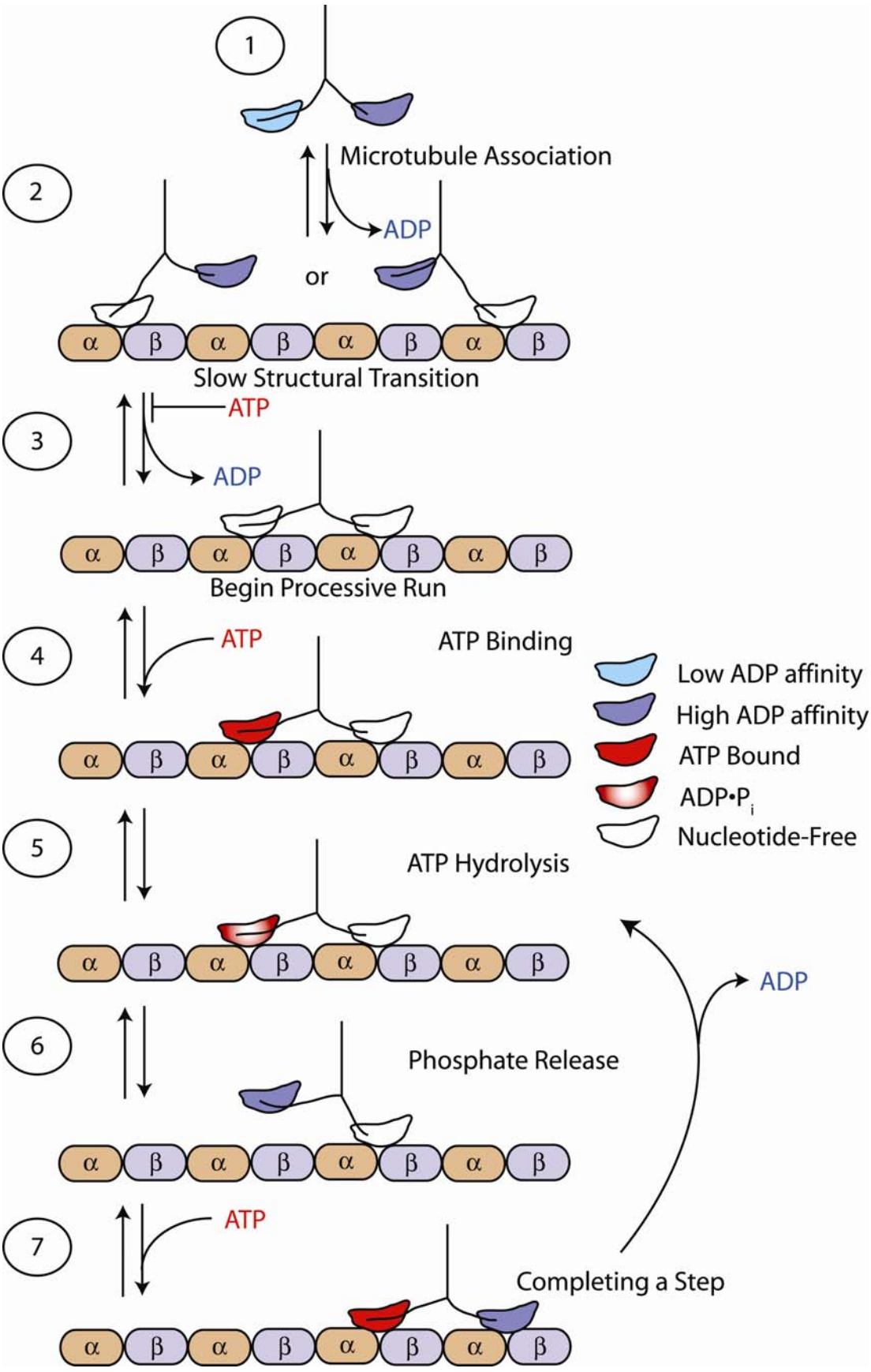
1
Microtubule Association
2
ADP
or
α β α β α β α β
Slow Structural Transition
ATP
3
ADP
α β α β α β α β
Begin Processive Run
ATP
4
ATP Binding
α β α β α β α β
Low ADP affinity
High ADP affinity
ATP Bound
ADP•P$_i$
Nucleotide-Free
5
ATP Hydrolysis
α β α β α β α β
ADP
6
Phosphate Release
α β α β α β α β
ATP
7
α β α β α β α β
Completing a Step

Figure 6.6 Mechanochemical Cycle of Dimeric Eg5

While in solution, the two motor domains of dimeric Eg5 have a different affinity for ADP (1). Upon association with the microtubule, ADP bound to the motor domain with the lower affinity for nucleotide releases its bound ADP rapidly. A slow conformational change occurs which limits both the rate of ADP release from the motor domain with the higher affinity for nucleotide off the microtubule and ATP binding to the motor that released its ADP rapidly (2). After the completion of these events the motor is now ready to begin its processive run. The rearward motor domain (head closest to the minus-end of the microtubule) will now bind ATP (3), proceed through catalysis (4), and release P_i (5) such that it now only has ADP bound to it (6). ATP binding and possibly ATP hydrolysis at the forward motor domain is necessary to complete the 16 nm advance of the rearward motor domain and trigger ADP release (7). Because ATP hydrolysis on the rearward head and ADP release on the forward head cannot be ordered, steps have been collapsed to the state of the motor in (5). In order for the motor to more processively, the new forward head must be nucleotide free before the rearward head enters the ADP state.

6.4.2 A Means for MT•Eg5-513 Complex Dissociation

At this point, the state of the motor that leads to the termination of the processive run is not explicitly known. It is tempting to speculate that the short run lengths of dimeric Eg5 [333] in comparison to conventional kinesin are due to an inability to keep the motor domains out-of-phase. The observed rate of ADP release at 8.4 s^{-1} after ATP binding is within the range seen for ATP hydrolysis (Figure 6.5). One possible interpretation of these data is that during stepping, there is an initial coupling between the two motor domains that requires ATP binding. Following ATP binding, which is the most rapid step in the cycle [Chapter 4 and [344]], the activities of the two motor domains are uncoupled allowing the rearward head to hydrolyze the bound ATP and the forward head to release its ADP. If the two rates are comparable, and since there isn't a slow step following ATP hydrolysis like there is for conventional kinesin [190], then the possibility of a dual ADP bound state is more prominent and could lead to dissociation of the motor from the microtubule. Alternatively, ADP release during stepping could be fast but occurs

in sequence after ATP hydrolysis. It is not known whether the ADP•P_i intermediate is a tight binding state for dimeric Eg5, but regardless, it is a very transient state in the cycle. A race would be set up between P_i release and ADP release; there would not be a guaranteed slow step guarding the transition from a tight binding to a weak binding state. These scenarios cannot be distinguished from the kinetics, but, nevertheless, both scenarios could allow for Eg5-513 to enter a dual bound ADP state fairly easily, which would cause motor to dissociate from the microtubule.

7.0 DISSERTATION SUMMARY

During a person's daily routine, various tasks need to be accomplished which require physical work. Often, the human body is sufficient for providing the force necessary to accomplish a task and when it is insufficient, there are a variety of different tools that can be used, powered by a motor capable of generating a sufficient force. Regardless of the scenario, though, there is a consciousness guiding the action of the particular motor. On the cellular level, there are many routine tasks to be accomplished. Molecular motors amazingly accomplish their tasks without the guidance of a consciousness and must usually do so much more rapidly than macromolecular motors. Guided by only the chemistry of the amino acids making up the molecular motor, the protein "knows" what it is to do, when it is to do it, what it is to do it on, and how it is to do it. Even more interesting is that apparently small changes in amino acid sequence can result in two motors that perform entirely different roles. The kinesin superfamily of molecular motors is an excellent example of this [58]. These motors have >35% amino acid identity in their enzymatic motor domains yet function in diverse roles from transporting various cargoes, to altering the dynamics of microtubules, to using microtubules as levers to separate the spindle poles during mitosis.

Most work regarding kinesin motors has involved studies on conventional kinesin. Besides being the founding member of the superfamily, conventional kinesin being a dimeric motor, provided a system amenable to studying a single engine as well as the effects of having

two engines work cooperatively. A dimeric state is not the highest level of complexity that a kinesin motor may take, and in the last decade, the importance of the homotetrameric members of the Kinesin-5 family has become increasingly apparent. These motors are the cornerstones of cell division. If their function is perturbed, cells cannot establish or maintain a bipolar spindle necessary to segregate the appropriate genetic material into two daughter cells [7, 8, 138, 217, 223-239, 303, 304]. Furthermore, when a cell cannot establish a bipolar spindle, apoptosis is triggered [7, 8].

At the beginning of this dissertation, an ample body of research was present on monomeric Eg5 motor domains but nothing was known regarding the cooperativity or lack there of between four motor domains. To begin to address this question, a truncation of the human Eg5 gene was engineered whose protein product, Eg5-513, resulted in a dimeric motor [Chapter 3 and [205]]. Equilibrium and transient kinetic studies were undertaken to examine how the two motor domains of a homotetramer modulate each others function.

As a result of studies using this dimeric Eg5, it was uncovered that the two motor domains interacting with the same microtubule are able to take multiple steps along the microtubule lattice before dissociating [333]. This was a very important finding because Eg5 had been invoked as part of the theoretical mitotic spindle matrix [347]. This implied that Eg5 was held at a particular position in the spindle through association with some unknown protein that is part of an undefined support matrix responsible for keeping the spindle together. In this theory, Eg5 is presumed to be a nonprocessive motor and relies on this undefined matrix to keep it in close contact with the microtubules so that it can successively impart force on the spindle. While processivity by dimeric Eg5 and later evidence that homotetrameric Eg5 is processive [348] cannot rule out the spindle matrix model, it established a mechanistic basis for the repeated

force generating events necessary to sustain the mitotic spindle instead of just relying on a hand-waving argument.

Work presented in this dissertation can account for the mechanism underlying processivity by dimeric Eg5. Comparison of the dimeric Eg5 mechanochemical cycle with that of the two other characterized dimeric Kinesins, conventional kinesin and Ncd, illustrates how each motor is uniquely tuned for a different degree of processivity. Finally, though dimeric Eg5 is not a physiological motor, its characteristics appear to be carried through to the homotetramer.

7.1 DIMERIC EG5 PROCESSIVITY

While dimeric Eg5 is a processive motor, the number of steps that the motor will take on average is only ~8 [333]. Convienently, the only other kinein motors with highly characterized mechanochemical cycles are either highly processive (conventional kinesin) or nonprocessive (Ncd); making dimeric Eg5 an excellent candidate to uncover the minimal requirements necessary for a kinesin to stay attached to a microtubule while it is transitioning one of its motor domains to the next binding spot.

7.1.1 Alternating Enzymatic Cycles

For a dimeric motor, the most basic requirement for processivity is to keep one motor domain tightly associated with the microtubule while the other temporarily dissociates in its search for the next binding spot. For all known kinesins, the nucleotide at the active-site has an alloseteric impact on the microtubule binding site via Switch-I and Switch-II. When ATP is bound at the

active-site a strong interaction with the microtubule is generated, however, if products of ATP hydrolysis were present at the active-site, either ADP or ADP•P_i depending on the motor, the motor tends to dissociate. Therefore, both motor domains of a dimer cannot contain the appropriate hydrolysis product at the active-sites simultaneously. An easy way to accomplish this is by having the motor alternate catalysis of ATP on its motor domains.

Two lines of data suggested that dimeric Eg5 alternated catalysis on its motor domains. (1) In single turnover experiments examining the rate of ATP hydrolysis, the observed rate was found to unexpectedly vary with the substrate concentration. A reduction in the observed rate was noticed when the substrate concentration was ≥ half the active-site concentration. This effect could be accounted for if the population of motor active-sites was not equivalent and there were really two distinct populations represented by the two heads of the Eg5 dimer. Sequential hydrolysis of ATP by the two motor domains would cause for an observed rate approximately half of the intrinsic value. (2) If the two motor domains of a dimer alternated catalysis of substrate, one would predict that the affinity for the substrate by the two active-sites would not be equivalent. In experiments that examined the interactions of ATP with only one motor domain, such as the mantATP binding experiment (Figure 4.1), an apparent $K_{d,ATP}$ was seen in the range of 5-10 μM. However, in pulse-chase ATP binding experiments where amount of active-sites participating in a reaction can be quantified, all active-sites, i.e. both motor domains of the dimer, were seen to participate in the reaction with a $K_{d,ATP}$ of ~60 μM (Figure 4.2). This difference in the dissociation constants between the experiments suggested that the two motor domains share different affinities for ATP.

By alternating catalysis on its motor domains, dimeric Eg5 fulfills a prerequisite for processive motion, however alternating catalytic cycles is not sufficient to guarantee

processivity. Even though Ncd is a nonprocessive motor it still alternated catalysis on its motor domains.

7.1.2 Position of "Slow Step"

Another important factor for the processive motion by a kinesin is the position of the slowest step in the cycle. This kinetic parameter substantially contributes to why conventional kinesin is processive and Ncd is nonprocessive. In the ATPase cycle of conventional kinesin, the slowest biochemical event for a single motor domain, the release of phosphate following ATP hydrolysis, occurs while the motor domain is still associated with the microtubule. Conventional kinesin takes a step upon the binding of ATP by the forward motor domain. The transition of the new forward motor domain to a tight binding state is rapid allowing the motor sufficient time to tightly associate the transitioning motor domain with the microtubule before the other motor domain dissociates. For Ncd, the situation is reversed. Following ATP hydrolysis, a Ncd motor domain will dissociate from its microtubule binding site in the ADP•P_i form [173]. The slowest step in the cycle is the transition from a weak to a strong microtubule binding state as ADP release upon association with the microtubule is rate-limiting [156, 174].

For dimeric Eg5, the relationship of the slow step in the ATPase cycle to the transitioning of the stepping motor domain from a weak to a strong microtubule associated state is very different from what was observed with conventional kinesin and Ncd. First off, the rate-limiting step in the ATPase cycle does not occur during processive stepping; instead it limits the transition of the motor from a stationary microtubule associated state to processive stepping. Motility rates by either single molecule optical trapping [333] or multiple motor microtubule gliding assays [Chapter 3 Addendum and [205]] indicated that the event controlling steady-state

ATP turnover and motor powered movement were not the same event. The step in the Eg5 ATPase cycle that is comparable in this discussion to P_i release by conventional kinesin and ADP release by Ncd would be the hydrolysis of ATP. ATP hydrolysis was measured at 5-10 s^{-1} (Figure 4.5), which is comparable to the rate of motility seen at 6-12 s^{-1} [205, 333]. Furthermore, events following ATP hydrolysis such as P_i release (Figure 4.6) and dissociation of the MT•Eg5 complex (Figure 4.7) displayed observed rates no faster than what was seen for ATP hydrolysis indicating that they were kinetically limited by the rate of ATP hydrolysis. Therefore, with regard to the concept of processive stepping, the slow step in the cycle for the motor domain that is transitioning from a strong to a weak microtubule binding state is the actual biochemical transition.

Regarding the motor domain transitioning from a weak binding to a strong microtubule binding state, the transition is dependent on the presence of ATP as is the case with both conventional kinesin and Ncd. ATP binding was seen to be sufficient to trigger transitions leading to the motor taking a step and releasing bound ADP (Figure 6.5). In the experiments that addressed this topic, nonhydrolyzable or slowly hydrolysable ATP analogues were seen to trigger the fluorescence decrease expected when mantADP, bound on one of the motor domains, gets released into solution, congruent with the motor taking a step. The fluorescence decrease was reduced in comparison to the amplitude of the decrease when the native substrate, ATP was used. Possibly, ATP binding can induce some of the necessary conformational changes required for the motor to take a step and release bound ADP, but hydrolysis is necessary to complete the transition. The observed rate of ADP release coincides with this possibility because at 8-9 s^{-1}, the release of ADP could be limited by ATP hydrolysis at 5-10 s^{-1}. Regarding processive stepping, this would imply that ADP release by the new forward motor domain occurs rapidly

upon ATP hydrolysis by the rearward motor domain. For the motor to be processive, the transition from a weak to a strong microtubule binding state, concurrent with ADP release, must be faster than (1) P_i release by the rearward motor domain if P_i release occurs before motor domain detachment, or (2) detachment of the rearward motor domain if P_i release occurs after the motor domain detaches. Unless the rate of ADP release is >> greater than the rapid events that occur on the microtubule bound motor domain, at best only a marginal probability would ensure that the two motor domains are not found in a weak microtubule binding state simultaneously, dissociating the motor from the microtubule.

ATP binding being sufficient to induce all the conformational changes necessary for dimeric Eg5 to take a step and release ADP cannot be overlooked, though. The amplitudes of the transients from mantADP release during motor stepping display a distinct trend where the more wild-type the motor and substrate are, the more ADP release is favored (Figure 6.6). In the case of Eg5-513, ATP elicited the greatest fluorescence response, followed by the slowly hydrolysable ATPγS, and the nonhydrolysable analogue AMPPNP gave the weakest response. The hydrolysis defective mutant, R234K, displayed the same trend, but in the presence of ATP, its response was merely comparable to that of Eg5-513 in the presence of ATPγS. Release of ADP from R234K in the presence of ATPγS was comparable to Eg5-513 in the presence of AMPPNP. Finally, in the most "mutant" situation, ADP release was least favored from R234K in the presence of AMPPNP. This trend argues that the more the communication pathway from the nucleotide to the microtubule binding domain is altered the more the communication between motor domains might be disrupted. If the ability to hydrolyze was truly necessary for the motor to undergo all the necessary structural transitions required to release ADP while stepping, the

different situations where ATP hydrolysis is inhibited should all produce a comparable transient. One would not expect hierarchical effects due to the severity of inhibition.

If ATP binding is sufficient to induce all the structural transitions required to release ADP while stepping, two possibilities open up regarding the timing of the strong to weak transition of the stationary motor domain and the weak to strong transition of the stepping motor domain. (1) Because of the comparable rates of ADP release during stepping and ATP hydrolysis, ATP hydrolysis could still occur before ADP release and set up the previously described scenario. (2) The alternative scenario introduced in this case is that ATP hydrolysis and ADP release could occur near simultaneously. This reciprocal effect on the strength of the interactions of each motor domain with the microtubule would promote processivity but also increase the probability of the two motor domains being both in a weak microtubule associated state if the timing was slightly off.

The length of a processive run by a kinesin motor may be predominantly governed by the ability to separate the biochemical states of the motor domains. Ncd, which is not processive, has an ATPase cycle which ensures that both motor domains exist in a weak microtubule binding state at the end of each ATP turnover. Eg5, which is mildly processive, is only marginally able to keep its motor domains from existing simultaneously in a weak microtubule binding state. Conventional kinesin, which is highly processive, uses a 5-fold difference in the rate constants governing the weak to strong transitions of its motor domains to keep both of its motor domains from being in weak microtubule binding states. It will be interesting to see if this pattern regarding the chronological separation of the microtubule binding state transitions of motor domains holds true for other multimeric kinesin motors.

7.2 POTENTIAL *IN VIVO* RELEVANCE OF DIMERIC EG5 STUDIES

There are two main mechanical differences between dimeric Eg5 and conventional kinesin: the initial two head microtubule bound state required to begin the processive run, and the mechanochemical cycle geared for lower processivity. Do either of these features of dimeric Eg5 reflect features of homotetrameric Eg5?

7.2.1 Binding the Microtubule with Both Heads

Regarding the steady-state rate-limiting transition leading to the novel intermediate of both motor domains associated with the microtubule at the start of the processive run, this dissertation has not experimentally determined an apparent advantage for a dimeric motor to begin in this state. Primarily, one might imagine that beginning a processive run with both heads associated with the microtubule might enhance the number of steps that the motor will take before dissociating. This is not the case because dimeric Eg5 is much less processive than conventional kinesin [196, 333]. An advantage to associating both motor domains with the microtubule prior to processivity might be able to be detected in work with the homotetramer. When Eg5 crosslinks two microtubules, intramolecular tension within the motor is probably generated. By having both motors domains of each dimeric half associated with a microtubule the tension will get dispersed over four motor domains instead of just two. This division of force might allow the homotetramer to move more processively than if only two of the four motor domains had to work against the the same amount of load. Future work will reveal if having four motor domains associated with two microtubules confers a particular mechanistic advantage to the motor. If so, then coupling a slow structural transition to the association of the second motor domain with the

microtubule (Figure 6.2) might be a way for the homotetramer to allow enough time to get four motor domains coordinated over two microtubules.

7.2.2 Utility of Marginal Processivity

The mechanism for dimeric Eg5 proposed in this dissertation (Figure 6.6) can account for the ability of dimeric Eg5 to move processively but detach from the microtubule much quicker than conventional kinesin. This type of mechanism can be directly correlated with *in vitro* observations made for the homotetramer. The homotetramer has been seen to undergo two types of motion along the microtubules, motor driven movement and diffusive movement [256]. The mechanism provided in this work can account for the motor driven movement during which force is repeatedly imparted on the microtubules crossbridged by the motor, and a means to allow the motor to easily switch to diffusive movement, which might be beneficial in preventing the motor from becoming stalled at a roadblock in the crowded mitotic spindle.

7.3 FUTURE DIRECTIONS

7.3.1 The Steady-state Limiting Structural Transition?

This dissertation has provided several lines of evidence first identifying as well as dissecting the nucleotide states of the two dimeric Eg5 motor domains during the slow steady-state limiting conformational change that primes the motor to move processively. The structural features moving during this isomerization event have not been experimentally verified. Work by

Rosenfeld *et al*. [251] has suggested that the neck-linker, a portion of the motor whose movement is responsible for the positioning of the second motor domain towards its microtubule binding site, reorients itself in response to microtubule binding. This is in contrast to conventional kinesin where neck-linker reorientation is dictated by ATP binding [194]. As proposed in Krzysiak *et al*. [344] the movement of the Eg5 neck-linker in response to microtubule binding makes it an excellent place to start in identifying the structural transition that occurs upon initial association with the microtubule. There are some requirements if neck-linker docking is to actually account for this slow structural transition.

For one requirement, the mechanism of neck-linker docking must be different during the initial encounter with the microtubule as compared to during processive motion. ADP release during processive motion has been observed to be at least an order of magnitude faster during processive motion than ADP release that is coupled to the slow steady-state limiting transition. The kinetic data presented in this dissertation do not rule out the possibility that the neck-linker behaves differently during different stages of the Eg5 ATPase cycle. In support of this idea, during the initial association of the motor with the microtubule ATP does not appear to affect ADP release; however, during processive motion an effect is seen. Of course, support by these data relies on a strict coupling of the neck-linker docking of one motor domain triggering ADP release from the other. This conventional kinesin like coupling might not be present in Eg5. In considering the model in Figure 6.6, specifically species 6, the position of what was the rearward microtubule bound motor domain is not known following ATP hydrolysis. Intramolecular strain established by having both motor domains associated with the microtubule could lead to a positioning of the rearward motor domain in front of what was the forward motor domain but unable to sufficiently interact with the microtubule binding site to stimulate ADP release. This

might itself lead to a partial docking of the neck-linker requiring ATP binding to complete. If this situation were true, the microtubule would still have the majority of the effect on the displacement of the neck-linker and ATP would only have a minor but detectable role.

A second requirement for neck-linker docking to structurally account for the steady-state rate-limiting transition is that another slower structural transition cannot precede or follow neck-linker movement. This is an important factor to consider because the observed rate for neck-linker reorientation by monomeric Eg5 was over 100-fold faster than the steady-state rate-limiting transition by dimeric Eg5 [251]. Maybe tethering a second motor domain at the end of the neck-linker inherently slows its movement. Alternatively, and probably more likely, neck-linker docking becomes limited by a structural transition on that second motor domain. Off the microtubule the two motor domains of dimeric Eg5 are biochemically different as seen by their different affinities for ADP (Figure 6.1). There is most likely a structural difference in those motor domains to account for that biochemical difference. Interaction with the microtubule might remove that structural difference, and in doing so, limit neck-linker docking. In terms of the ADP release measurements in this dissertation that lead to the discover of the steady-state rate-limiting transition (Figure 4.9), the biochemical/structural difference between dimeric Eg5 motor domains off the microtubule might not affect neck-linker docking at all, but lead to another structural rearrangement of unknown origin. Future structural and dynamics studies, hopefully including a crystal structure, will be necessary to determine the nature of the steady-state rate-limiting structural transition.

7.3.2 Eg5 Inhibitors and Diffusive Movement?

Another important area to pursue in regards to Eg5 is its inhibition by the multitude of Eg5 specific inhibitors. Work with monomeric Eg5 motors has indicated that these inhibitors cause microtubule association defects, slowed ADP release, and a propensity to go off pathway into an ATP bound state that will not hydrolyze the bound ATP. To by no means diminish the contribution of the inhibitor work on monomeric Eg5 motors; however, these features displayed by the monomer cannot truly account for the inhibition of force production by Eg5 *in vivo*. Microtubule association was slowed but it could still happen. ADP release was slowed but it was still rapid in the cycle. The nonproductive ATP bound complex significantly impacted the observed rate of steady-state turnover but was reversible, and therefore could not account for a mechanism of spindle collapse by means of suicide inhibition.

Work presented in Chapter 3 along with the cryo-EM results from the Hoenger lab [205] have led to the proposal that inhibition of dimeric Eg5 by these specific inhibitiors results from trapping both motor domains in an ATP-like state; thereby causing steric problems in the interaction of motor with the microtubule. Work with homotetrameric Eg5 and the inhibitor monastrol has indicated that inhibition does result in defects in associating with the microtubule [348]. The diffusive component to homotetrameric motility in the absence of any motor driven movement was observed. This implies that very weak interactions with the microtubule can be made but nothing sufficiently strong is made for the motor to impart a normal level of force on the microtubule. Alternatively, the motor might still be able to make a strong interaction with the microtubule, though at a much reduced frequency. This would prevent the motor from moving processively, drastically reducing force production on a given time scale.

These inhibitors might unlock the mechanism by which a motor is able to diffuse longitudinally along the microtubule axis without diffusing away from the microtubule, a mode of movement also important for the Kinesin-13 subfamily. The observation that Eg5 begins its ATPase cycle with both motor domains associated with the microtubule seems very intriguing in relation to this question. Potentially, if ADP release could be blocked from the motor domain that releases ADP slowly, the motor should also be blocked from entering a force producing state. This dissertation has demonstrated that ATP cannot bind until the slow structural transition kinetically coupled with ADP release from the second motor domain occurs. The motor might then only engage in many successive, rapid, weak microtubule interactions and appear as though it is diffusing along the microtubule lattice. *In vivo*, a particular microtubule structure might accelerate the motor entering into a dual head bound state from which it can generate force. A recent report [349] suggested that the ATP-promoted, motor-based movement by Eg5 becomes favored when the motor can crosslink two microtubules. The literature lacks a comparable mechanistic analysis to this dissertation on the Kinesin-13s, but they also seem like a good candidate to have a step in the cycle regulatable by microtubule architecture. In the case of the Kinesin-13s, the architectural cue has been established to be the microtubule ends. The Kinesin-13s have an affinity for the microtubule ends and display a stimulated steady-state ATPase when bound at a microtubule end [98, 119, 350].

ABBREVIATIONS AND TERMS

AMPPNP—adenosine 5′-(β,γ-imido)triphosphate, an ATP analogue that is not hydrolysable by Kinesin motors.

Apyrase—(Grade VII, Sigma-Aldrich Co.) an enzyme that preferentially cleaves the β-phosphate off of ADP leaving AMP, which does not bind kinesin motors, and inorganic phosphate.

ATPγS—adenosine-5′(γ-thio)triphosphate, an ATP analogue that kinesin motors hydrolyze much slower than ATP.

AXP—refers to any adenosine nucleotide (ADP, ATP, ATPγS, or AMPPNP).

Eg5-367$_{NF}$—monomeric Eg5 motor domains comprised of the first 367 amino acids of the human gene. The purification process resulted in motor without ADP on the active-site. The motor was purified by Jared C. Cochran.

Eg5-513—dimeric Eg5 comprised of the first 513 amino acids of the human gene.

Eg5-513-5His—dimeric Eg5-513 with a 5X histag at the C-terminus.

MantAXP—refers to a racemate (Invitrogen) of 2′(3′)-O-(N-methylanthraniloyl) labeled ADP or ATP. These nucleotides are more highly fluorescent when bound at the active-site of a Kinesin motor as compared to being free in solution.

MDCC-PBP—the phosphate binding protein from the lab of Martin Webb. It has been labeled with 7-diethylamino-3-((((2-maleimidyl)ethyl)amino)carbonyl)coumarin which responds to changes in the local environment around the fluorophore. When the protein binds inorganic phosphate, a fluorescence enhancement is observed.

***S*-monastrol**—a specific inhibitor to the ATPase of Eg5.

Monoaster—when Eg5 is inhibited a normal bipolar spindle collapses into a structure containing all γ-tubulin foci located in a central region with microtubules emanating outward in all directions. The chromosomes are located in a circular pattern surrounding microtubule aster.

P_i—inorganic phosphate.

PNPase—purine nucleoside phosphorylase (Sigma-Aldrich Co.) will covalently attach inorganic phosphate to 7-methylguanosine.

Processivity—the degree to which a motor is able to stay bound to its protofilament partner over multiple rounds of its ATPase cycle.

PuTP—refers to a purine nucleotide triphosphate. The purine bases are Adenine and Guanine.

R234K—refers to Eg5-513-5His that has had arginine 234 mutated to a lysine. This mutant displays predominantly wild-type kinetics but has >100 fold reduction in the rate of ATP hydrolysis.

Taxol—Paclitaxel (Sigma-Aldrich Co.) from *Taxus brevifoli*a acts as a stabilizer of microtubule dynamics through binding to the β-subunit of the tubulin dimer.

BIBLIOGRAPHY

1. Sauer G., Korner R., Hanisch A., Ries A., Nigg E.A., and Sillje H.H. (2005). Proteome analysis of the human mitotic spindle**.** Mol. Cell Proteomics. *4***:** 35-43.

2. Goshima G., Wollman R., Goodwin S.S., Zhang N., Scholey J.M., Vale R.D., and Stuurman N. (2007). Genes Required for Mitotic Spindle Assembly in Drosophila S2 Cells**.** Science *316***:** 417-421.

3. Erenpreisa J. and Cragg M. (2001). Mitotic death: a mechanism of survival? A review**.** Cancer Cell International *1***:** 1.

4. Lew D.J. and Burke D.J. (2003). The spindle assembly and spindle position checkpoints**.** Annu. Rev. Genet. *37***:** 251-282.

5. Michel L., Benezra R., and az-Rodriguez E. (2004). MAD2 dependent mitotic checkpoint defects in tumorigenesis and tumor cell death: a double edged sword**.** Cell Cycle *3***:** 990-992.

6. Xie S., Xie B., Lee M.Y., and Dai W. (2005). Regulation of cell cycle checkpoints by polo-like kinases**.** Oncogene *24***:** 277-286.

7. Tao W., South V.J., Zhang Y., Davide J.P., Farrell L., Kohl N.E., Sepp-Lorenzino L., and Lobell R.B. (2005). Induction of apoptosis by an inhibitor of the mitotic kinesin KSP requires both activation of the spindle assembly checkpoint and mitotic slippage**.** Cancer Cell *8***:** 49-59.

8. Marcus A.I., Peters U., Thomas S.L., Garrett S., Zelnak A., Kapoor T.M., and Giannakakou P. (2005). Mitotic kinesin inhibitors induce mitotic arrest and cell death in Taxol-resistant and -sensitive cancer cells**.** J. Biol. Chem. *280***:** 11569-11577.

9. Giono L.E. and Manfredi J.J. (2006). The p53 tumor suppressor participates in multiple cell cycle checkpoints**.** J. Cell Physiol *209***:** 13-20.

10. Nakanishi M., Shimada M., and Niida H. (2006). Genetic instability in cancer cells by impaired cell cycle checkpoints**.** Cancer Science *97***:** 984-989.

11. Sharp D.J., Rogers G.C., and Scholey J.M. (2000). Microtubule motors in mitosis**.** Nature *407***:** 41-47.

12. Mitchison T.J. and Salmon E.D. (2001). Mitosis: a history of division**.** Nat. Cell Biol. *3***:** E17-E21.

13. Karsenti E. and Vernos I. (2001). The Mitotic Spindle: A Self-Made Machine**.** Science *294***:** 543-547.

14. Wittmann T., Hyman A., and Desai A. (2001). The spindle: a dynamic assembly of microtubules and motors**.** Nat. Cell Biol. *3***:** E28-E34.

15. Brust-Mascher I. and Scholey J.M. (2002). Microtubule flux and sliding in mitotic spindles of Drosophila embryos**.** Mol. Biol. Cell *13***:** 3967-3975.

16. McIntosh J.R., Grishchuk E.L., and West R.R. (2002). Chromosome-microtubule interactions during mitosis**.** Annu. Rev. Cell Dev. Biol *18***:** 193-219.

17. Nedelec F. (2002). Computer simulations reveal motor properties generating stable antiparallel microtubule interactions**.** J. Cell Biol. *158***:** 1005-1015.

18. Scholey J.M., Brust-Mascher I., and Mogilner A. (2003). Cell division**.** Nature *422***:** 746-752.

19. Kwon M. and Scholey J. (2004). Spindle mechanics and dynamics during mitosis in *Drosophila***.** Trends Cell Biol. *14***:** 194-205.

20. Desai A. and Mitchison T.J. (1997). Microtubule polymerization dynamics**.** Annu. Rev. Cell Dev. Biol. *13***:** 83-117.

21. Nogales E., Wolf S.G., and Downing K.H. (1998). Structure of the alpha beta tubulin dimer by electron crystallography**.** Nature *391***:** 199-203.

22. Downing K.H. and Nogales E. (1998). New insights into microtubule structure and function from the atomic model of tubulin**.** Eur. Biophys. J. *27***:** 431-436.

23. Chretien D. and Wade R.H. (1991). New data on the microtubule surface lattice**.** Biol. Cell *71***:** 161-174.

24. Wade R.H. and Chretien D. (1993). Cryoelectron microscopy of microtubules**.** J. Struct. Biol. *110***:** 1-27.

25. Li H., DeRosier D.J., Nicholson W.V., Nogales E., and Downing K.H. (2002). Microtubule Structure at 8 A Resolution**.** Structure *10***:** 1317-1328.

26. Mitchison T.J. (1993). Localization of an exchangeable GTP binding site at the plus end of microtubules**.** Science *261***:** 1044-1047.

27. Hirose K., Fan J., and Amos L.A. (1995). Re-examination of the polarity of microtubules and sheets decorated with kinesin motor domain**.** J. Mol. Biol. *251***:** 329-333.

28. Fan J., Griffiths A.D., Lockhart A., Cross R.A., and Amos L.A. (1996). Microtubule minus ends can be labelled with a phage display antibody specific to alpha-tubulin**.** J. Mol. Biol. *259***:** 325-330.

29. Nogales E., Whittaker M., Milligan R.A., and Downing K.H. (1999). High-resolution model of the microtubule**.** Cell *96***:** 79-88.

30. Allen C. and Borisy G.G. (1974). Structural polarity and directional growth of microtubules of Chlamydomonas flagella**.** J. Mol. Biol. *90***:** 381-402.

31. Weisenberg R.C., Deery W.J., and Dickinson P.J. (1976). Tubulin-nucleotide interactions during the polymerization and depolymerization of microtubules**.** Biochemistry *15***:** 4248-4254.

32. Carlier M.F. and Pantaloni D. (1981). Kinetic analysis of guanosine 5'-triphosphate hydrolysis associated with tubulin polymerization**.** Biochemistry *20***:** 1918-1924.

33. Gelfand V.I. and Bershadsky A.D. (1991). Microtubule dynamics: mechanism, regulation, and function**.** Annu. Rev. Cell Biol. *7***:** 93-116.

34. Nogales E. and Wang H.W. (2006). Structural mechanisms underlying nucleotide-dependent self-assembly of tubulin and its relatives**.** Current Opinion in Structural Biology *16***:** 221-229.

35. Dammermann A., Desai A., and Oegema K. (2003). The minus end in sight**.** Current Biology *13***:** R614-R624.

36. Mitchison T. and Kirschner M. (1984). Dynamic instability of microtubule growth**.** Nature *312***:** 237-242.

37. Kristofferson D., Mitchison T., and Kirschner M. (1986). Direct observation of steady-state microtubule dynamics**.** J. Cell Biol. *102***:** 1007-1019.

38. Cassimeris L., Pryer N.K., and Salmon E.D. (1988). Real-time observations of microtubule dynamic instability in living cells**.** J. Cell Biol. *107***:** 2223-2231.

39. Walker R.A., O'Brien E.T., Pryer N.K., Soboeiro M.F., Voter W.A., Erickson H.P., and Salmon E.D. (1988). Dynamic instability of individual microtubules analyzed by video light microscopy: rate constants and transition frequencies**.** J. Cell Biol. *107***:** 1437-1448.

40. Mandelkow E.M., Mandelkow E., and Milligan R.A. (1991). Microtubule dynamics and microtubule caps: a time-resolved cryo-electron microscopy study**.** J. Cell Biol. *114***:** 977-991.

41. Drechsel D.N. and Kirschner M.W. (1994). The minimum GTP cap required to stabilize microtubules**.** Curr. Biol. *4***:** 1053-1061.

42. Hyman A.A., Chretien D., Arnal I., and Wade R.H. (1995). Structural changes accompanying GTP hydrolysis in microtubules: information from a slowly hydrolyzable analogue guanylyl-(alpha,beta)-methylene-diphosphonate**.** J. Cell Biol. *128***:** 117-125.

43. Alberts B., Johnson A., Lewis J., Raff M., Roberts K., and Walter P. (2007). Molecular Biology of the Cell, 4 edn. (New York: Garland Science).

44. Lowe J., Li H., Downing K.H., and Nogales E. (2001). Refined structure of [alpha][beta]-tubulin at 3.5 A resolution**.** Journal of Molecular Biology *313***:** 1045-1057.

45. Hirokawa N. and Takemura R. (2004). Kinesin superfamily proteins and their various functions and dynamics**.** Exp. Cell Res. *301***:** 50-59.

46. Caviston J.P. and Holzbaur E.L. (2006). Microtubule motors at the intersection of trafficking and transport**.** Trends Cell Biol. *16***:** 530-537.

47. Lakamper S. and Meyhofer E. (2006). Back on track - On the role of the microtubule for kinesin motility and cellular function**.** J. Muscle Res. Cell Motil. 1-11.

48. Salmon E.D., Leslie R.J., Saxton W.M., Karow M.L., and McIntosh J.R. (1984). Spindle microtubule dynamics in sea urchin embryos: analysis using a fluorescein-labeled tubulin and measurements of fluorescence redistribution after laser photobleaching**.** J. Cell Biol. *99***:** 2165-2174.

49. Saxton W.M., Stemple D.L., Leslie R.J., Salmon E.D., Zavortink M., and McIntosh J.R. (1984). Tubulin dynamics in cultured mammalian cells**.** J. Cell Biol. *99***:** 2175-2186.

50. McNally F.J. (1996). Modulation of microtubule dynamics during the cell cycle**.** Curr. Opin. Cell Biol. *8***:** 23-29.

51. Kirschner M. and Mitchison T. (1986). Beyond self-assembly: from microtubules to morphogenesis**.** Cell *45***:** 329-342.

52. Holy T.E. and Leibler S. (1994). Dynamic instability of microtubules as an efficient way to search in space**.** Proc. Natl. Acad. Sci. U. S. A *91***:** 5682-5685.

53. Mogilner A., Wollman R., Civelekoglu-Scholey G., and Scholey J. (2006). Modeling mitosis**.** Trends Cell Biol. *16***:** 88-96.

54. Skibbens R.V., Skeen V.P., and Salmon E.D. (1993). Directional instability of kinetochore motility during chromosome congression and segregation in mitotic newt lung cells: a push-pull mechanism**.** J. Cell Biol. *122***:** 859-875.

55. Hyman A.A. (1995). Microtubule dynamics. Kinetochores get a grip**.** Curr. Biol. *5***:** 483-484.

56. Maiato H., DeLuca J., Salmon E.D., and Earnshaw W.C. (2004). The dynamic kinetochore-microtubule interface**.** J. Cell Sci. *117***:** 5461-5477.

57. Ganem N.J. and Compton D.A. (2006). Functional roles of poleward microtubule flux during mitosis**.** Cell Cycle *5***:** 481-485.

58. Vale R.D. (1996). Switches, latches, and amplifiers: common themes of G proteins and molecular motors**.** J. Cell Biol. *135***:** 291-302.

59. Mallik R. and Gross S.P. (2004). Molecular motors: strategies to get along**.** Curr. Biol. *14***:** R971-R982.

60. Burgess S.A. and Knight P.J. (2004). Is the dynein motor a winch? Curr. Opin. Struct. Biol. *14***:** 138-146.

61. Hook P. and Vallee R.B. (2006). The dynein family at a glance**.** J. Cell Sci. *119***:** 4369-4371.

62. Cross R.A. (2004). Molecular motors: Dynein's gearbox**.** Curr. Biol. *14***:** R355-R356.

63. Koonce M.P. and Samso M. (2004). Of rings and levers: the dynein motor comes of age**.** Trends Cell Biol. *14***:** 612-619.

64. Mocz G. and Gibbons I.R. (1996). Phase Partition Analysis of Nucleotide Binding to Axonemal Dynein**.** Biochemistry *35***:** 9204-9211.

65. Mocz G., Helms M.K., Jameson D.M., and Gibbons I.R. (1998). Probing the Nucleotide Binding Sites of Axonemal Dynein with the Fluorescent Nucleotide Analogue 2'(3')-O-(-N-Methylanthraniloyl)-adenosine 5'-Triphosphate**.** Biochemistry *37***:** 9862-9869.

66. Sakato M. and King S.M. (2004). Design and regulation of the AAA+ microtubule motor dynein**.** Journal of Structural Biology *146***:** 58-71.

67. Mallik R., Carter B.C., Lex S.A., King S.J., and Gross S.P. (2004). Cytoplasmic dynein functions as a gear in response to load**.** Nature *427***:** 649-652.

68. Silvanovich A., Li M.g., Serr M., Mische S., and Hays T.S. (2003). The Third P-loop Domain in Cytoplasmic Dynein Heavy Chain Is Essential for Dynein Motor Function and ATP-sensitive Microtubule Binding**.** Mol. Biol. Cell *14***:** 1355-1365.

69. Berg J.S., Powell B.C., and Cheney R.E. (2001). A Millennial Myosin Census**.** Mol. Biol. Cell *12***:** 780-794.

70. Mermall V., Post P.L., and Mooseker M.S. (1998). Unconventional myosins in cell movement, membrane traffic, and signal transduction**.** Science *279***:** 527-533.

71. Sellers J.R. (2000). Myosins: a diverse superfamily**.** Biochim. Biophys. Acta *1496***:** 3-22.

72. Hofmann W.A., Johnson T., Klapczynski M., Fan J.L., and de L.P. (2006). From transcription to transport: emerging roles for nuclear myosin I**.** Biochem. Cell Biol. *84***:** 418-426.

73. Kull F.J., Vale R.D., and Fletterick R.J. (1998). The case for a common ancestor: kinesin and myosin motor proteins and G proteins**.** J. Muscle Res. Cell Motil. *19***:** 877-886.

74. Sablin E.P. and Fletterick R.J. (2001). Nucleotide switches in molecular motors: structural analysis of kinesins and myosins**.** Curr. Opin. Struct. Biol. *11***:** 716-724.

75. De La Cruz E.M. and Ostap E.M. (2004). Relating biochemistry and function in the myosin superfamily**.** Curr. Opin. Cell Biol. *16***:** 61-67.

76. Kambara T. and Ikebe M. (2006). A Unique ATP Hydrolysis Mechanism of Single-headed Processive Myosin, Myosin IX**.** J. Biol. Chem. *281***:** 4949-4957.

77. Lymn R.W. and Taylor E.W. (1971). Mechanism of adenosine triphosphate hydrolysis by actomyosin**.** Biochemistry *10***:** 4617-4624.

78. Marston S.B. and Taylor E.W. (1980). Comparison of the myosin and actomyosin ATPase mechanisms of the four types of vertebrate muscles**.** Journal of Molecular Biology *139***:** 573-600.

79. Ritchie M.D., Geeves M.A., Woodward S.K.A., and Manstein D.J. (1993). Kinetic Characterization of a Cytoplasmic Myosin Motor Domain Expressed in Dictyostelium discoideum**.** PNAS *90***:** 8619-8623.

80. Ostap E.M. and Pollard T.D. (1996). Biochemical kinetic characterization of the Acanthamoeba myosin-I ATPase**.** J. Cell Biol. *132***:** 1053-1060.

81. Geeves M.A. and Holmes K.C. (1999). STRUCTURAL MECHANISM OF MUSCLE CONTRACTION**.** Annual Review of Biochemistry *68***:** 687-728.

82. De La Cruz E.M., Wells A.L., Rosenfeld S.S., Ostap E.M., and Sweeney H.L. (1999). The kinetic mechanism of myosin V**.** Proc. Natl. Acad. Sci. U. S. A *96***:** 13726-13731.

83. De La Cruz E.M., Sweeney H.L., and Ostap E.M. (2000). ADP Inhibition of Myosin V ATPase Activity**.** Biophys. J. *79***:** 1524-1529.

84. De La Cruz E.M., Ostap E.M., and Sweeney H.L. (2001). Kinetic Mechanism and Regulation of Myosin VI**.** J. Biol. Chem. *276***:** 32373-32381.

85. Yengo C.M., De La Cruz E.M., Safer D., Ostap E.M., and Sweeney H.L. (2002). Kinetic Characterization of the Weak Binding States of Myosin V**.** Biochemistry *41***:** 8508-8517.

86. Robblee J.P., Olivares A.O., and De La Cruz E.M. (2004). Mechanism of Nucleotide Binding to Actomyosin VI: EVIDENCE FOR ALLOSTERIC HEAD-HEAD COMMUNICATION**.** J. Biol. Chem. *279***:** 38608-38617.

87. Rosenfeld S.S. and Sweeney H.L. (2004). A model of myosin V processivity**.** J. Biol. Chem. *279***:** 40100-40111.

88. Hannemann D.E., Cao W., Olivares A.O., Robblee J.P., and DeLaCruz E.M. (2005). Magnesium, ADP, and Actin Binding Linkage of Myosin V: Evidence for Multiple Myosin V-ADP and Actomyosin V-ADP States**.** Biochemistry *44***:** 8826-8840.

89. Olivares A.O. and De La Cruz E.M. (2005). Holding the reins on Myosin V**.** PNAS *102***:** 13719-13720.

90. Rosenfeld S.S., Houdusse A., and Sweeney H.L. (2005). Magnesium Regulates ADP Dissociation from Myosin V**.** J. Biol. Chem. *280***:** 6072-6079.

91. Sweeney H.L., Park H., Zong A.B., Yang Z., Selvin P.R., and Rosenfeld S.S. (2007). How myosin VI coordinates its heads during processive movement**.** EMBO J. *26***:** 2682-2692.

92. Vale R.D., Reese T.S., and Sheetz M.P. (1985). Identification of a novel force-generating protein, kinesin, involved in microtubule-based motility**.** Cell *42***:** 39-50.

93. Brady S.T. (1985). A novel brain ATPase with properties expected for the fast axonal transport motor**.** Nature *317***:** 73-75.

94. Gilbert S.P. and Sloboda R.D. (1986). Identification of a MAP 2-like ATP-binding protein associated with axoplasmic vesicles that translocate on isolated microtubules**.** J. Cell Biol. *103***:** 947-956.

95. Dagenbach E.M. and Endow S.A. (2004). A new kinesin tree**.** J. Cell Sci. *117***:** 3-7.

96. Lawrence C.J., Malmberg R.L., Muszynski M.G., and Dawe R.K. (2002). Maximum likelihood methods reveal conservation of function among closely related kinesin families**.** J. Mol. Evol. *54***:** 42-53.

97. Lawrence C.J., Dawe R.K., Christie K.R., Cleveland D.W., Dawson S.C., Endow S.A., Goldstein L.S., Goodson H.V., Hirokawa N., Howard J. et al. (2004). A standardized kinesin nomenclature**.** J. Cell Biol. *167***:** 19-22.

98. Hunter A.W., Caplow M., Coy D.L., Hancock W.O., Diez S., Wordeman L., and Howard J. (2003). The kinesin-related protein MCAK is a microtubule depolymerase that forms an ATP-hydrolyzing complex at microtubule ends**.** Mol. Cell *11***:** 445-457.

99. Helenius J., Brouhard G., Kalaidzidis Y., Diez S., and Howard J. (2006). The depolymerizing kinesin MCAK uses lattice diffusion to rapidly target microtubule ends**.** Nature *441***:** 115-119.

100. Stenoien D.L. and Brady S.T. (1997). Immunochemical analysis of kinesin light chain function**.** Mol. Biol. Cell *8***:** 675-689.

101. Khodjakov A., Lizunova E.M., Minin A.A., Koonce M.P., and Gyoeva F.K. (1998). A specific light chain of kinesin associates with mitochondria in cultured cells**.** Mol. Biol. Cell *9***:** 333-343.

102. Gyoeva F.K., Bybikova E.M., and Minin A.A. (2000). An isoform of kinesin light chain specific for the Golgi complex**.** J. Cell Sci. *113 (Pt 11)***:** 2047-2054.

103. McCart A.E., Mahony D., and Rothnagel J.A. (2003). Alternatively spliced products of the human kinesin light chain 1 (KNS2) gene**.** Traffic. *4***:** 576-580.

104. Sawin K.E., LeGuellec K., Philippe M., and Mitchison T.J. (1992). Mitotic spindle organization by a plus-end-directed microtubule motor**.** Nature *359***:** 540-543.

105. Grancell A. and Sorger P.K. (1998). Chromosome movement: Kinetochores motor along**.** Current Biology *8***:** R382-R385.

106. Chakravarty A., Howard L., and Compton D.A. (2004). A mechanistic model for the organization of microtubule asters by motor and non-motor proteins in a mammalian mitotic extract**.** Mol. Biol. Cell *15***:** 2116-2132.

107. Maney T., Hunter A.W., Wagenbach M., and Wordeman L. (1998). Mitotic centromere-associated kinesin is important for anaphase chromosome segregation**.** J. Cell Biol. *142***:** 787-801.

108. Desai A., Verma S., Mitchison T.J., and Walczak C.E. (1999). Kin I kinesins are microtubule-destabilizing enzymes**.** Cell *96***:** 69-78.

109. Sharp D.J., McDonald K.L., Brown H.M., Matthies H.J., Walczak C., Vale R.D., Mitchison T.J., and Scholey J.M. (1999). The bipolar kinesin, KLP61F, cross-links microtubules within interpolar microtubule bundles of Drosophila embryonic mitotic spindles**.** J. Cell Biol. *144***:** 125-138.

110. Kline-Smith S.L., Khodjakov A., Hergert P., and Walczak C.E. (2004). Depletion of centromeric MCAK leads to chromosome congression and segregation defects due to improper kinetochore attachments**.** Mol. Biol. Cell *15***:** 1146-1159.

111. Kwok B.H., Yang J.G., and Kapoor T.M. (2004). The rate of bipolar spindle assembly depends on the microtubule-gliding velocity of the mitotic kinesin Eg5**.** Curr. Biol. *14***:** 1783-1788.

112. Cui W., Sproul L.R., Gustafson S.M., Matthies H.J., Gilbert S.P., and Hawley R.S. (2005). Drosophila Nod protein binds preferentially to the plus ends of microtubules and promotes microtubule polymerization in vitro**.** Mol. Biol. Cell *16***:** 5400-5409.

113. Sproul L.R., Anderson D.J., Mackey A.T., Saunders W.S., and Gilbert S.P. (2005). Cik1 targets the minus-end kinesin depolymerase kar3 to microtubule plus ends**.** Curr. Biol. *15***:** 1420-1427.

114. Wordeman L. (2005). Microtubule-depolymerizing kinesins**.** Curr. Opin. Cell Biol. *17***:** 82-88.

115. Kinoshita K., Noetzel T.L., Arnal I., Drechsel D.N., and Hyman A.A. (2006). Global and local control of microtubule destabilization promoted by a catastrophe kinesin MCAK/XKCM1**.** J. Muscle Res. Cell Motil. 1-8.

116. Maney T., Wagenbach M., and Wordeman L. (2001). Molecular dissection of the microtubule depolymerizing activity of mitotic centromere-associated kinesin**.** J. Biol. Chem. *276***:** 34753-34758.

117. Ovechkina Y., Wagenbach M., and Wordeman L. (2002). K-loop insertion restores microtubule depolymerizing activity of a "neckless" MCAK mutant**.** J. Cell Biol. *159***:** 557-562.

118. Newton C.N., Wagenbach M., Ovechkina Y., Wordeman L., and Wilson L. (2004). MCAK, a Kin I kinesin, increases the catastrophe frequency of steady-state HeLa cell microtubules in an ATP-dependent manner in vitro**.** FEBS Lett. *572***:** 80-84.

119. Hertzer K.M., Ems-McClung S.C., Kline-Smith S.L., Lipkin T.G., Gilbert S.P., and Walczak C.E. (2006). Full-length dimeric MCAK is a more efficient microtubule depolymerase than minimal domain monomeric MCAK**.** Mol. Biol. Cell *17***:** 700-710.

120. Moores C.A., Cooper J., Wagenbach M., Ovechkina Y., Wordeman L., and Milligan R.A. (2006). The role of the kinesin-13 neck in microtubule depolymerization**.** Cell Cycle *5***:** 1812-1815.

121. Ems-McClung S.C., Hertzer K.M., Zhang X., Miller M.W., and Walczak C.E. (2007). The Interplay of the N- and C-Terminal Domains of MCAK Control Microtubule Depolymerization Activity and Spindle Assembly**.** Mol. Biol. Cell *18***:** 282-294.

122. Howard J. and Hyman A.A. (2007). Microtubule polymerases and depolymerases**.** Current Opinion in Cell Biology *19***:** 31-35.

123. Chu H.M., Yun M., Anderson D.E., Sage H., Park H.W., and Endow S.A. (2005). Kar3 interaction with Cik1 alters motor structure and function**.** EMBO J. *24***:** 3214-3223.

124. Yen T.J., Compton D.A., Wise D., Zinkowski R.P., Brinkley B.R., Earnshaw W.C., and Cleveland D.W. (1991). CENP-E, a novel human centromere-associated protein required for progression from metaphase to anaphase**.** EMBO J. *10***:** 1245-1254.

125. Liao H., Li G., and Yen T.J. (1994). Mitotic regulation of microtubule cross-linking activity of CENP-E kinetochore protein**.** Science *265***:** 394-398.

126. Lombillo V.A., Nislow C., Yen T.J., Gelfand V.I., and McIntosh J.R. (1995). Antibodies to the kinesin motor domain and CENP-E inhibit microtubule depolymerization-dependent motion of chromosomes in vitro**.** J. Cell Biol. *128***:** 107-115.

127. Schaar B.T., Chan G.K., Maddox P., Salmon E.D., and Yen T.J. (1997). CENP-E function at kinetochores is essential for chromosome alignment**.** J. Cell Biol. *139***:** 1373-1382.

128. Wood K.W., Sakowicz R., Goldstein L.S., and Cleveland D.W. (1997). CENP-E is a plus end-directed kinetochore motor required for metaphase chromosome alignment**.** Cell *91***:** 357-366.

129. Yao X., Anderson K.L., and Cleveland D.W. (1997). The microtubule-dependent motor centromere-associated protein E (CENP-E) is an integral component of kinetochore corona fibers that link centromeres to spindle microtubules**.** J. Cell Biol. *139***:** 435-447.

130. Putkey F.R., Cramer T., Morphew M.K., Silk A.D., Johnson R.S., McIntosh J.R., and Cleveland D.W. (2002). Unstable kinetochore-microtubule capture and chromosomal instability following deletion of CENP-E**.** Dev. Cell *3***:** 351-365.

131. Tanudji M., Shoemaker J., L'Italien L., Russell L., Chin G., and Schebye X.M. (2004). Gene silencing of CENP-E by small interfering RNA in HeLa cells leads to missegregation of chromosomes after a mitotic delay**.** Mol. Biol. Cell *15***:** 3771-3781.

132. Schafer-Hales K., Iaconelli J., Snyder J.P., Prussia A., Nettles J.H., El-Naggar A., Khuri F.R., Giannakakou P., and Marcus A.I. (2007). Farnesyl transferase inhibitors impair chromosomal maintenance in cell lines and human tumors by compromising CENP-E and CENP-F function**.** Mol Cancer Ther *6***:** 1317-1328.

133. Mountain V., Simerly C., Howard L., Ando A., Schatten G., and Compton D.A. (1999). The kinesin-related protein, HSET, opposes the activity of Eg5 and cross-links microtubules in the mammalian mitotic spindle**.** J. Cell Biol. *147***:** 351-366.

134. Mountain V. and Compton D.A. (2000). Dissecting the role of molecular motors in the mitotic spindle**.** Anat. Rec. *261***:** 14-24.

135. Wilde A., Lizarraga S.B., Zhang L., Wiese C., Gliksman N.R., Walczak C.E., and Zheng Y. (2001). Ran stimulates spindle assembly by altering microtubule dynamics and the balance of motor activities**.** Nat. Cell Biol. *3***:** 221-227.

136. Goshima G. and Vale R.D. (2005). Cell cycle-dependent dynamics and regulation of mitotic kinesins in Drosophila S2 cells**.** Mol. Biol. Cell *16***:** 3896-3907.

137. Tao L., Mogilner A., Civelekoglu-Scholey G., Wollman R., Evans J., Stahlberg H., and Scholey J.M. (2006). A homotetrameric kinesin-5, KLP61F, bundles microtubules and antagonizes Ncd in motility assays**.** Curr. Biol. *16***:** 2293-2302.

138. Chin G.M. and Herbst R. (2006). Induction of apoptosis by monastrol, an inhibitor of the mitotic kinesin Eg5, is independent of the spindle checkpoint**.** Mol. Cancer Ther. *5***:** 2580-2591.

139. Kull F.J., Sablin E.P., Lau R., Fletterick R.J., and Vale R.D. (1996). Crystal structure of the kinesin motor domain reveals a structural similarity to myosin**.** Nature *380***:** 550-555.

140. Sablin E.P., Kull F.J., Cooke R., Vale R.D., and Fletterick R.J. (1996). Crystal structure of the motor domain of the kinesin-related motor ncd**.** Nature *380***:** 555-559.

141. Marx A., Muller J., and Mandelkow E. (2005). The structure of microtubule motor proteins**.** Adv. Protein Chem. *71***:** 299-344.

142. Kikkawa M., Sablin E.P., Okada Y., Yajima H., Fletterick R.J., and Hirokawa N. (2001). Switch-based mechanism of kinesin motors**.** Nature *411***:** 439-445.

143. Gilbert S.P., Webb M.R., Brune M., and Johnson K.A. (1995). Pathway of processive ATP hydrolysis by kinesin**.** Nature *373***:** 671-676.

144. Hirose K., Lockhart A., Cross R.A., and Amos L.A. (1995). Nucleotide-dependent angular change in kinesin motor domain bound to tubulin**.** Nature *376***:** 277-279.

145. Rosenfeld S.S., Rener B., Correia J.J., Mayo M.S., and Cheung H.C. (1996). Equilibrium studies of kinesin-nucleotide intermediates**.** J. Biol. Chem. *271***:** 9473-9482.

146. Jiang W. and Hackney D.D. (1997). Monomeric kinesin head domains hydrolyze multiple ATP molecules before release from a microtubule**.** J. Biol. Chem. *272***:** 5616-5621.

147. Kawaguchi K. and Ishiwata S. (2001). Nucleotide-dependent single- to double-headed binding of kinesin**.** Science *291***:** 667-669.

148. Howard J., Hudspeth A.J., and Vale R.D. (1989). Movement of microtubules by single kinesin molecules**.** Nature *342***:** 154-158.

149. Block S.M., Goldstein L.S., and Schnapp B.J. (1990). Bead movement by single kinesin molecules studied with optical tweezers**.** Nature *348***:** 348-352.

150. Hackney D.D. (1995). Highly processive microtubule-stimulated ATP hydrolysis by dimeric kinesin head domains**.** Nature *377***:** 448-450.

151. Vale R.D., Funatsu T., Pierce D.W., Romberg L., Harada Y., and Yanagida T. (1996). Direct observation of single kinesin molecules moving along microtubules**.** Nature *380***:** 451-453.

152. Chandra R., Endow S.A., and Salmon E.D. (1993). An N-terminal truncation of the ncd motor protein supports diffusional movement of microtubules in motility assays**.** J. Cell Sci. *104 (Pt 3)***:** 899-906.

153. Case R.B., Pierce D.W., Hom-Booher N., Hart C.L., and Vale R.D. (1997). The directional preference of kinesin motors is specified by an element outside of the motor catalytic domain**.** Cell *90***:** 959-966.

154. Crevel I.M., Lockhart A., and Cross R.A. (1997). Kinetic evidence for low chemical processivity in ncd and Eg5**.** J. Mol. Biol. *273***:** 160-170.

155. deCastro M.J., Ho C.H., and Stewart R.J. (1999). Motility of dimeric ncd on a metal-chelating surfactant: evidence that ncd is not processive**.** Biochemistry *38***:** 5076-5081.

156. Pechatnikova E. and Taylor E.W. (1999). Kinetics processivity and the direction of motion of Ncd**.** Biophys. J. *77***:** 1003-1016.

157. deCastro M.J., Fondecave R.M., Clarke L.A., Schmidt C.F., and Stewart R.J. (2000). Working strokes by single molecules of the kinesin-related microtubule motor ncd**.** Nat. Cell Biol. *2***:** 724-729.

158. Foster K.A. and Gilbert S.P. (2000). Kinetic studies of dimeric Ncd: evidence that Ncd is not processive**.** Biochemistry *39***:** 1784-1791.

159. Vale R.D., Schnapp B.J., Mitchison T., Steuer E., Reese T.S., and Sheetz M.P. (1985). Different axoplasmic proteins generate movement in opposite directions along microtubules in vitro**.** Cell *43***:** 623-632.

160. McDonald H.B., Stewart R.J., and Goldstein L.S. (1990). The kinesin-like ncd protein of Drosophila is a minus end-directed microtubule motor**.** Cell *63***:** 1159-1165.

161. Walker R.A., Salmon E.D., and Endow S.A. (1990). The Drosophila claret segregation protein is a minus-end directed motor molecule**.** Nature *347***:** 780-782.

162. Hackney D.D. (1994). Evidence for alternating head catalysis by kinesin during microtubule-stimulated ATP hydrolysis**.** Proc. Natl. Acad. Sci. U. S. A *91***:** 6865-6869.

163. Lockhart A., Crevel I.M., and Cross R.A. (1995). Kinesin and ncd bind through a single head to microtubules and compete for a shared MT binding site**.** J. Mol. Biol. *249***:** 763-771.

164. Arnal I., Metoz F., Debonis S., and Wade R.H. (1996). Three-dimensional structure of functional motor proteins on microtubules**.** Curr. Biol. *6***:** 1265-1270.

165. Crevel I.M., Lockhart A., and Cross R.A. (1996). Weak and strong states of kinesin and ncd**.** J. Mol. Biol. *257***:** 66-76.

166. Hirose K., Lockhart A., Cross R.A., and Amos L.A. (1996). Three-dimensional cryoelectron microscopy of dimeric kinesin and ncd motor domains on microtubules**.** Proc. Natl. Acad. Sci. U. S. A *93***:** 9539-9544.

167. Sosa H., Dias D.P., Hoenger A., Whittaker M., Wilson-Kubalek E., Sablin E., Fletterick R.J., Vale R.D., and Milligan R.A. (1997). A model for the microtubule-Ncd motor protein complex obtained by cryo-electron microscopy and image analysis**.** Cell *90***:** 217-224.

168. Gilbert S.P., Moyer M.L., and Johnson K.A. (1998). Alternating site mechanism of the kinesin ATPase**.** Biochemistry *37***:** 792-799.

169. Hirose K., Cross R.A., and Amos L.A. (1998). Nucleotide-dependent structural changes in dimeric NCD molecules complexed to microtubules**.** J. Mol. Biol. *278***:** 389-400.

170. Hackney D.D. (2002). Pathway of ADP-stimulated ADP release and dissociation of tethered kinesin from microtubules. Implications for the extent of processivity**.** Biochemistry *41***:** 4437-4446.

171. Yun M., Bronner C.E., Park C.G., Cha S.S., Park H.W., and Endow S.A. (2003). Rotation of the stalk/neck and one head in a new crystal structure of the kinesin motor protein, Ncd**.** EMBO J. *22***:** 5382-5389.

172. Ma Y.Z. and Taylor E.W. (1997). Interacting head mechanism of microtubule-kinesin ATPase**.** J. Biol. Chem. *272***:** 724-730.

173. Foster K.A., Correia J.J., and Gilbert S.P. (1998). Equilibrium binding studies of non-claret disjunctional protein (Ncd) reveal cooperative interactions between the motor domains**.** J. Biol. Chem. *273***:** 35307-35318.

174. Foster K.A., Mackey A.T., and Gilbert S.P. (2001). A mechanistic model for Ncd directionality**.** J. Biol. Chem. *276***:** 19259-19266.

175. Hackney D.D., Malik A.S., and Wright K.W. (1989). Nucleotide-free kinesin hydrolyzes ATP with burst kinetics**.** J. Biol. Chem. *264***:** 15943-15948.

176. Sadhu A. and Taylor E.W. (1992). A kinetic study of the kinesin ATPase**.** J. Biol. Chem. *267***:** 11352-11359.

177. Ma Y.Z. and Taylor E.W. (1995). Kinetic mechanism of kinesin motor domain**.** Biochemistry *34***:** 13233-13241.

178. Ma Y.Z. and Taylor E.W. (1995). Mechanism of microtubule kinesin ATPase**.** Biochemistry *34***:** 13242-13251.

179. Ma Y.Z. and Taylor E.W. (1997). Kinetic mechanism of a monomeric kinesin construct**.** J. Biol. Chem. *272***:** 717-723.

180. Pechatnikova E. and Taylor E.W. (1997). Kinetic mechanism of monomeric non-claret disjunctional protein (Ncd) ATPase**.** J. Biol. Chem. *272***:** 30735-30740.

181. Moyer M.L., Gilbert S.P., and Johnson K.A. (1998). Pathway of ATP hydrolysis by monomeric and dimeric kinesin**.** Biochemistry *37***:** 800-813.

182. Mackey A.T. and Gilbert S.P. (2000). Moving a microtubule may require two heads: a kinetic investigation of monomeric Ncd**.** Biochemistry *39***:** 1346-1355.

183. Berliner E., Young E.C., Anderson K., Mahtani H.K., and Gelles J. (1995). Failure of a single-headed kinesin to track parallel to microtubule protofilaments**.** Nature *373***:** 718-721.

184. Hancock W.O. and Howard J. (1998). Processivity of the motor protein kinesin requires two heads**.** J. Cell Biol. *140***:** 1395-1405.

185. Hancock W.O. and Howard J. (1999). Kinesin's processivity results from mechanical and chemical coordination between the ATP hydrolysis cycles of the two motor domains**.** Proc. Natl. Acad. Sci. U. S. A *96***:** 13147-13152.

186. Rosenfeld S.S., Fordyce P.M., Jefferson G.M., King P.H., and Block S.M. (2003). Stepping and stretching. How kinesin uses internal strain to walk processively**.** J. Biol. Chem. *278***:** 18550-18556.

187. Uemura S. and Ishiwata S. (2003). Loading direction regulates the affinity of ADP for kinesin**.** Nat Struct Mol Biol *10***:** 308-311.

188. Schief W.R., Clark R.H., Crevenna A.H., and Howard J. (2004). Inhibition of kinesin motility by ADP and phosphate supports a hand-over-hand mechanism**.** Proc. Natl. Acad. Sci. U. S. A *101***:** 1183-1188.

189. Crevel I.M., Nyitrai M., Alonso M.C., Weiss S., Geeves M.A., and Cross R.A. (2004). What kinesin does at roadblocks: the coordination mechanism for molecular walking**.** EMBO J. *23***:** 23-32.

190. Klumpp L.M., Hoenger A., and Gilbert S.P. (2004). Kinesin's second step**.** Proc. Natl. Acad. Sci. U. S. A *101***:** 3444-3449.

191. Guydosh N.R. and Block S.M. (2006). Backsteps induced by nucleotide analogs suggest the front head of kinesin is gated by strain**.** PNAS *103***:** 8054-8059.

192. Hackney D.D. (1988). Kinesin ATPase: rate-limiting ADP release**.** Proc. Natl. Acad. Sci. U. S. A *85***:** 6314-6318.

193. Alonso M.C., Drummond D.R., Kain S., Hoeng J., Amos L., and Cross R.A. (2007). An ATP Gate Controls Tubulin Binding by the Tethered Head of Kinesin-1**.** Science *316***:** 120-123.

194. Rice S., Lin A.W., Safer D., Hart C.L., Naber N., Carragher B.O., Cain S.M., Pechatnikova E., Wilson-Kubalek E.M., Whittaker M. et al. (1999). A structural change in the kinesin motor protein that drives motility**.** Nature *402***:** 778-784.

195. Hua W., Young E.C., Fleming M.L., and Gelles J. (1997). Coupling of kinesin steps to ATP hydrolysis**.** Nature *388***:** 390-393.

196. Schnitzer M.J. and Block S.M. (1997). Kinesin hydrolyses one ATP per 8-nm step**.** Nature *388***:** 386-390.

197. Coy D.L., Wagenbach M., and Howard J. (1999). Kinesin takes one 8-nm step for each ATP that it hydrolyzes**.** J. Biol. Chem. *274***:** 3667-3671.

198. Endres N.F., Yoshioka C., Milligan R.A., and Vale R.D. (2006). A lever-arm rotation drives motility of the minus-end-directed kinesin Ncd**.** Nature *439***:** 875-878.

199. Hoenger A., Sack S., Thormahlen M., Marx A., Muller J., Gross H., and Mandelkow E. (1998). Image reconstructions of microtubules decorated with monomeric and dimeric kinesins: comparison with x-ray structure and implications for motility**.** J. Cell Biol. *141***:** 419-430.

200. Hoenger A., Thormahlen M., az-Avalos R., Doerhoefer M., Goldie K.N., Muller J., and Mandelkow E. (2000). A new look at the microtubule binding patterns of dimeric kinesins**.** J. Mol. Biol. *297***:** 1087-1103.

201. Sosa H. and Milligan R.A. (1996). Three-dimensional structure of ncd-decorated microtubules obtained by a back-projection method**.** J. Mol. Biol. *260***:** 743-755.

202. Cole D.G., Saxton W.M., Sheehan K.B., and Scholey J.M. (1994). A "slow" homotetrameric kinesin-related motor protein purified from Drosophila embryos**.** J. Biol. Chem. *269***:** 22913-22916.

203. Kashina A.S., Baskin R.J., Cole D.G., Wedaman K.P., Saxton W.M., and Scholey J.M. (1996). A bipolar kinesin**.** Nature *379***:** 270-272.

204. Hildebrandt E.R., Gheber L., Kingsbury T., and Hoyt M.A. (2006). Homotetrameric Form of Cin8p, a Saccharomyces cerevisiae Kinesin-5 Motor, Is Essential for Its in Vivo Function**.** J. Biol. Chem. *281***:** 26004-26013.

205. Krzysiak T.C., Wendt T., Sproul L.R., Tittmann P., Gross H., Gilbert S.P., and Hoenger A. (2006). A structural model for monastrol inhibition of dimeric kinesin Eg5**.** EMBO J. *25***:** 2263-2273.

206. Whitehead C.M. and Rattner J.B. (1998). Expanding the role of HsEg5 within the mitotic and post-mitotic phases of the cell cycle**.** J. Cell Sci. *111 (Pt 17)***:** 2551-2561.

207. Uzbekov R., Prigent C., and rlot-Bonnemains Y. (1999). Cell cycle analysis and synchronization of the Xenopus laevis XL2 cell line: study of the kinesin related protein XlEg5**.** Microsc. Res. Tech. *45***:** 31-42.

208. Enos A.P. and Morris N.R. (1990). Mutation of a gene that encodes a kinesin-like protein blocks nuclear division in A. nidulans**.** Cell *60***:** 1019-1027.

209. Sawin K.E. and Mitchison T.J. (1995). Mutations in the kinesin-like protein Eg5 disrupting localization to the mitotic spindle**.** Proc. Natl. Acad. Sci. U. S. A *92***:** 4289-4293.

210. Blangy A., Lane H.A., d'Herin P., Harper M., Kress M., and Nigg E.A. (1995). Phosphorylation by p34cdc2 regulates spindle association of human Eg5, a kinesin-related motor essential for bipolar spindle formation in vivo**.** Cell *83***:** 1159-1169.

211. Giet R., Uzbekov R., Cubizolles F., Le G.K., and Prigent C. (1999). The Xenopus laevis aurora-related protein kinase pEg2 associates with and phosphorylates the kinesin-related protein XlEg5**.** J. Biol. Chem. *274***:** 15005-15013.

212. Drummond D.R. and Hagan I.M. (1998). Mutations in the bimC box of Cut7 indicate divergence of regulation within the bimC family of kinesin related proteins**.** J. Cell Sci. *111 (Pt 7)***:** 853-865.

213. Saunders W.S. and Hoyt M.A. (1992). Kinesin-related proteins required for structural integrity of the mitotic spindle**.** Cell *70***:** 451-458.

214. Roof D.M., Meluh P.B., and Rose M.D. (1992). Kinesin-related proteins required for assembly of the mitotic spindle**.** J. Cell Biol. *118***:** 95-108.

215. Heck M.M., Pereira A., Pesavento P., Yannoni Y., Spradling A.C., and Goldstein L.S. (1993). The kinesin-like protein KLP61F is essential for mitosis in Drosophila**.** J. Cell Biol. *123***:** 665-679.

216. Walczak C.E., Vernos I., Mitchison T.J., Karsenti E., and Heald R. (1998). A model for the proposed roles of different microtubule-based motor proteins in establishing spindle bipolarity**.** Curr. Biol. *8***:** 903-913.

217. Mayer T.U., Kapoor T.M., Haggarty S.J., King R.W., Schreiber S.L., and Mitchison T.J. (1999). Small molecule inhibitor of mitotic spindle bipolarity identified in a phenotype-based screen**.** Science *286***:** 971-974.

218. Kapoor T.M., Mayer T.U., Coughlin M.L., and Mitchison T.J. (2000). Probing spindle assembly mechanisms with monastrol, a small molecule inhibitor of the mitotic kinesin, Eg5**.** J. Cell Biol. *150***:** 975-988.

219. Goshima G. and Vale R.D. (2003). The roles of microtubule-based motor proteins in mitosis: comprehensive RNAi analysis in the Drosophila S2 cell line**.** J. Cell Biol. *162***:** 1003-1016.

220. Zhu C., Zhao J., Bibikova M., Leverson J.D., Bossy-Wetzel E., Fan J.B., Abraham R.T., and Jiang W. (2005). Functional analysis of human microtubule-based motor proteins, the kinesins and dyneins, in mitosis/cytokinesis using RNA interference**.** Mol. Biol. Cell *16***:** 3187-3199.

221. Sharp D.J., Brown H.M., Kwon M., Rogers G.C., Holland G., and Scholey J.M. (2000). Functional Coordination of Three Mitotic Motors in Drosophila Embryos**.** Mol. Biol. Cell *11***:** 241-253.

222. Wilson P.G. (1999). BimC motor protein KLP61F cycles between mitotic spindles and fusomes in Drosophila germ cells**.** Curr. Biol. *9***:** 923-926.

223. Kaiser A., Brembeck F.H., Nicke B., Wiedenmann B., Riecken E.O., and Rosewicz S. (1999). All-trans-retinoic acid-mediated growth inhibition involves inhibition of human kinesin-related protein HsEg5**.** J. Biol. Chem. *274***:** 18925-18931.

224. Maliga Z., Kapoor T.M., and Mitchison T.J. (2002). Evidence that monastrol is an allosteric inhibitor of the mitotic kinesin Eg5**.** Chem. Biol. *9***:** 989-996.

225. Nakazawa J., Yajima J., Usui T., Ueki M., Takatsuki A., Imoto M., Toyoshima Y.Y., and Osada H. (2003). A novel action of terpendole E on the motor activity of mitotic Kinesin Eg5**.** Chem. Biol. *10***:** 131-137.

226. Brier S., Lemaire D., Debonis S., Forest E., and Kozielski F. (2004). Identification of the protein binding region of S-trityl-L-cysteine, a new potent inhibitor of the mitotic kinesin Eg5**.** Biochemistry *43***:** 13072-13082.

227. Debonis S., Skoufias D.A., Lebeau L., Lopez R., Robin G., Margolis R.L., Wade R.H., and Kozielski F. (2004). In vitro screening for inhibitors of the human mitotic kinesin Eg5 with antimitotic and antitumor activities**.** Mol. Cancer Ther. *3***:** 1079-1090.

228. Funk C.J., Davis A.S., Hopkins J.A., and Middleton K.M. (2004). Development of high-throughput screens for discovery of kinesin adenosine triphosphatase modulators**.** Anal. Biochem. *329***:** 68-76.

229. Cox C.D., Breslin M.J., Mariano B.J., Coleman P.J., Buser C.A., Walsh E.S., Hamilton K., Huber H.E., Kohl N.E., Torrent M. et al. (2005). Kinesin spindle protein (KSP) inhibitors. Part 1: The discovery of 3,5-diaryl-4,5-dihydropyrazoles as potent and selective inhibitors of the mitotic kinesin KSP**.** Bioorg. Med. Chem. Lett. *15***:** 2041-2045.

230. Duhl D.M. and Renhowe P.A. (2005). Inhibitors of kinesin motor proteins--research and clinical progress**.** Curr. Opin. Drug Discov. Devel. *8***:** 431-436.

231. Gartner M., Sunder-Plassmann N., Seiler J., Utz M., Vernos I., Surrey T., and Giannis A. (2005). Development and biological evaluation of potent and specific inhibitors of mitotic Kinesin Eg5**.** Chembiochem. *6***:** 1173-1177.

232. Sarli V., Huemmer S., Sunder-Plassmann N., Mayer T.U., and Giannis A. (2005). Synthesis and biological evaluation of novel EG5 inhibitors**.** Chembiochem. *6***:** 2005-2013.

233. Sunder-Plassmann N., Sarli V., Gartner M., Utz M., Seiler J., Huemmer S., Mayer T.U., Surrey T., and Giannis A. (2005). Synthesis and biological evaluation of new tetrahydro-beta-carbolines as inhibitors of the mitotic kinesin Eg5**.** Bioorg. Med. Chem. *13***:** 6094-6111.

234. Okumura H., Nakazawa J., Tsuganezawa K., Usui T., Osada H., Matsumoto T., Tanaka A., and Yokoyama S. (2006). Phenothiazine and carbazole-related compounds inhibit mitotic kinesin Eg5 and trigger apoptosis in transformed culture cells**.** Toxicol. Lett. *166***:** 44-52.

235. Cox C.D., Torrent M., Breslin M.J., Mariano B.J., Whitman D.B., Coleman P.J., Buser C.A., Walsh E.S., Hamilton K., Schaber M.D. et al. (2006). Kinesin spindle protein (KSP) inhibitors. Part 4: Structure-based design of 5-alkylamino-3,5-diaryl-4,5-dihydropyrazoles as potent, water-soluble inhibitors of the mitotic kinesin KSP**.** Bioorg. Med. Chem. Lett.

236. Kim K.S., Lu S., Cornelius L.A., Lombardo L.J., Borzilleri R.M., Schroeder G.M., Sheng C., Rovnyak G., Crews D., Schmidt R.J. et al. (2006). Synthesis and SAR of pyrrolotriazine-4-one based Eg5 inhibitors**.** Bioorg. Med. Chem. Lett. *16***:** 3937-3942.

237. Skoufias D.A., Debonis S., Saoudi Y., Lebeau L., Crevel I., Cross R., Wade R.H., Hackney D., and Kozielski F. (2006). S-trityl-l-cysteine is a reversible, tight-binding inhibitor of the human kinesin eg5 that specifically blocks mitotic progression**.** J. Biol. Chem.

238. Tarby C.M., Kaltenbach R.F., III, Huynh T., Pudzianowski A., Shen H., Ortega-Nanos M., Sheriff S., Newitt J.A., McDonnell P.A., Burford N. et al. (2006). Inhibitors of human mitotic kinesin Eg5: characterization of the 4-phenyl-tetrahydroisoquinoline lead series**.** Bioorg. Med. Chem. Lett. *16***:** 2095-2100.

239. Garcia-Saez I., Debonis S., Lopez R., Trucco F., Rousseau B., Thuery P., and Kozielski F. (2007). Structure of human Eg5 in complex with a new monastrol-based inhibitor bound in the R configuration**.** J. Biol. Chem. *282***:** 9740-9747.

240. Brier S., Lemaire D., Debonis S., Forest E., and Kozielski F. (2006). Molecular dissection of the inhibitor binding pocket of mitotic kinesin Eg5 reveals mutants that confer resistance to antimitotic agents**.** J. Mol. Biol. *360***:** 360-376.

241. Brier S., Lemaire D., Debonis S., Kozielski F., and Forest E. (2006). Use of hydrogen/deuterium exchange mass spectrometry and mutagenesis as a tool to identify the binding region of inhibitors targeting the human mitotic kinesin Eg5**.** Rapid Commun. Mass Spectrom. *20***:** 456-462.

242. Maliga Z. and Mitchison T.J. (2006). Small-molecule and mutational analysis of allosteric Eg5 inhibition by monastrol**.** BMC. Chem. Biol. *6***:** 2.

243. Turner J., Anderson R., Guo J., Beraud C., Fletterick R., and Sakowicz R. (2001). Crystal structure of the mitotic spindle kinesin Eg5 reveals a novel conformation of the neck-linker**.** J. Biol. Chem. *276***:** 25496-25502.

244. Yan Y., Sardana V., Xu B., Homnick C., Halczenko W., Buser C.A., Schaber M., Hartman G.D., Huber H.E., and Kuo L.C. (2004). Inhibition of a mitotic motor protein: where, how, and conformational consequences**.** J. Mol. Biol. *335***:** 547-554.

245. Crevel I.M., Alonso M.C., and Cross R.A. (2004). Monastrol stabilises an attached low-friction mode of Eg5**.** Curr. Biol. *14***:** R411-R412.

246. Cochran J.C. and Gilbert S.P. (2005). ATPase mechanism of Eg5 in the absence of microtubules: insight into microtubule activation and allosteric inhibition by monastrol**.** Biochemistry *44***:** 16633-16648.

247. Maliga Z., Xing J., Cheung H., Juszczak L.J., Friedman J.M., and Rosenfeld S.S. (2006). A pathway of structural changes produced by monastrol binding to Eg5**.** J. Biol. Chem. *281***:** 7977-7982.

248. Cochran J.C., Gatial J.E., III, Kapoor T.M., and Gilbert S.P. (2005). Monastrol inhibition of the mitotic kinesin Eg5**.** J. Biol. Chem. *280***:** 12658-12667.

249. Moyer M.L., Gilbert S.P., and Johnson K.A. (1996). Purification and characterization of two monomeric kinesin constructs**.** Biochemistry *35***:** 6321-6329.

250. Cochran J.C., Sontag C.A., Maliga Z., Kapoor T.M., Correia J.J., and Gilbert S.P. (2004). Mechanistic analysis of the mitotic kinesin Eg5**.** J. Biol. Chem. *279***:** 38861-38870.

251. Rosenfeld S.S., Xing J., Jefferson G.M., and King P.H. (2005). Docking and rolling, a model of how the mitotic motor Eg5 works**.** J. Biol. Chem. *280***:** 35684-35695.

252. Lockhart A. and Cross R.A. (1994). Origins of reversed directionality in the ncd molecular motor**.** EMBO J. *13***:** 751-757.

253. Shimizu T., Sablin E., Vale R.D., Fletterick R., Pechatnikova E., and Taylor E.W. (1995). Expression, purification, ATPase properties, and microtubule-binding properties of the ncd motor domain**.** Biochemistry *34***:** 13259-13266.

254. Whitehead C.M., Winkfein R.J., and Rattner J.B. (1996). The relationship of HsEg5 and the actin cytoskeleton to centrosome separation**.** Cell Motil. Cytoskeleton *35***:** 298-308.

255. Kapitein L.C., Peterman E.J., Kwok B.H., Kim J.H., Kapoor T.M., and Schmidt C.F. (2005). The bipolar mitotic kinesin Eg5 moves on both microtubules that it crosslinks**.** Nature *435***:** 114-118.

256. Kwok B.H., Kapitein L.C., Kim J.H., Peterman E.J., Schmidt C.F., and Kapoor T.M. (2006). Allosteric inhibition of kinesin-5 modulates its processive directional motility**.** Nat. Chem. Biol. *2***:** 480-485.

257. Debonis S., Simorre J.P., Crevel I., Lebeau L., Skoufias D.A., Blangy A., Ebel C., Gans P., Cross R., Hackney D.D. et al. (2003). Interaction of the mitotic inhibitor monastrol with human kinesin Eg5**.** Biochemistry *42***:** 338-349.

258. Sack S., Kull F.J., and Mandelkow E. (1999). Motor proteins of the kinesin family. Structures, variations, and nucleotide binding sites**.** Eur. J. Biochem. *262***:** 1-11.

259. Marx A., Muller J., Mandelkow E.M., Hoenger A., and Mandelkow E. (2005). Interaction of kinesin motors, microtubules, and MAPs**.** J. Muscle Res. Cell Motil. 1-13.

260. Woehlke G., Ruby A.K., Hart C.L., Ly B., Hom-Booher N., and Vale R.D. (1997). Microtubule interaction site of the kinesin motor**.** Cell *90***:** 207-216.

261. Song H. and Endow S.A. (1998). Decoupling of nucleotide- and microtubule-binding sites in a kinesin mutant**.** Nature *396***:** 587-590.

262. Yun M., Zhang X., Park C.G., Park H.W., and Endow S.A. (2001). A structural pathway for activation of the kinesin motor ATPase**.** EMBO J. *20***:** 2611-2618.

263. Farrell C.M., Mackey A.T., Klumpp L.M., and Gilbert S.P. (2002). The role of ATP hydrolysis for kinesin processivity**.** J. Biol. Chem. *277***:** 17079-17087.

264. Kull F.J. and Endow S.A. (2002). Kinesin: switch I & II and the motor mechanism**.** J. Cell Sci. *115***:** 15-23.

265. Klumpp L.M., Mackey A.T., Farrell C.M., Rosenberg J.M., and Gilbert S.P. (2003). A kinesin switch I arginine to lysine mutation rescues microtubule function**.** J. Biol. Chem. *278***:** 39059-39067.

266. Auerbach S.D. and Johnson K.A. (2005). Kinetic effects of kinesin switch I and switch II mutations**.** J. Biol. Chem. *280***:** 37061-37068.

267. Alonso M.C., van D.J., Vandekerckhove J., and Cross R.A. (1998). Proteolytic mapping of kinesin/ncd-microtubule interface: nucleotide-dependent conformational changes in the loops L8 and L12**.** EMBO J. *17***:** 945-951.

268. Hirose K., Lowe J., Alonso M., Cross R.A., and Amos L.A. (1999). Congruent docking of dimeric kinesin and ncd into three-dimensional electron cryomicroscopy maps of microtubule-motor ADP complexes**.** Mol. Biol. Cell *10***:** 2063-2074.

269. Vale R.D. and Milligan R.A. (2000). The way things move: looking under the hood of molecular motor proteins**.** Science *288***:** 88-95.

270. Woehlke G. (2001). A look into kinesin's powerhouse**.** FEBS Lett. *508***:** 291-294.

271. Al-Bassam J., Cui Y., Klopfenstein D., Carragher B.O., Vale R.D., and Milligan R.A. (2003). Distinct conformations of the kinesin Unc104 neck regulate a monomer to dimer motor transition**.** J. Cell Biol. *163***:** 743-753.

272. Nitta R., Kikkawa M., Okada Y., and Hirokawa N. (2004). KIF1A alternately uses two loops to bind microtubules**.** Science *305***:** 678-683.

273. Hirose K., Akimaru E., Akiba T., Endow S.A., and Amos L.A. (2006). Large Conformational Changes in a Kinesin Motor Catalyzed by Interaction with Microtubules**.** Molecular Cell *23***:** 913-923.

274. Sindelar C.V. and Downing K.H. (2007). The beginning of kinesin's force-generating cycle visualized at 9-A resolution**.** J. Cell Biol. *177***:** 377-385.

275. Kozielski F., Arnal I., and Wade R.H. (1998). A model of the microtubule-kinesin complex based on electron cryomicroscopy and X-ray crystallography**.** Curr. Biol. *8***:** 191-198.

276. Mandelkow E. and Hoenger A. (1999). Structures of kinesin and kinesin-microtubule interactions**.** Curr. Opin. Cell Biol. *11***:** 34-44.

277. Kikkawa M., Okada Y., and Hirokawa N. (2000). 15 A resolution model of the monomeric kinesin motor, KIF1A**.** Cell *100***:** 241-252.

278. Kozielski F., Sack S., Marx A., Thormahlen M., Schonbrunn E., Biou V., Thompson A., Mandelkow E.M., and Mandelkow E. (1997). The crystal structure of dimeric kinesin and implications for microtubule-dependent motility**.** Cell *91***:** 985-994.

279. Sablin E.P., Case R.B., Dai S.C., Hart C.L., Ruby A., Vale R.D., and Fletterick R.J. (1998). Direction determination in the minus-end-directed kinesin motor ncd**.** Nature *395***:** 813-816.

280. Henningsen U. and Schliwa M. (1997). Reversal in the direction of movement of a molecular motor**.** Nature *389***:** 93-96.

281. Endow S.A. and Waligora K.W. (1998). Determinants of kinesin motor polarity**.** Science *281***:** 1200-1202.

282. Wade R.H. and Kozielski F. (2000). Structural links to kinesin directionality and movement**.** Nat. Struct. Biol. *7***:** 456-460.

283. Kasprzak A.A. and Hajdo L. (2002). Directionality of kinesin motors**.** Acta Biochim. Pol. *49***:** 813-821.

284. Vale R.D. and Fletterick R.J. (1997). The design plan of kinesin motors**.** Annu. Rev. Cell Dev. Biol. *13***:** 745-777.

285. Romberg L., Pierce D.W., and Vale R.D. (1998). Role of the kinesin neck region in processive microtubule-based motility**.** J. Cell Biol. *140***:** 1407-1416.

286. Sack S., Muller J., Marx A., Thormahlen M., Mandelkow E.M., Brady S.T., and Mandelkow E. (1997). X-ray structure of motor and neck domains from rat brain kinesin**.** Biochemistry *36***:** 16155-16165.

287. Hoenger A. and Milligan R.A. (1997). Motor domains of kinesin and ncd interact with microtubule protofilaments with the same binding geometry**.** J. Mol. Biol. *265***:** 553-564.

288. Case R.B., Rice S., Hart C.L., Ly B., and Vale R.D. (2000). Role of the kinesin neck linker and catalytic core in microtubule-based motility**.** Curr. Biol. *10***:** 157-160.

289. Xing J., Wriggers W., Jefferson G.M., Stein R., Cheung H.C., and Rosenfeld S.S. (2000). Kinesin has three nucleotide-dependent conformations. Implications for strain-dependent release**.** J. Biol. Chem. *275***:** 35413-35423.

290. Sindelar C.V., Budny M.J., Rice S., Naber N., Fletterick R., and Cooke R. (2002). Two conformations in the human kinesin power stroke defined by X-ray crystallography and EPR spectroscopy**.** Nat. Struct. Biol. *9***:** 844-848.

291. Tomishige M., Stuurman N., and Vale R.D. (2006). Single-molecule observations of neck linker conformational changes in the kinesin motor protein**.** Nat Struct Mol Biol *13***:** 887-894.

292. Shelanski M.L., Gaskin F., and Cantor C.R. (1973). Microtubule assembly in the absence of added nucleotides**.** Proc. Natl. Acad. Sci. U. S. A *70***:** 765-768.

293. Sloboda R.D., Dentler W.L., and Rosenbaum J.L. (1976). Microtubule-associated proteins and the stimulation of tubulin assembly in vitro**.** Biochemistry *15***:** 4497-4505.

294. Borisy G.G., Olmsted J.B., Marcum J.M., and Allen C. (1974). Microtubule assembly in vitro**.** Fed. Proc. *33***:** 167-174.

295. Omoto C.K. and Johnson K.A. (1986). Activation of the dynein adenosinetriphosphatase by microtubules**.** Biochemistry *25***:** 419-427.

296. Johnson K.A. and Borisy G.G. (1977). Kinetic analysis of microtubule self-assembly in vitro**.** Journal of Molecular Biology *117***:** 1-31.

297. LOWRY O.H., ROSEBROUGH N.J., FARR A.L., and RANDALL R.J. (1951). Protein measurement with the Folin phenol reagent**.** J. Biol Chem. *193***:** 265-275.

298. Schacterle G.R. and Pollack R.L. (1973). A simplified method for the quantitative assay of small amounts of protein in biologic material**.** Analytical Biochemistry *51***:** 654-655.

299. Brune M., Hunter J.L., Corrie J.E., and Webb M.R. (1994). Direct, real-time measurement of rapid inorganic phosphate release using a novel fluorescent probe and its application to actomyosin subfragment 1 ATPase**.** Biochemistry *33***:** 8262-8271.

300. Haldimann A., Daniels L.L., and Wanner B.L. (1998). Use of New Methods for Construction of Tightly Regulated Arabinose and Rhamnose Promoter Fusions in Studies of the Escherichia coli Phosphate Regulon**.** J. Bacteriol. *180***:** 1277-1286.

301. Gilbert S.P. and Johnson K.A. (1993). Expression, purification, and characterization of the Drosophila kinesin motor domain produced in Escherichia coli**.** Biochemistry *32***:** 4677-4684.

302. Gordon D.M. and Roof D.M. (1999). The kinesin-related protein Kip1p of Saccharomyces cerevisiae is bipolar**.** J. Biol. Chem. *274***:** 28779-28786.

303. Carter B.Z., Mak D.H., Shi Y., Schober W.D., Wang R.Y., Konopleva M., Koller E., Dean N.M., and Andreeff M. (2006). Regulation and targeting of Eg5, a mitotic motor protein in blast crisis CML: overcoming imatinib resistance**.** Cell Cycle *5***:** 2223-2229.

304. Liu M., Aneja R., Liu C., Sun L., Gao J., Wang H., Dong J.T., Sarli V., Giannis A., Joshi H.C. et al. (2006). Inhibition of the mitotic kinesin Eg5 up-regulates Hsp70 through the phosphatidylinositol 3-kinase/Akt pathway in multiple myeloma cells**.** J. Biol. Chem. *281***:** 18090-18097.

305. Hoenger A., Doerhoefer M., Woehlke G., Tittmann P., Gross H., Song Y.H., and Mandelkow E. (2000). Surface topography of microtubule walls decorated with monomeric and dimeric kinesin constructs**.** Biol. Chem. *381***:** 1001-1011.

306. Gilbert S.P. and Mackey A.T. (2000). Kinetics: a tool to study molecular motors**.** Methods *22***:** 337-354.

307. Correia J.J., Gilbert S.P., Moyer M.L., and Johnson K.A. (1995). Sedimentation studies on the kinesin motor domain constructs K401, K366, and K341**.** Biochemistry *34***:** 4898-4907.

308. De La Cruz E.M., Ostap E.M., and Sweeney H.L. (2001). Kinetic mechanism and regulation of myosin VI**.** J. Biol. Chem. *276***:** 32373-32381.

309. Sakamoto T., Wang F., Schmitz S., Xu Y., Xu Q., Molloy J.E., Veigel C., and Sellers J.R. (2003). Neck length and processivity of myosin V**.** J. Biol. Chem. *278***:** 29201-29207.

310. Cross R.A. (2004). The kinetic mechanism of kinesin**.** Trends Biochem. Sci. *29***:** 301-309.

311. Jiang W., Stock M.F., Li X., and Hackney D.D. (1997). Influence of the kinesin neck domain on dimerization and ATPase kinetics**.** J. Biol. Chem. *272***:** 7626-7632.

312. Kallipolitou A., Deluca D., Majdic U., Lakamper S., Cross R., Meyhofer E., Moroder L., Schliwa M., and Woehlke G. (2001). Unusual properties of the fungal conventional kinesin neck domain from Neurospora crassa**.** EMBO J. *20***:** 6226-6235.

313. Lupas A., Van Dyke M., and Stock J. (1991). Predicting coiled coils from protein sequences**.** Science *252***:** 1162-1164.

314. Berger B., Wilson D.B., Wolf E., Tonchev T., Milla M., and Kim P.S. (1995). Predicting coilied coils by use of pairwise residue correlations**.** Proc. Natl. Acad. Sci. USA *92***:** 8259-8263.

315. De M., V, Burkhard P., Le B.N., Vernos I., and Hoenger A. (2001). Analysis of heterodimer formation by Xklp3A/B, a newly cloned kinesin-II from Xenopus laevis**.** EMBO J. *20***:** 3370-3379.

316. De M., V, de M.A., Goldie K.N., Correia J.J., and Hoenger A. (2003). Dimerization properties of a Xenopus laevis kinesin-II carboxy-terminal stalk fragment**.** EMBO Rep. *4***:** 717-722.

317. Wendt T.G., Volkmann N., Skiniotis G., Goldie K.N., Muller J., Mandelkow E., and Hoenger A. (2002). Microscopic evidence for a minus-end-directed power stroke in the kinesin motor ncd**.** EMBO J. *21***:** 5969-5978.

318. Muto E., Sakai H., and Kaseda K. (2005). Long-range cooperative binding of kinesin to a microtubule in the presence of ATP**.** J. Cell Biol. *168***:** 691-696.

319. Asenjo A.B., Krohn N., and Sosa H. (2003). Configuration of the two kinesin motor domains during ATP hydrolysis**.** Nat. Struct. Biol. *10***:** 836-842.

320. Valentine M.T., Fordyce P.M., and Block S.M. (2006). Eg5 steps it up! Cell Div. *1***:** 31.

321. Valentine M.T. and Gilbert S.P. (2007). To step or not to step? How biochemistry and mechanics influence processivity in Kinesin and Eg5**.** Curr. Opin. Cell Biol. *19***:** 75-81.

322. Whitehead C.M. and Rattner J.B. (1998). Expanding the role of HsEg5 within the mitotic and post-mitotic phases of the cell cycle**.** J. Cell Sci. *111***:** 2551-2561.

323. Wilde A., Lizarraga S.B., Zhang L., Wiese C., Gliksman N.R., Walczak C.E., and Zheng Y. (2001). Ran stimulates spindle assemblyby alterin microtubule dynamics and the balance of motor activities**.** Nat. Cell Biol. *3***:** 221-227.

324. Kwok B.H., Yang J.G., and Kapoor T.M. (2004). The Rate of Bipolar Spindle Assembly Depends on the Microtubule-Gliding Velocity of the Mitotic Kinesin Eg5**.** Curr. Biol. *14***:** 1783-1788.

325. Shirasu-Hiza M., Perlman Z.E., Wittmann T., Karsenti E., and Mitchison T.J. (2004). Eg5 Causes Elongation of Meiotic Spindles When Flux-Associated Microtubule Depolymerization Is Blocked**.** Curr. Biol. *14***:** 1941-1945.

326. Miyamoto D.T., Perlman Z.E., Burbank K.S., Groen A.C., and Mitchison T.J. (2004). The kinesin Eg5 drives poleward microtubule flux in Xenopus laevis egg extract spindles**.** J. Cell Biol. *167***:** 813-818.

327. Kapitein L.C., Peterman E.J.G., Kwok B.H., Kim J.H., Kapoor T.M., and Schmidt C.F. (2005). The bipolar mitotic kinesin Eg5 moves on both microtubules that it crosslinks**.** Nature *435***:** 114-118.

328. Blangy A., Lane H.A., d'Herin P., Harper M., Kress M., and Nigg E.A. (1995). Phosphorylation by $p34^{cdc2}$ Regulates Spindle Association of Human Eg5, a Kinesin-Related Motor Essential for Bipolar Spindle Formation In Vivo**.** Cell *83***:** 1159-1169.

329. Sakowicz R., Finer J.T., Beraud C., Crompton A., Lewis E., Fritsch A., Lee Y., Mak J., Moody R., Turincio R. et al. (2004). Antitumor activity of a kinesin inhibitor**.** Cancer Res. *64***:** 3276-3280.

330. Okumura H., Nakazawa J., Tsuganezawa K., Usui T., Osada H., Matsumoto T., Tanaka A., and Yokoyama S. (2006). Phenothiazine and carbazole-related compounds inhibit mitotic kinesin Eg5 and trigger apoptosis in transformed culture cells**.** Toxicol. Lett.

331. Tao W., South V.J., Zhang Y., Davide J.P., Farrell L., Kohl N.E., Sepp-Lorenzino L., and Lobell R.B. (2005). Induction of apoptosis by an inhibitor of the mitotic kinesin KSP requires both activation of the spindle assembly checkpoint and mitotic slippage**.** Cancer Cell *8***:** 49-59.

332. Lockhart A. and Cross R.A. (1996). Kinetics and motility of the Eg5 microtubule motor**.** Biochemistry *35***:** 2365-2373.

333. Valentine M.T., Fordyce P.M., Krzysiak T.C., Gilbert S.P., and Block S.M. (2006). Individual dimers of the mitotic kinesin motor Eg5 step processively and support substantial loads in vitro**.** Nat. Cell Biol. *8***:** 470-476.

334. Klumpp L.M., Hoenger A., and Gilbert S.P. (2004). Kinesin's second step**.** Proc. Natl. Acad. Sci. USA *101***:** 3444-3449.

335. Klumpp L.M., Brendza K.M., Rosenberg J.M., Hoenger A., and Gilbert S.P. (2003). Motor domain mutation traps kinesin as a microtubule rigor complex**.** Biochemistry *42***:** 2595-2606.

336. Gilbert S.P. and Mackey A.T. (2000). Kinetics: A Tool to Study Molecular Motors*1**.** Methods *22***:** 337-354.

337. Mackey A.T. and Gilbert S.P. (2003). The ATPase Cross-bridge Cycle of the Kar3 Motor Domain. IMPLICATIONS FOR SINGLE HEAD MOTILITY**.** J. Biol. Chem. *278***:** 3527-3535.

338. Mackey A.T. and Gilbert S.P. (2003). The ATPase Cross-bridge Cycle of the Kar3 Motor Domain. IMPLICATIONS FOR SINGLE HEAD MOTILITY**.** J. Biol. Chem. *278***:** 3527-3535.

339. Nalavadi V., Nyitrai M., Bertolini C., Adamek N., Geeves M.A., and Bahler M. (2005). Kinetic mechanism of myosin IXB and the contributions of two class IX-specific regions**.** J. Biol. Chem. *280***:** 38957-38968.

340. Kambara T. and Ikebe M. (2006). A Unique ATP Hydrolysis Mechanism of Single-headed Processive Myosin, Myosin IX**.** J. Biol. Chem. *281***:** 4949-4957.

341. Klumpp L.M., Brendza K.M., Gatial J.E., III, Hoenger A., Saxton W.M., and Gilbert S.P. (2004). Microtubule-kinesin interface mutants reveal a site critical for communication**.** Biochemistry *43***:** 2792-2803.

342. Shirasu-Hiza M., Perlman Z.E., Wittmann T., Karsenti E., and Mitchison T.J. (2004). Eg5 causes elongation of meiotic spindles when flux-associated microtubule depolymerization is blocked**.** Curr. Biol. *14***:** 1941-1945.

343. Miyamoto D.T., Perlman Z.E., Burbank K.S., Groen A.C., and Mitchison T.J. (2004). The kinesin Eg5 drives poleward microtubule flux in Xenopus laevis egg extract spindles**.** J. Cell Biol. *167***:** 813-818.

344. Krzysiak T.C. and Gilbert S.P. (2006). Dimeric Eg5 Maintains Processivity through Alternating-site Catalysis with Rate-limiting ATP Hydrolysis**.** J. Biol. Chem. *281***:** 39444-39454.

345. Cochran J.C., Krzysiak T.C., and Gilbert S.P. (2006). Pathway of ATP hydrolysis by monomeric Kinesin eg5**.** Biochemistry *45***:** 12334-12344.

346. Patel S.S. and Bandwar R.P. (2003). Fluorescence Methods for Studying the Kinetics and Thermodynamics of Transcription Initiation**.** In Methods in Enzymology RNA Polymerases and Associated Factors, Part C, Sankar Adhya and Susan Garges, ed. Academic Press), pp. 668-686.

347. Kapoor T.M. and Mitchison T.J. (2001). Eg5 is static in bipolar spindles relative to tubulin: evidence for a static spindle matrix**.** J. Cell Biol. *154***:** 1125-1133.

348. Korneev M.J., Lakamper S., and Schmidt C.F. (2007). Load-dependent release limits the processive stepping of the tetrameric Eg5 motor**.** Eur. Biophys. J.

349. Kapitein, L. C., Kwok, B. H., Schmidt, C. F., Kapoor, T. M., and Peterman, E. J., (2007) Microtubule crosslinking triggers the directional motility of Kinesin-5. *Biophysical Journal*, Supplement, 494a, Abstract, 2358-Pos

350. Moores C.A., Hekmat-Nejad M., Sakowicz R., and Milligan R.A. (2003). Regulation of KinI kinesin ATPase activity by binding to the microtubule lattice**.** J. Cell Biol. *163***:** 963-971.